

**Mapping a Brazilian deforestation
frontier using multi-temporal
TerraSAR-X data and supervised
machine learning**

Ron Hagensieker

Department of Earth Sciences
Freie Universität Berlin

Inaugural-Dissertation to obtain the academic degree
Doctor rerum naturalium (Dr. rer. nat.)

2018

First supervisor: Prof. Dr. Björn Waske
Second supervisor: Prof. Dr. Patrick Hostert
Day of disputation: September 10, 2018

Abstract

Satellite remote sensing enables a repeated survey of the earth's surface. With machine learning it is possible to recognize complex patterns from extensive data sets. Using methods from machine learning, remote sensing images are utilized to derive large scale land use and land cover (LULC) maps, carrying discrete information on the human management of land and intact primary forests, as well as change processes. Such information is particularly relevant in little developed regions, and areas which are undergoing transformation. Therefore, satellite remote sensing is generally the preferred method for generating LULC products within tropical regions, and particularly useful to assist tracking of change processes with regard to deforestation or land management. The Amazon is the largest area of continuous tropical forest in the world, and of substantial importance with regard to biodiversity, its influence on global climate, as well as providing living space for a large number of indigenous tribes. As tropical region, the Amazon is particularly affected by cloudy conditions, which pose a serious challenge to many remote sensing efforts. Utilization of Synthetic Aperture Radar (SAR) hence is promoted, as this warrants data availability at fixed intervals.

Performing land cover mapping at the deforestation frontier in the Brazilian states of Pará and Mato Grosso, the aim of this thesis is to evaluate latest concepts from machine learning and SAR remote sensing in the light of real world applicability. As a cumulative effort, this thesis provides a scalable method based on Markov Random Fields, to increase classification performance. This method is especially useful to enhance the outcome of SAR classifications, as it directly addresses inherent SAR properties such as multi-temporality and speckle. Furthermore, ALOS-2, RADARSAT-2, and TerraSAR-X, which are current SAR sensors fulfilling different properties with regard to ground resolution and wavelength, are being investigated concerning their synergetic potentials for the mapping of vegetated LULC classes of the Brazilian Amazon. Here, the additional value of combining multiple frequencies is evaluated using reliable validation techniques based on area adjustment. Additionally, single performance of the three sensors is evaluated and their potentials concerning the task of tropical mapping are estimated. Lastly, different potentials of TanDEM-X for the purpose of tropical mapping are investigated. TanDEM-X is the first continuous spaceborne mission

to offer a bi-static acquisition of data, enabling the generation of height models and the collection of coherence layers via a single pass.

Zusammenfassung

Satellitenfernerkundung ermöglicht eine periodische Erhebung der Erdoberfläche. Durch Machine Learning besteht zudem die Möglichkeit, Muster aus umfassenden Datensätzen abzuleiten. Unter Verwendung von Methoden des Machine Learning, werden Fernerkundungsbilder eingesetzt um großskalige Landnutzungs- und Landbedeckungskarten zu generieren, die diskrete Informationen über Bewirtschaftungspraktiken und intakte Primärwälder, als auch über Änderungsprozesse aufzeigen. Diese Informationen sind insbesondere von Interesse in wenig entwickelten Regionen sowie Gebieten, die Transformationsprozessen ausgesetzt sind. Daher ist satellitengestützte Fernerkundung generell die bevorzugte Methode um Landbedeckungs- und Landnutzungsprodukte tropischer Regionen zu generieren. Sie ist insbesondere nützlich Transformationsprozesse hinsichtlich Entwaldung oder Landbewirtschaftung zu erfassen.

Der Amazonas ist das weltgrößte Gebiet zusammenhängenden tropischen Waldes und von substantieller Bedeutung hinsichtlich Biodiversität, globalen Klimas sowie als Lebensgrundlage für eine große Anzahl indigener Völker. Als tropische Region ist der Amazonas insbesondere von bewölkten Bedingungen betroffen, die eine große Herausforderung für viele Fernerkundungsansätze darstellen. Die Verwendung von Verfahren basierend auf Synthetic Aperture Radar (SAR) ist aus diesem Grund bevorzugt, da somit die Datenverfügbarkeit in festen Intervallen gewährleistet werden kann.

Durch Landbedeckungskartierungen an der aktuellen Entwaldungsfront der brasilianischen Staaten Pará und Mato Grosso sollen in dieser Arbeit aktuelle Konzepte des Machine Learnings und SAR basierender Fernerkundung angewandt und ihre Verwendbarkeit unter realweltlichen Bedingungen geprüft werden. Als kumulativer Ansatz wird in der vorliegenden Arbeit eine skalierbare Methode basierend auf Markov Random Fields vorgestellt, die zur Verbesserung von Klassifizierungsgenauigkeiten verwendet werden kann. Der Nutzen dieser Methode betrifft insbesondere auf SAR basierende Klassifizierungen, da durch sie inherente SAR Eigenschaften wie Körnung und multi-temporale Datensätze adressiert werden. Weiterhin wird die Verwendbarkeit der aktuellen SAR Sensoren ALOS-2, RADARSAT-2 sowie TerraSAR-X, welche über individuelle Eigenschaften hinsichtlich Bodenauflösung sowie

Wellenlänge verfügen, auf ihre Tauglichkeit hinsichtlich synergetischer Nutzung als auch zur Kartierung tropischer Vegetationsklassen des Amazonas untersucht. Diese Validierung wird anhand moderner flächenbereinigter Metriken durchgeführt, um eine verlässliche Validierung zu gewährleisten. Weiterhin werden alle drei Sensoren bezüglich ihrer Eignung, tropische Kartierungen durchzuführen, verglichen. Abschließend folgt eine Bewertung der Potenziale von TanDEM-X vor dem Hintergrund tropischer Kartierung. TanDEM-X ist die erste orbitale Satellitenmission, die eine bistatische Akquise von SAR-Daten ermöglicht, sodass Höhenmodelle und Kohärenzinformationen mit einem einfachen Überflug abgeleitet werden können.

Table of contents

Abstract	v
Zusammenfassung	vii
Abstract	vii
List of figures	xiii
List of tables	xv
1 Introduction	1
1.1 Motivation	2
1.2 Brazilian Amazon	3
1.3 Synthetic Aperture Radar	6
1.3.1 Background	6
1.3.2 SAR for tropical Remote Sensing	8
1.4 Classification Overview	9
1.5 Adjusted Validation	10
1.6 Aims and Structure	12
2 Tropical land use land cover mapping in Pará (Brazil) using discriminative Markov random fields and multi-temporal TerraSAR-X data	23
2.1 Introduction	24
2.2 Study Area & Data	27
2.2.1 Study Area	27
2.2.2 Remote Sensing Data	29
2.2.3 Reference Data	30
2.3 Methods	33
2.3.1 Import Vector Machines	33

2.3.2	Markov Random Field	34
2.3.3	Passing scheme & transition matrices	35
2.3.4	Classification & Validation	38
2.4	Results	39
2.5	Discussion	45
2.6	Conclusion	48
3	Evaluation of Multi-Frequency SAR Images for Tropical Land Cover Mapping	57
3.1	Introduction	58
3.2	Study Area	61
3.3	Data	62
3.3.1	Remote Sensing Data	62
3.3.2	Reference Data	65
3.4	Methods	66
3.4.1	Preprocessing	66
3.4.2	Classification	66
3.5	Results	67
3.6	Discussion	75
3.7	Conclusions	77
4	Land Cover Classification based on interferometric TanDEM-X Imagery in the Brazilian Amazon	85
4.1	Introduction	86
4.2	Data & Study area	87
4.3	Methods	90
4.4	Results	91
4.5	Discussion	95
4.6	Conclusion	95
5	Mapping Deforestation from Height Differences of Tandem-X Images	99
5.1	Introduction	100
5.2	Data & Study area	101
5.3	Methods	103
5.4	Reference Data	103
5.5	Methods	104
5.6	Results	105
5.7	Discussion	107

5.8	Conclusion	108
6	Synthesis	113
6.1	Main findings	114
6.1.1	Chapter 2 - Discriminative MRF	114
6.1.2	Chapter 3 - Multi-frequency SAR	114
6.1.3	Chapters 4 and 5 - Interferometric SAR	115
6.2	Conclusion and prospects	115

List of figures

1.1	Location of the two study areas in Pará and Mato Grosso.	5
2.1	Composite of three TerraSAR-X acquisitions (Red: VV June 8, Green: HH September 4, Blue: VV November 9 of 2014). True color ETM (L8, 12 September 2014) in the background shows the diverse LULC properties. . .	28
2.2	Photograph illustrating the fluent transitions and interactions of different land cover types in the study region.	29
2.3	Temporal (green) and spatial (yellow) neighbors of a given pixel (blue). . .	34
2.4	Passing schedule as applied in this study. One pass over all layers corresponds to one iteration of LBP.	36
2.5	Factor-graph as implemented in this study. Variable nodes illustrated by yellow (spatial neighbor) and green nodes (temporal). Circles mark the corresponding factor nodes and the unary IVM-based energy.	37
2.6	User's and Producer's Accuracy for all the classes at each date.	40
2.7	Growth of burnt areas over the 2014 dry season. Error bars are indicative of the 95% confidence interval.	43
2.8	Final classification results using the st-MRF approach.	44
2.9	Difference map between 2014-06-30 classifications of st-MRF and IVM. Light colors indicate agreement between the two maps. Dark colors indicate class ambiguities, while the class of the final st-MRF classification is presented.	46
3.1	The study area is defined in an area of severe LULC processes and as the intersection of the available L-, C-, and X-band swaths.	62
3.2	Composites of the available SAR images consisting of January (red), March (green), and June (blue) acquisitions.	64
3.3	Comparison of the single scene mapping capabilities. Scenes are shown that yield the highest overall accuracy per sensor. The bottom right shows the TerraClass reference image.	69

3.4	Subsets of the classification result, achieved after each iteration of the wrapper. The classification is based on all specified data sets, e.g.,: the RS2-Jan is selected as the third data set and added to the AL2-Jan and TSX-Jun, which have been selected beforehand. The classification of these three datasets results in an accuracy of 67.79%.	70
3.5	Gains in User and Producer Accuracy for wrapper iterations 2–5.	72
3.6	Final classification product using multi-temporal, multi-frequency imagery compared to TerraClass reference data set. Note that inconsistent classes from the TerraClass dataset are masked out white.	74
4.1	The utilized StripMap scene. Position of the subset in the lower part is indicated by the red window.	88
4.2	Comparison of UA's and PA's.	92
4.3	Visual comparison of generated land cover products.	92
4.4	Final land cover map using the <i>InSAR+T</i> data set.	94
5.1	Location and extent of the study region in central Brazil.	102
5.2	Summary of relevant input layers: differences in height, differences in intensity, and digitized areas of change, respectively.	105
5.3	Deforestation map of the study region.	106

List of tables

2.1	Scenes utilized in this study. All scenes were collected over the same area using the same incidence angle.	27
2.2	Number of sample points available for training distinguished by class, extracted from polygons.	31
2.3	Classification scheme.	32
2.4	Area adjusted overall accuracies for different dates. The shown values are means over 10 iterations.	39
2.5	Comparison of different classifications inside the subsetting area of Figure 2.1.	41
3.1	SAR images included in wrapper analysis. TerraSAR-X data acquired as StripMap, RADARSAT-2 in Standard Beam mode, and ALOS-2 as Fine Beam StripMap, at 5 m, 20 m, and 10 m targeted ground resolution, respectively.	64
3.2	Area adjusted overall accuracy (%) for each dataset and iteration of the wrapper.	68
3.3	Population error matrix derived from classification of the full dataset and TerraClass reference data. Numbers reflect area adjusted percentages as introduced by Equation (4.1).	75
4.1	Area proportion matrix for the InSAR+T approach.	93
5.1	Confusion matrix for the classification. Test data was sampled over the entire extent of the available data.	107

Chapter 1

Introduction

1.1 Motivation

In 2015 natural forests encompassed roughly 40 000 000 km², with tropical and subtropical forests accounting for more than half of total forest area (Keenan et al., 2015). They function as hotspots for biodiversity (Pimm et al., 2014), carbon sinks (Pan et al., 2011), and reservoirs of freshwater. Yet, following land pressure and global demand for growable as well as fleeting resources, there exists a strong economic drive to transform these areas for cultivation and exploitation purposes (Verburg et al., 1999; Koh et al., 2008; Mantz, 2008).

Land Use and Land Cover (LULC) science is concerned with analyzing the multi-faceted structure and utilization of the earth's surface (Lambin et al., 2001; Cihlar et al., 2001). While land cover is defined as the physical surface of earth, with land use anthropogenous practices such as management regimes can be characterized. With an estimated 40 % of all land surfaces being under direct human use (Foley, 2005), a strong need exists to map and assess processes which affect tropical ecosystems to contribute to conservation efforts, assist land management, and safeguard efficient as well as sustainable growth. Information on LULC is further an integral part of various fields of research, including but not limited to hydrology (Wagner et al., 2013), epidemiology (Kienberger et al., 2014), and climatology (Broxton et al., 2014). Its relevance is underlined by a variety of non-governmental organizations and international Programmes, e.g. Reducing Emissions from Deforestation and Forest Degradation by the United Nations (UN-REDD), the Worldbank, the World Wildlife Fund (WWF), or UN's Food and Agriculture Organization (FAO), whose work is predominantly based on LULC information.

In this framework of gathering spatial measures on different types of land cover, satellite remote sensing plays an important role, as it offers comparable periodical surface measurements on a global scale. Surveying the earth on polar orbits, modern constellations, such as Sentinel-2, allow the acquisition of images at up to 10 m ground pixel resolution within a five day repeat window (Drusch et al., 2012), enabling an exhaustive monitoring even of small scale processes. Representative programmes highlighting the capabilities of such systems include Brazilian Prodes and Deter (Valeriano et al., 2004; Initiative et al., 2013), which are based primarily on data by Landsat and the Moderate-resolution Imaging Spectroradiometer (MODIS) to perform deforestation and degradation mapping.

In practice, tropical regions are particularly affected by the diurnal cycle in convection (Yang et al., 2001), which often coincides with the sensors' acquisition schedule at highly illuminated daytimes (Asner, 2001b). Therefore, multi-spectral remote sensing is influenced negatively by atmospheric interferences, i.e. haze and cloud cover, hampering its potentials to collect continuous time series data. Contrary to multi-spectral sensors, Synthetic Aperture Radar (SAR) operates at microwave frequencies, with wavelengths generally longer than

2.5 cm. Its signals can pass through the atmosphere and clouds, enabling SAR a guaranteed collection of gapless images at fixed revisit rates. For example, the Sentinel-1 constellation, consisting of two structurally identical satellites, comes with an orbital revisit of six days, and offers wall to wall mapping capabilities within a one week time window (Torres et al., 2012). Despite advantages in coverage, SAR images are inherently affected by speckle, terrain effects, and the operational limitations of a given wavelength (Woodhouse, 2005). For this reason, development of new instruments and methods in the context of SAR is of particular interest.

Within this chapter, the aim is to outline the overall motivation for the conducted research, and to elaborate on the chosen structure for the thesis. Overarching topics include the utilization of SAR images for the derivation of LULC maps within Amazonian study regions, while particular chapters refer to standalone methods for the improvement of mapping accuracy. Furthermore, the following sections of Chapter 1 are concerned with communicating a high level introduction to the given subjects, i.e. land cover mapping of the Amazon, SAR, validation, and classification methods.

1.2 Brazilian Amazon

The Brazilian Amazon is the largest area of tropical rain forest shared by a single country, covering nearly 40 % of Brazil's entire area. It is of global importance due to its function as a carbon sink (Brienen et al., 2015), and is expected to harbor at least 10 % of total global biodiversity. Moreover, many of its effects on global systems are just recently being investigated. For example, Medvigy et al. (2013) discuss the significant impact of the Amazon on weather patterns within the USA. The Amazon further plays an important role in the subcontinental water cycle, affecting regional precipitation, with single trees emitting an estimated 1000l of water vapor per day (Nobre et al., 2014; Makarieva et al., 2006). For this reason, the potential effects of deforestation on the increasing number of droughts in south-eastern metropolitan regions of Brazil are discussed (Nazareno et al., 2015).

Over the last decades, the Amazon became threatened by a variety of anthropogenic factors (Davidson et al., 2012; Oliveira et al., 2013; Lapola et al., 2014). By spatial extent, cattle ranching might be the most severe, and due to the negative effects of cattle on CO₂ cycles, large scale ranching in the Amazon has global implications. By extension, increased herding of cattle also raises demand for soy, which is traditionally grown outside of the Brazilian tropics. Yet, high demand and advances in agriculture are causing a northward spread leading to further deforestation in the Amazon (Aide et al., 2004; Coy et al., 2014).

Overall, Brazil is the top global producer for many agriculturally extensive products, like soybean, coffee, sugar, and beef (Rada, 2013).

Within the last years, a debate on a potential full stop of Amazonian deforestation has been brought up in scientific literature and global political conversation alike (Nepstad et al., 2009; Soares-Filho et al., 2014; Nepstad et al., 2014a). Recent changes in policy, i.e. the beef and soy moratoria (Tollefson, 2015; Gibbs et al., 2015), and the increased utilization of remote sensing have been presented as potential reasons for a strong decline in deforestation rates starting in 2005. Yet, more recent statistics from 2012 onward show rates to be gradually increasing, raising questions on the long-term effectiveness and the effects of cyclic regimes on deforestation rates (Fearnside, 2015; INPE, 2015). Within Brazil, the federal states Mato Grosso and Pará are the largest contributors to Brazil's greenhouse gas emissions (Bustamante et al., 2012). As deforestation in Mato Grosso set in earlier than in Pará, it is just since 2006 that Pará is the state with the highest forest losses. Today, in Mato Grosso large parts of the Cerrado and the Amazon are already removed, yet, particularly in northern Mato Grosso, large scale deforestation remains a regular occurrence. On the other hand, many recent deforestation frontiers exist today in Pará. While Mato Grosso has traditionally played a bigger role infrastructurally, development of Pará is specifically linked to the Transamazonian highway BR-230, and the intersecting BR-163, which connects Santarém and Cuiabá.

Figure 1.1 introduces the study sites of this thesis. The general focus lies on a region just north of Novo Progresso, in south-western Pará, which in the last years came into public attention for its strong deforestation dynamics. Due to constraints in data availability, for Chapter 5 a second study site is introduced in northern Mato Grosso. It is characterized by similar dynamics, and results are assumed to be transferable. It was chosen due to the availability of a set of multi-temporal TanDEM-X (TD-X) scenes.

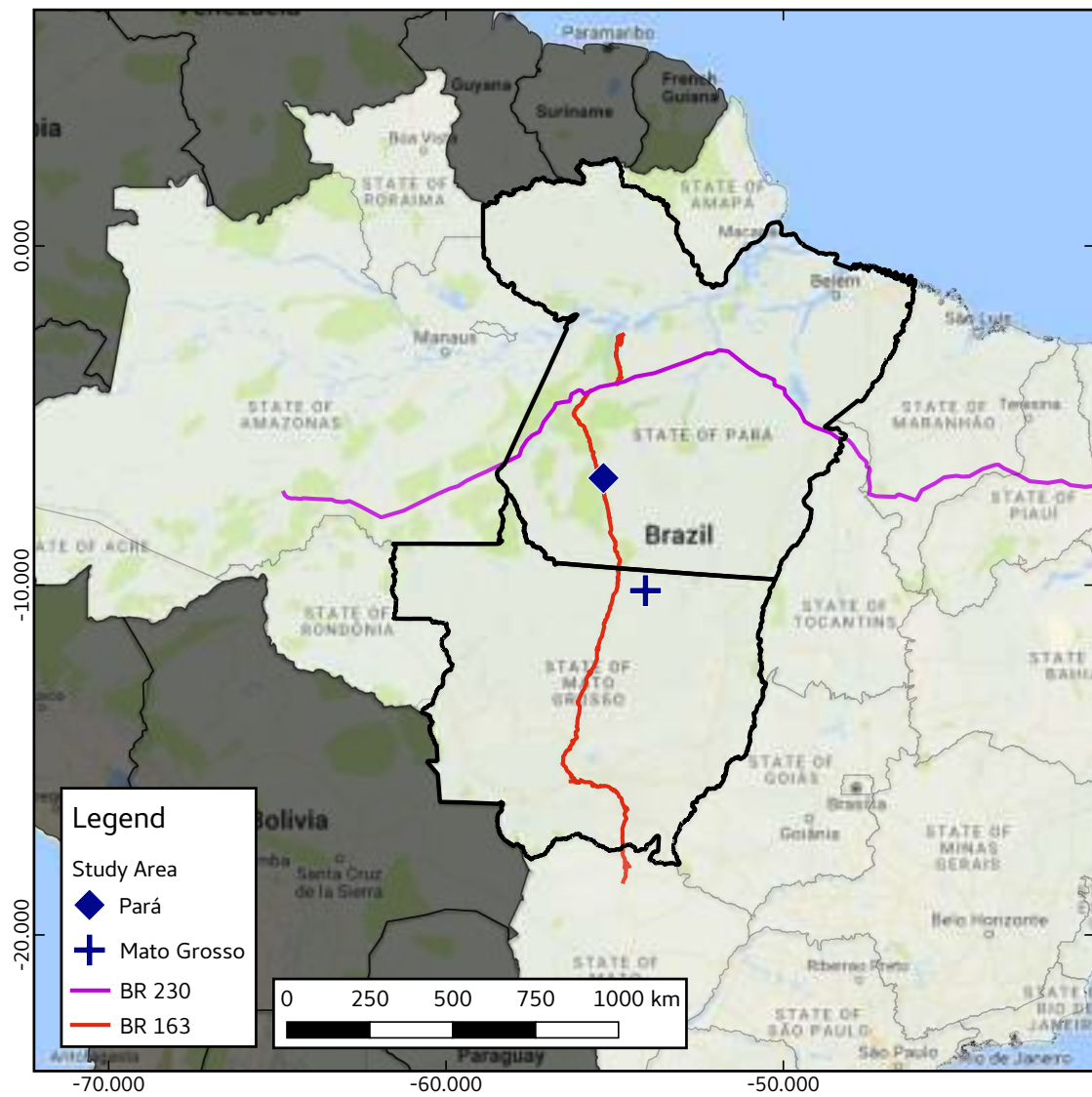


Fig. 1.1 Location of the two study areas in Pará and Mato Grosso.

1.3 Synthetic Aperture Radar

1.3.1 Background

The functioning principles of SAR allow for a cloud-free survey of land surface even under cloudy conditions (Moreira et al., 2013a). Contrary to multi-spectral systems, which in general sense the sun's radiation as it is reflected back by earth, SAR is an active system that measures its own sent out chirps (sweep signals), called backscatter. To achieve an acceptable pixel resolution, SAR is a side looking system that synthetically forms an antenna through its own forward motion. Image formation, also called focusing, relies on a two dimensional construction of the image, which is conventionally achieved through Fourier transformations (Moreira et al., 2013a).

SAR backscatter is comprised of two parts. As product of an active acquisition, the backscatter's intensity as well as its phase can be interpreted to infer information on scatterers on the ground (real world objects). While the intensity carries information on properties such as the surface's roughness, exposition, or dielectricity, the phase of coherent acquisitions can be used to derive information on the elevation of terrain, or, in the case of differential interferometry, to detect miniscule changes in elevation over time. In general, intensity is associated with the wavelength of the SAR system relative to scatterers on the ground. Additionally, the wavelength also determines the penetration of signals into different surfaces, such as tree canopy, certain soils, or ice sheets. Therefore, and due to SAR sensors operating at specific frequencies, different applications favor different sensors. Here, Enghart et al. (2011) highlight the advantageous properties of long wavelengths for the estimation of biomass, while in the agricultural domain short wavelengths help with the detection of early growing stages for certain crops. Still, if additional factors are taken into consideration, such as ground resolution or revisit rates, vagueness with regard to applicability remains due to the specific capabilities of different sensors. Moreover, some studies highlight possible benefits of the combined utilization of different wavelengths (Enghart et al., 2011; Schmullius et al., 1997).

Besides intensity, phase information of multiple SAR acquisitions can be utilized to determine detailed information on the surface structure by resolving the ambiguity of direction resulting in topographic distortion (Woodhouse, 2005). It is overall based on the time delay of an echoed signal not being equivalent to the distance, if topographic features on the ground are present (Woodhouse, 2005). Interferometry is often achieved through antennas with an across-track displacement, i.e. a displacement perpendicular to the flight direction. In the aerial case, this displacement is usually achieved through the wingspan of a plane, while in case of the Shuttle Radar Topography Mission (SRTM) a mast attached

to the space shuttle Endeavour was utilized. Across-track interferometry, for this reason, is often associated with single-pass interferometry, which describes utilization of two slightly displaced sensors to achieve the angular variation needed for estimating topography. On the other hand, repeat-pass interferometry describes one collecting sensor, which, in the case of space-borne SAR, gathers several scenes at revisiting orbits, either in an across-track or an along-track geometry. This is particularly useful to quantify processes over time, e.g. vertical movements, (Ferretti et al., 2000), and also falls under the category of differential interferometry.

Since commissioning of TD-X, a constellation of two twin satellites allowing to gather single-pass interferometric data, first studies have been published to use this data for land cover mapping. Schlund et al. (2013) utilize interferometric coherence, a by-product from the creation of the Digital Surface Model (DSM), to assist classification of a forest site in Indonesia. Other studies include the detection of urban footprints (Esch et al., 2013), or biomass classifications (Caicoya et al., 2012).

Another key principle of SAR is the polarization of transmitted and received signals, which is described as the movement in time and at a fixed location, of the tip of the electric field vector in space (Woodhouse, 2005). While radiation is in general non-polarized, chirps of a SAR system are transmitted, either with horizontal or vertical polarization. Modern sensors are able to operate different polarizations in quick succession, in a way that they can transmit and collect polarimetric information. For example, current systems are, in general, able to specify the transmission to be either horizontally or vertically polarized, and are able to subsequently receive both horizontal as well as vertical backscatter from both transmissions. In an optimal, fully polarimetric setup, the received signal can then be stored, on a pixel-level, in backscatter matrices (1.1).

$$\mathbf{S} = \begin{pmatrix} S_{VV} & S_{VH} \\ S_{HV} & S_{HH} \end{pmatrix} \quad (1.1)$$

Here, S are complex numbers representing amplitude and phase of the wave, while S_{HV} describes the received vertical signal for the associated horizontal transmission. In this ideal case of a filled matrix, \mathbf{S} can be *decomposed* into a covariance matrix, which can then be used to precisely characterize scatterers on the ground (Moreira et al., 2013a; Woodhouse, 2005). Yet, as fully polarimetric spaceborne sensors remain experimental, such potentials are not investigated as part of this work. Instead, cross-polarized data is utilized (e.g. VH+VV), and analysis is targeted on amplitudes neglecting interferometric phase.

1.3.2 SAR for tropical Remote Sensing

Since its introduction, SAR data has played an important role for remote sensing of tropical forests. With the launch of the Japanese Earth Resource Satellite 1 (JERS-1), and the European Remote-Sensing Satellite (ERS-1) in the early 90s, two spaceborne SAR sensors were commissioned to gather orbital images at L- and C-band, respectively. Backscatter of both sensors has been investigated with regard to estimations of above-ground biomass. Luckman et al. (1998) found that with JERS-1 data, only three broad classes of regenerating forest biomass density could be distinguished for a Brazilian study site, yet Santos et al. (2002) show applicability for biomass estimations for certain forest types and conditions. For boreal forests, albeit transferable also to tropical stands, Kurvonen et al. (1999) show a higher correlation coefficients for JERS-1 at L-band than ERS-1 when estimating biomass. Similarly, Luckman (1997) show ERS-1 to be merely able to separate forest from non-forest areas, while JERS-1 and the L-band instrument of SIR-C could be used for biomass estimations. Shimabukuro et al. (1998) investigate the capabilities of the C-band sensor RADARSAT (RS) for the distinction of several vegetation classes in Brazil, but due to the lack of spatial features could not achieve convincing results using automated approaches. Enabled by the utilization of spatial features, such as texture parameters, and the advancement of techniques from machine learning, such as decision trees and neural networks, first successes could also be achieved to perform vegetation based classifications using these data sources. (Dobson et al., 1996; Miranda et al., 1998). Especially for the distinction of inundated areas and mangroves SAR has proven useful (Simard et al., 2000).

The 2000s saw the rise of interferometric methods for forestry applications, and the commission of succeeding missions such as the Advanced Synthetic Aperture Radar (ASAR), RS-2, the Phased Array type L-band Synthetic Aperture Radar (PALSAR), as well as TerraSAR-X (TS-X) and TD-X. Here, Luckman et al. (2000) demonstrate for a Brazilian study site that repeat-pass interferometric coherence can help with the detection of forest disturbances, while the additional inclusion of interferometric ERS data yields no measurable benefits. These results are achieved accordingly by Takeuchi et al. (2003) for a site in Sumatra, underlining the capabilities of both sensors to detect deforestation, yet also showing the higher potentials of JERS-1 for more complex applications. While the focus of short wavelength SAR for forestry lies on boreal forests, some studies evaluate the potentials of the new missions within the tropical context. In particular logging and deforestation are topics of interest, which can be detected reliably even at X- and C-band ().

Because of the growing data volume, recent topics of investigation include multi-sensoral integration as well as the utilization of archive data for data mining purposes. Very prominently, Shimada et al. (2014) produce global forest maps using annual PALSAR data gathered

between 2007 and 2010, and transfer this approach for a 2014-2015 dataset of its successor ALOS-2 (Advanced Land Observing Satellite) to also perform change detection (Shimada et al., 2016). Using multi-sensoral data, land cover mapping accuracy can be optimized (Gessner et al., 2015), and also the performance of monitoring efforts can be increased (Reiche et al., 2016).

In summary, over the last decades areas of application for different types of SAR data have been outlined, yet also the development of new methods and the availability of abundant data enables applications under non-optimal conditions.

1.4 Classification Overview

Classification algorithms, so called classifiers, form the basis of any modern land cover mapping effort (Jin et al., 2014; Waske et al., 2009b; Moser et al., 2011). In the case of land cover mapping, a classifier commonly describes a program to transform pixel values into meaningful, discrete classes of land cover. Within the scope of this thesis, different classifiers from the field of non-parametric supervised learning are applied, namely Import Vector Machine (IVM) and Random Forest (RF) (Zhu et al., 2005a; Breiman, 2001a). Supervised learning describes the algorithms' property of utilizing labeled data for model adjustment (Mohri et al., 2012), and hence the gradual process of finding a set of model parameters in order to produce sensible outcome. In the case of a classification task, labeled data is understood to be of a discrete kind. This type of training is called non-parametric, since it does not aim to model the target classes via a set of distribution parameters μ, σ . In contrast to non-parametric methods, popular parametric methods include maximum likelihood (Hastie et al., 2009), as well as the recent and promising developments surrounding Generative Adversarial Nets (Goodfellow et al., 2014).

For training, the first step is to collect representative samples from the target classes, and a second, independent set for model validation (Hastie et al., 2009). After training and application of the model on unlabeled data, this validation set in conjunction with the classified outcome can be used to form a cross table to achieve a comprising evaluation. While this high level description outlines the general supervised learning approach, classification of image and remote sensing data come with additional potentials and challenges.

Many methods in the field of remote sensing are derived from approaches stemming from the domains of computer vision and image processing, which at their basis have the analysis of images (Parker, 2010). Besides training a model via a set of random samples, the images' intrinsic spatial properties are recognized and exploited to assist the classification task. Most relevantly, images are viewed as a matrix (or grid) of features. Each sample, called a pixel,

consists of an identical number of features, the channels, which are usually between one (greyscale), and four (RGBA), in the case of traditional image analysis. Each pixel is hence located at a distinct position in the image grid, and its appearance is highly correlated with its neighbors. Methods which address this structure outperform naive approaches, which do not pose these restrictions on the feature space. Examples are superpixels (Achanta et al., 2012), quadtrees (Samet, 1984), but also filtering techniques in general (He et al., 2013), and the recent technique of convolutional neural networks (Lee et al., 2009). Lastly, image processing in most cases is only concerned with the classification of entire images, or sometimes the classification of image subsets (Wang et al., 2010; Shi et al., 2000), for example, to recognize the presence of certain objects, like numbers, faces, or animals. In this case, classification of single pixels is generally not of interest.

Just as images offer a binding structure, remote sensing images fulfill a couple of additional properties. The number of channels, in remote sensing called bands, is highly variable and differs for each sensor and the chosen preprocessing. For example, Schlund et al. (2013) use a mixture of experimental SAR and texture bands, and Waske et al. (2010) use hundreds of hyperspectral bands, highlighting the diversity in potential data sets. While the high number of bands promotes class separability, it also increases computational cost of the conducted analysis and enhances the effect of the curse of dimensionality, thus increasing demands on a representative sampling and classifier (Shultz et al., 2011). In addition to the spatial grid, remote sensing images are usually collected in repeated intervals over the same location, which allows extension of the grid by an additional, temporal axis. Just like spatial vicinity, temporal vicinity is highly indicative on pixel appearance and class affiliation, yet, normalization is required for analyzing multiple dates (Small, 2011; Vermote et al., 2016). Furthermore, challenges can arise from different sensors collecting multi-temporal data, which means that the associated land cover (the discrete label at a certain pixel), is highly correlated, while the feature space is not comparable, neither in bands nor pixel alignment (Reiche et al., 2015a). Contrary to conventional image recognition, remote sensing is usually concerned with assigning classifications to each single pixel, as these represent ground areas associated with distinct land covers.

1.5 Adjusted Validation

Validation is particularly aimed at estimating the quality of the generated land cover maps. The land cover map is a combination of a certain number of independent classification (i.e. the number of pixels in the image). This poses additional challenges on the validation procedure, as different types of land cover are not present in similar proportions. For this

purpose, accuracy measures within this thesis are mostly based on practices as proposed by Foody (2002), Olofsson et al. (2013), and Olofsson et al. (2014). In particular, area adjusted measures are utilized to better reflect the effects of unevenly distributed land cover within study areas.

A conventional confusion matrix carries information on the actual state and target states of classifications. Items of known class get classified by the algorithm, and depending on their outcome they are associated with a certain cell in the confusion matrix. Contrary to a conventional confusion matrix, Olofsson et al. (2014) define the population error matrix through entries p_{ij} , with i representing the algorithm's output, and j the known reference. Instead of counted occurrences, entries within the population error matrix are normalized by the total number of available reference samples. For this reason, each entry is associated as a proportion, and the diagonal sum of the matrix expresses the overall accuracy, while user's (U) and producer's (P) accuracies can be inferred using the ratios of the columns' and rows' sums, respectively.

Afterwards, poststratification is applied, which is achieved through multiplication of the proportion of area mapped of a certain class W_i , by the ratio n_{ij}/n_{j+} . Here, n_{j+} describes the iterated sum over all columns for the j th row. The resulting matrix is the foundation to derive additional variance metrics, such as the variance of the overall accuracy (1.2)

$$\hat{V}(\hat{O}) = \sum_{i=1}^q W_i^2 \hat{U}_i (1 - \hat{U}_i) / (n_{i+} - 1). \quad (1.2)$$

Note that elements n refer to entries of the post-stratified error matrix. Additionally, the variance of user's accuracy can be estimated using (1.3)

$$\hat{V}(\hat{U}) = \hat{U}_i (1 - \hat{U}_i) / (n_{i+} - 1), \quad (1.3)$$

while the variance of producer's accuracy for some reference class $j = k$ is estimated by (1.4)

$$V(P) = \frac{1}{N_{+j}^2} \left[\frac{N_{j+}^2 (1 - P_j)^2 U_j (1 - U_j)}{n_{j+} - 1} + P_j^2 \sum_{i \neq j}^q N_{i+}^2 \frac{n_{ij}}{n_{i+}} \left(1 - \frac{n_{ij}}{n_{i+}} / (n_{i+} - 1) \right) \right], \quad (1.4)$$

with $N_{+j} = \sum_{i=1}^q \frac{N_{i+}}{n_{i+}} n_{ij}$, the estimated marginal total number of pixels of reference class j , N_j the corresponding marginal total of map class j , and n_j the number of samples in map class j .

Building upon such metrics, it is possible to define other sophisticated measures such as confidence intervals or area estimates.

Please note that the above explanation is an abbreviated version of Olofsson et al. (2014), with the purpose of keeping the chosen accuracy metrics transparent. To get a full understanding and explanation of the utilized method, please see the referred articles.

1.6 Aims and Structure

This thesis is a cumulative effort consisting of four scientific manuscripts, which propose methods for different stages in the processing chain of SAR-based land cover mapping of the Brazilian Amazon. All methods aim at introducing a different aspect to assist with the task of tropical land cover classification with SAR data, and the evaluation of the proposed methodology in terms of accuracy measures. Within this section, an argument is offered for its logical structure as well as the contents of the associated manuscripts. The overarching goal is to advance SAR-based tropical mapping. The following research questions are addressed:

- Are discriminative Markov Random Fields (MRF) viable for integrating multi-temporal datasets showing many occurrences of land cover change? It further poses the question, which methods can be used for MRF inference given the constraints of the multi-temporal setup as well as the size of the dataset.
- How well suited for the task of tropical land cover mapping are standard products by TS-X, RS-2, and ALOS-2?
- What are the current potentials of multi-frequent land cover classification in this context?
- What is the additional value of TD-X' interferometric features, in particular with regard to the separation of different vegetation types?
- What additional value can be generated by subtraction two height models derived from TD-X within a one year interval, with the purpose of mapping deforestation?

As part of Chapter 2, modern algorithms from the field of machine learning are adapted and their performance is evaluated for the purpose of tropical vegetation mapping. The goal is to develop a classification method, which can utilize spatial-temporal context to enhance classification accuracies. To achieve this, discriminative Markov Random Fields are applied in unison with a probabilistic Import Vector Machine classifier. MRF's are a

method to integrate information about pixel neighborhoods on top of the classification procedure. The classification procedure gets complemented by the integration of spatio-temporal neighborhoods, meaning each pixel is directly linked to its four spatial, and additionally to its two temporal neighbors. This way, land cover trajectories can be defined to prohibit temporally illogical changes in land cover, and spatially it enforces Tobler's first law of Geography (Tobler, 1970), that near things are more related than distant things, to sharpen classification quality. The method directly addresses various properties as highlighted in the previous Section 1.4. Besides the spatial-temporal integration, it is by definition transferable to multi-sensor cases, and is based on the intra-image classifications within the land cover map.

As part of Chapter 3, current spaceborne SAR sensors are evaluated with regard to tropical mapping. The goal is to evaluate the mapping potentials at different wavelengths, and also to gather knowledge on multi-frequency applicability. With TS-X, RS-2, and ALOS-2, this study utilizes data from three systems which are currently operational. Multiple scenes from each sensor are acquired in different seasons, allowing for a comparative study of these satellites' multi-temporal capabilities. A wrapper is set up to compare both, the mono- as well as the multi-frequent classification potentials. This is a method to concatenate input features based on their performance in previous iterations. In a first step, all scenes are classified independently. Afterwards, the best outcome is concatenated with each of the remaining scenes, again logging the classification accuracies. This procedure is iterated until the entire stack of images is classified. The order is considered a reliable indicator for the information gain of each scene.

Finally, two chapters (Chapter 4 and Chapter 5) are dedicated to an evaluation of interferometric TD-X data. Chapter 4 investigates the capabilities of including information on interferometric into a LULC classification within the Pará study region. As part of Chapter 5, two interferometric datasets within a one year interval are acquired. Both datasets are processed independently to derive height maps, which are afterwards subtracted to indicate land cover change, in particular deforestation.

The chapters of this work are written as autonomous manuscripts:

- R. Hagensieker, R. Roscher, J. Rosentreter, B. Jakimow, and B. Waske (2017a). "Tropical land use land cover mapping in Pará (Brazil) using discriminative Markov random fields and multi-temporal TerraSAR-X data". In: *International Journal of Applied Earth Observation and Geoinformation* 63, pp. 244–256
- R. Hagensieker and B. Waske (2018). "Evaluation of Multi-Frequency SAR Images for Tropical Land Cover Mapping". In: *Remote Sensing* 10.2, p. 257

- R. Hagensieker, I. Zeller, and B. Waske (submitted[a]). “Land Cover Classification based on interferometric TanDEM-X Imagery in the Brazilian Amazon”. In: *Geoscience and Remote Sensing Letters*
- R. Hagensieker, P. Lubig, and B. Waske (submitted[b]). “Mapping Deforestation from Height Differences of multi-temporal Tandem-X Images”. In: *Remote Sensing Letters*

References

- Achanta, R., A. Shaji, K. Smith, A. Lucchi, P. Fua, and S. Süsstrunk (2012). “SLIC Superpixels Compared to State-of-the-Art Superpixel Methods”. In: *IEEE Transactions on Pattern Analysis and Machine Intelligence* 34.11, pp. 2274–2282.
- Aide, T. M. and H. R. Grau (2004). “Globalization, migration, and Latin American ecosystems”. In: *Science* 305.5692, pp. 1915–1916.
- Asner, G. P. (2001b). “Cloud cover in Landsat observations of the Brazilian Amazon”. In: *International Journal of Remote Sensing* 22.18, pp. 3855–3862.
- Breiman, L. (2001a). “Random forests”. In: *Machine learning* 45.1, pp. 5–32.
- Brienen, R. J. W., O. L. Phillips, T. R. Feldpausch, E. Gloor, T. R. Baker, J. Lloyd, G. Lopez-Gonzalez, A. Monteagudo-Mendoza, Y. Malhi, S. L. Lewis, et al. (2015). “Long-term decline of the Amazon carbon sink”. In: *Nature* 519.7543, pp. 344–348.
- Broxton, P. D., X. Zeng, D. Sulla-Menashe, and P. A. Troch (2014). “A global land cover climatology using MODIS data”. In: *Journal of Applied Meteorology and Climatology* 53.6, pp. 1593–1605.
- Bustamante, M. M., C. A. Nobre, R. Smeraldi, A. P. Aguiar, L. G. Barioni, L. G. Ferreira, K. Longo, P. May, A. S. Pinto, and J. P. Ometto (2012). “Estimating greenhouse gas emissions from cattle raising in Brazil”. In: *Climatic change* 115.3-4, pp. 559–577.
- Caicoya, A. T., F. Kugler, I. Hajnsek, and K. Papathanassiou (2012). “Boreal forest biomass classification with TanDEM-X”. In: *2012 IEEE International Geoscience and Remote Sensing Symposium*. IEEE.
- Cihlar, J. and L. J. Jansen (2001). “From land cover to land use: a methodology for efficient land use mapping over large areas”. In: *The Professional Geographer* 53.2, pp. 275–289.
- Coy, M. and M. Klingler (2014). “Frentes pioneiras em transformação: o eixo da BR-163 e os desafios socioambientais”. In: *Territórios e Fronteiras* 7.1, pp. 1–26.
- Davidson, E. A., A. C. de Araújo, P. Artaxo, J. K. Balch, I. F. Brown, M. M. Bustamante, M. T. Coe, R. S. DeFries, M. Keller, M. Longo, et al. (2012). “The Amazon basin in transition”. In: *Nature* 481.7381, pp. 321–328.
- Dobson, M., L. Pierce, and F. Ulaby (1996). “Knowledge-based land-cover classification using ERS-1/JERS-1 SAR composites”. In: *IEEE Transactions on Geoscience and Remote Sensing* 34.1, pp. 83–99.
- Drusch, M., U. Del Bello, S. Carlier, O. Colin, V. Fernandez, F. Gascon, B. Hoersch, C. Isola, P. Laberinti, P. Martimort, and et al. (2012). “Sentinel-2: ESA’s Optical High-Resolution Mission for GMES Operational Services”. In: *Remote Sensing of Environment* 120, 25–36.

- Englhart, S., V. Keuck, and F. Siegert (2011). “Aboveground biomass retrieval in tropical forests – The potential of combined X- and L-band SAR data use”. In: *Remote Sensing of Environment* 115.5, pp. 1260–1271.
- Esch, T., M. Marconcini, A. Felbier, A. Roth, W. Heldens, M. Huber, M. Schwinger, H. Taubenbock, A. Muller, and S. Dech (2013). “Urban Footprint Processor—Fully Automated Processing Chain Generating Settlement Masks From Global Data of the TanDEM-X Mission”. In: *IEEE Geoscience and Remote Sensing Letters* 10.6, pp. 1617–1621.
- Fearnside, P. M. (2015). “Environment: deforestation soars in the Amazon”. In: *Nature* 521.7553, pp. 423–423.
- Ferretti, A., C. Prati, and F. Rocca (2000). “Nonlinear subsidence rate estimation using permanent scatterers in differential SAR interferometry”. In: *IEEE Transactions on Geoscience and Remote Sensing* 38.5, pp. 2202–2212.
- Foley, J. A. (2005). “Global Consequences of Land Use”. In: *Science* 309.5734, pp. 570–574.
- Foody, G. M. (2002). “Status of land cover classification accuracy assessment”. In: *Remote Sensing of Environment* 80.1, pp. 185–201.
- Gessner, U., M. Machwitz, T. Esch, A. Tillack, V. Naeimi, C. Kuenzer, and S. Dech (2015). “Multi-sensor mapping of West African land cover using MODIS, ASAR and TanDEM-X/TerraSAR-X data”. In: *Remote Sensing of Environment* 164, pp. 282–297.
- Gibbs, H. K., L. Rausch, J. Munger, I. Schelly, D. C. Morton, P. Noojipady, B. Soares-Filho, P. Barreto, L. Micol, and N. F. Walker (2015). “Brazil’s soy moratorium”. In: *Science* 347.6220, pp. 377–378.
- Goodfellow, I., J. Pouget-Abadie, M. Mirza, B. Xu, D. Warde-Farley, S. Ozair, A. Courville, and Y. Bengio (2014). “Generative Adversarial Nets”. In: *Advances in Neural Information Processing Systems* 27. Ed. by Z. Ghahramani, M. Welling, C. Cortes, N. D. Lawrence, and K. Q. Weinberger. Curran Associates, Inc., pp. 2672–2680.
- Hagensieker, R. and B. Waske (2018). “Evaluation of Multi-Frequency SAR Images for Tropical Land Cover Mapping”. In: *Remote Sensing* 10.2, p. 257.
- Hagensieker, R., I. Zeller, and B. Waske (submitted[a]). “Land Cover Classification based on interferometric TanDEM-X Imagery in the Brazilian Amazon”. In: *Geoscience and Remote Sensing Letters*.
- Hagensieker, R., P. Lubig, and B. Waske (submitted[b]). “Mapping Deforestation from Height Differences of multi-temporal Tandem-X Images”. In: *Remote Sensing Letters*.
- Hagensieker, R., R. Roscher, J. Rosentreter, B. Jakimow, and B. Waske (2017a). “Tropical land use land cover mapping in Pará (Brazil) using discriminative Markov random fields and multi-temporal TerraSAR-X data”. In: *International Journal of Applied Earth Observation and Geoinformation* 63, pp. 244–256.

- Hastie, T., R. Tibshirani, and J. Friedman (2009). *The Elements of Statistical Learning*. New York: Springer.
- He, K., J. Sun, and X. Tang (2013). “Guided Image Filtering”. In: *IEEE Transactions on Pattern Analysis and Machine Intelligence* 35.6, pp. 1397–1409.
- Initiative, C. P., J. Assunção, C. Gandour, and R. Rocha (2013). “DETERring Deforestation in the Brazilian Amazon: Environmental Monitoring and Law Enforcement”. In: INPE (2015). *Projeto PRODES - Monitoramento da Floresta Amazonica Brasileira por Satelite*.
- Jin, H., G. Mountrakis, and S. V. Stehman (2014). “Assessing integration of intensity, polarimetric scattering, interferometric coherence and spatial texture metrics in PALSAR-derived land cover classification”. In: *ISPRS Journal of Photogrammetry and Remote Sensing* 98, 70–84.
- Keenan, R. J., G. A. Reams, F. Achard, J. V. de Freitas, A. Grainger, and E. Lindquist (2015). “Dynamics of global forest area: Results from the FAO Global Forest Resources Assessment 2015”. In: *Forest Ecology and Management* 352, pp. 9–20.
- Kienberger, S. and M. Hagenlocher (2014). “Spatial-explicit modeling of social vulnerability to malaria in East Africa”. In: *International journal of health geographics* 13.1, p. 29.
- Koh, L. P. and D. S. Wilcove (2008). “Is oil palm agriculture really destroying tropical biodiversity?” In: *Conservation Letters* 1.2, pp. 60–64.
- Kurvonen, L., J. Pulliainen, and M. Hallikainen (1999). “Retrieval of biomass in boreal forests from multitemporal ERS-1 and JERS-1 SAR images”. In: *IEEE Transactions on Geoscience and Remote Sensing* 37.1, 198–205.
- Lambin, E. F., B. Turner, H. J. Geist, S. B. Agbola, A. Angelsen, J. W. Bruce, O. T. Coomes, R. Dirzo, G. Fischer, C. Folke, and et al. (2001). “The causes of land-use and land-cover change: moving beyond the myths”. In: *Global Environmental Change* 11.4, 261–269.
- Lapola, D. M., L. A. Martinelli, C. A. Peres, J. P. Ometto, M. E. Ferreira, C. A. Nobre, A. P. D. Aguiar, M. M. Bustamante, M. F. Cardoso, M. H. Costa, et al. (2014). “Pervasive transition of the Brazilian land-use system”. In: *Nature climate change* 4.1, pp. 27–35.
- Lee, H., R. Grosse, R. Ranganath, and A. Y. Ng (2009). “Convolutional deep belief networks for scalable unsupervised learning of hierarchical representations”. In: *Proceedings of the 26th Annual International Conference on Machine Learning - ICML 2009*.
- Luckman, A (1997). “A study of the relationship between radar backscatter and regenerating tropical forest biomass for spaceborne SAR instruments”. In: *Remote Sensing of Environment* 60.1, pp. 1–13.

- Luckman, A., J. Baker, and U. Wegmüller (2000). “Repeat-Pass Interferometric Coherence Measurements of Disturbed Tropical Forest from JERS and ERS Satellites”. In: *Remote Sensing of Environment* 73.3, pp. 350–360.
- Luckman, A., J. Baker, M. Honzák, and R. Lucas (1998). “Tropical Forest Biomass Density Estimation Using JERS-1 SAR: Seasonal Variation, Confidence Limits, and Application to Image Mosaics”. In: *Remote Sensing of Environment* 63.2, pp. 126–139.
- Makarieva, A. M. and V. G. Gorshkov (2006). “Biotic pump of atmospheric moisture as driver of the hydrological cycle on land”. In: *Hydrology and Earth System Sciences Discussions* 3.4, pp. 2621–2673.
- Mantz, J. W. (2008). “Improvisational economies: Coltan production in the eastern Congo”. In: *Social Anthropology* 16.1, pp. 34–50.
- Medvigy, D., R. L. Walko, M. J. Otte, and R. Avissar (2013). “Simulated Changes in Northwest US Climate in Response to Amazon Deforestation*”. In: *Journal of Climate* 26.22, pp. 9115–9136.
- Miranda, F. P., L. E. N. Fonseca, and J. R. Carr (1998). “Semivariogram textural classification of JERS-1 (Fuyo-1) SAR data obtained over a flooded area of the Amazon rainforest”. In: *International Journal of Remote Sensing* 19.3, pp. 549–556.
- Mohri, M., A. Rostamizadeh, and A. Talwalkar (2012). *Foundations of machine learning*. MIT press.
- Moreira, A., P. Pratstiraola, M. Younis, G. Krieger, I. Hajnsek, and K. P. Papathanassiou (2013a). “A Tutorial on Synthetic Aperture Radar”. In:
- Moser, G., E. Angiati, and S. B. Serpico (2011). “Multiscale unsupervised change detection on optical images by Markov random fields and wavelets”. In: *Geoscience and Remote Sensing Letters, IEEE* 8.4, pp. 725–729.
- Nazareno, A. G. and W. F. Laurance (2015). “Brazil's drought: Beware deforestation”. In: *Science* 347.6229, pp. 1427–1427.
- Nepstad, D., D. McGrath, C. Stickler, A. Alencar, A. Azevedo, B. Swette, T. Bezerra, M. DiGiano, J. Shimada, R. S. da Motta, et al. (2014a). “Slowing Amazon deforestation through public policy and interventions in beef and soy supply chains”. In: *Science* 344.6188, pp. 1118–1123.
- Nepstad, D., B. S. Soares-Filho, F. Merry, A. Lima, P. Moutinho, J. Carter, M. Bowman, A. Cattaneo, H. Rodrigues, S. Schwartzman, et al. (2009). “The end of deforestation in the Brazilian Amazon”. In: *Science* 326.5958, pp. 1350–1351.
- Nobre, A. D., M. D. Oyama, and G. S. Oliveira (2014). “The Future Climate of Amazonia”. In: *Scientific Assessment Report. Articulación Regional Amazonica (ARA), São José dos Campos*.

- Oliveira, L. J., M. H. Costa, B. S. Soares-Filho, and M. T. Coe (2013). "Large-scale expansion of agriculture in Amazonia may be a no-win scenario". In: *Environmental Research Letters* 8.2, p. 024021.
- Olofsson, P., G. M. Foody, M. Herold, S. V. Stehman, C. E. Woodcock, and M. A. Wulder (2014). "Good practices for estimating area and assessing accuracy of land change". In: *Remote Sensing of Environment* 148, pp. 42–57.
- Olofsson, P., G. M. Foody, S. V. Stehman, and C. E. Woodcock (2013). "Making better use of accuracy data in land change studies: Estimating accuracy and area and quantifying uncertainty using stratified estimation". In: *Remote Sensing of Environment* 129, pp. 122–131.
- Pan, Y., R. A. Birdsey, J. Fang, R. Houghton, P. E. Kauppi, W. A. Kurz, O. L. Phillips, A. Shvidenko, S. L. Lewis, J. G. Canadell, P. Ciais, R. B. Jackson, S. W. Pacala, A. D. McGuire, S. Piao, A. Rautiainen, S. Sitch, and D. Hayes (2011). "A Large and Persistent Carbon Sink in the World's Forests". In: *Science* 333.6045, pp. 988–993.
- Parker, J. R. (2010). *Algorithms for image processing and computer vision*. John Wiley & Sons.
- Pimm, S. L., C. N. Jenkins, R. Abell, T. M. Brooks, J. L. Gittleman, L. N. Joppa, P. H. Raven, C. M. Roberts, and J. O. Sexton (2014). "The biodiversity of species and their rates of extinction, distribution, and protection". In: *Science* 344.6187, pp. 1246752–1246752.
- Rada, N. (2013). "Assessing Brazil's Cerrado agricultural miracle". In: *Food Policy* 38, pp. 146–155.
- Reiche, J., R. Lucas, A. L. Mitchell, J. Verbesselt, D. H. Hoekman, J. Haarpaintner, J. M. Kellndorfer, A. Rosenqvist, E. A. Lehmann, C. E. Woodcock, F. M. Seifert, and M. Herold (2016). "Combining satellite data for better tropical forest monitoring". In: *Nature Climate Change* 6.2, pp. 120–122.
- Reiche, J., J. Verbesselt, D. Hoekman, and M. Herold (2015a). "Fusing Landsat and SAR time series to detect deforestation in the tropics". In: *Remote Sensing of Environment* 156, pp. 276–293.
- Samet, H. (1984). "The Quadtree and Related Hierarchical Data Structures". In: *ACM Computing Surveys* 16.2, pp. 187–260.
- Santos, J. R., M. S. P. Lacruz, L. S. Araujo, and M. Keil (2002). "Savanna and tropical rainforest biomass estimation and spatialization using JERS-1 data". In: *International Journal of Remote Sensing* 23.7, pp. 1217–1229.
- Schlund, M., F. von Poncet, D. H. Hoekman, S. Kuntz, and C. Schmullius (2013). "Importance of bistatic SAR features from TanDEM-X for forest mapping and monitoring". In: *Remote Sensing of Environment*.

- Schmullius, C. C. and D. L. Evans (1997). “Review article Synthetic aperture radar (SAR) frequency and polarization requirements for applications in ecology, geology, hydrology, and oceanography: A tabular status quo after SIR-C/X-SAR”. In: *International Journal of Remote Sensing* 18.13, 2713–2722.
- Shi, J. and J. Malik (2000). “Normalized cuts and image segmentation”. In: *IEEE Transactions on Pattern Analysis and Machine Intelligence* 22.8, pp. 888–905.
- Shimabukuro, Y., S. Amaral, F. Ahern, and R. Pietsch (1998). “Land Cover Classification from RADARSAT Data of the Tapajós National Forest, Brazil”. In: *Canadian Journal of Remote Sensing* 24.4, pp. 393–401.
- Shimada, M., T. Itoh, T. Motooka, M. Watanabe, and R. Thapa (2016). “Generation of the first PALSAR-2 global mosaic 2014/2015 and change detection between 2007 and 2015 using the PALSAR and PALSAR-2”. In: *2016 IEEE International Geoscience and Remote Sensing Symposium (IGARSS)*. IEEE.
- Shimada, M., T. Itoh, T. Motooka, M. Watanabe, T. Shiraishi, R. Thapa, and R. Lucas (2014). “New global forest/non-forest maps from ALOS PALSAR data (2007–2010)”. In: *Remote Sensing of Environment* 155, pp. 13–31.
- Shultz, T. R., S. E. Fahlman, S. Craw, P. Andritsos, P. Tsaparas, R. Silva, C. Drummond, C. X. Ling, V. S. Sheng, C. Drummond, P. L. Lanzi, J. Gama, R. P. Wiegand, P. Sen, G. Namata, M. Bilgic, L. Getoor, J. He, S. Jain, F. Stephan, S. Jain, F. Stephan, C. Sammut, M. Harries, C. Sammut, K. M. Ting, B. Pfahringer, J. Case, S. Jain, K. L. Wagstaff, S. Nijssen, A. Wirth, C. X. Ling, V. S. Sheng, X. Zhang, C. Sammut, N. Cancedda, J.-M. Renders, P. Michelucci, D. Oblinger, E. Keogh, and A. Mueen (2011). “Curse of Dimensionality”. In: *Encyclopedia of Machine Learning*. Springer US, pp. 257–258.
- Simard, M., S. Saatchi, and G. D. Grandi (2000). “The use of decision tree and multiscale texture for classification of JERS-1 SAR data over tropical forest”. In: *IEEE Transactions on Geoscience and Remote Sensing* 38.5, pp. 2310–2321.
- Small, D. (2011). “Flattening Gamma: Radiometric Terrain Correction for SAR Imagery”. In: *IEEE Transactions on Geoscience and Remote Sensing* 49.8, 3081–3093.
- Soares-Filho, B., R. Rajão, M. Macedo, A. Carneiro, W. Costa, M. Coe, H. Rodrigues, and A. Alencar (2014). “Cracking Brazil’s Forest Code”. In: *Science* 344.6182, pp. 363–364.
- Takeuchi, S. and Y. Oguro (2003). “A comparative study of coherence patterns in C-band and L-band interferometric SAR from tropical rain forest areas”. In: *Advances in Space Research* 32.11, pp. 2305–2310.
- Tobler, W. R. (1970). “A computer movie simulating urban growth in the Detroit region”. In: *Economic geography* 46.sup1, pp. 234–240.
- Tollefson, J. (2015). “Battle for the Amazon”. In: *Nature* 520.7545, p. 20.

- Torres, R., P. Snoeij, D. Geudtner, D. Bibby, M. Davidson, E. Attema, P. Potin, B. Rommen, N. Floury, M. Brown, and et al. (2012). “GMES Sentinel-1 mission”. In: *Remote Sensing of Environment* 120, 9–24.
- Valeriano, D., E. Mello, J. Moreira, Y. E. Shimabukuro, V Duarte, I. Souza, J. Santos, C. Barbosa, and R. Souza (2004). “Monitoring tropical forest from space: the PRODES digital project”. In: *International Archives of Photogrammetry Remote Sensing and Spatial Information Sciences* 35, pp. 272–274.
- Verburg, P. H., T. A. Veldkamp, and J. Bouma (1999). “Land use change under conditions of high population pressure: the case of Java”. In: *Global Environmental Change* 9.4, pp. 303–312.
- Vermote, E., C. Justice, M. Claverie, and B. Franch (2016). “Preliminary analysis of the performance of the Landsat 8/OLI land surface reflectance product”. In: *Remote Sensing of Environment* 185, pp. 46–56.
- Wagner, P., S Kumar, and K Schneider (2013). “An assessment of land use change impacts on the water resources of the Mula and Mutha Rivers catchment upstream of Pune, India”. In: *Hydrology and Earth System Sciences* 17.6, pp. 2233–2246.
- Wang, J., J. Yang, K. Yu, F. Lv, T. Huang, and Y. Gong (2010). “Locality-constrained Linear Coding for image classification”. In: *2010 IEEE Computer Society Conference on Computer Vision and Pattern Recognition*. IEEE.
- Waske, B. and M. Braun (2009b). “Classifier ensembles for land cover mapping using multitemporal SAR imagery”. In: *ISPRS Journal of Photogrammetry and Remote Sensing* 64.5, pp. 450–457.
- Waske, B., S. van der Linden, J. A. Benediktsson, A. Rabe, and P. Hostert (2010). “Sensitivity of support vector machines to random feature selection in classification of hyperspectral data”. In: *Geoscience and Remote Sensing, IEEE Transactions on* 48.7, pp. 2880–2889.
- Woodhouse, I. H. (2005). *Introduction to microwave remote sensing*. CRC press.
- Yang, G.-Y. and J. Slingo (2001). “The Diurnal Cycle in the Tropics”. In: *Monthly Weather Review* 129.4, 784–801.
- Zhu, J. and T. Hastie (2005a). “Kernel logistic regression and the import vector machine”. In: *Journal of Computational and Graphical Statistics* 14.1, pp. 185–205.

Chapter 2

Tropical land use land cover mapping in Pará (Brazil) using discriminative Markov random fields and multi-temporal TerraSAR-X data

International Journal of Applied Earth Observation and Geoinformation, Elsevier, 2017, 63,
244-256

<https://doi.org/10.1016/j.jag.2017.07.019>

Ron Hagensieker, Ribana Roscher, Johannes Rosentreter, Benjamin Jakimow, and Björn
Waske

Abstract

Remote sensing satellite data offer the unique possibility to map land use land cover transformations by providing spatially explicit information. However, detection of short-term processes and land use patterns of high spatial-temporal variability is a challenging task.

We present a novel framework using multi-temporal TerraSAR-X data and machine learning techniques, namely Discriminative Markov Random Fields with spatio-temporal priors, and Import Vector Machines, in order to advance the mapping of land cover characterized by short-term changes. Our study region covers a current deforestation frontier in the Brazilian state Pará with land cover dominated by primary forests, different types of pasture land and secondary vegetation, and land use dominated by short-term processes such as slash-and-burn activities. The data set comprises multi-temporal TerraSAR-X imagery acquired over the course of the 2014 dry season, as well as optical data (RapidEye, Landsat) for reference. Results show that land use land cover is reliably mapped, resulting in spatially adjusted overall accuracies of up to 79% in a five class setting, yet limitations for the differentiation of different pasture types remain.

The proposed method is applicable on multi-temporal data sets, and constitutes a feasible approach to map land use land cover in regions that are affected by high-frequent temporal changes.

2.1 Introduction

The Brazilian Amazon is the largest area of tropical rain forest shared by a single country. In the last decades it has become increasingly threatened by large scale deforestation, forest degradation, and the expansion of agriculture (Davidson et al., 2012; Lapola et al., 2014). They affect the Earth's ecosystems and ecosystem services far beyond the boundaries of the original region, and can influence the climate directly at local and even regional scales (Foley, 2005; Vitousek, 1997). Thus, detailed knowledge and information on land use and land cover (LULC) offers valuable input for decision support and environmental monitoring systems.

Remote sensing satellite data offers the unique possibility to generate consistent LULC maps over large areas at a temporally high resolution. Mapping of LULC change in the Amazon is predominantly achieved by analyzing multi-spectral remote sensing data (INPE, 2015; Wulder et al., 2012a; Hansen et al., 2013). However, a limitation of the analysis of multi-spectral remote sensing data is imposed by its dependency on cloud-free conditions. These are rare in tropical regions and in general not met during wet season (e.g. Rufin et al., 2015; Müller et al., 2015). Synthetic aperture radar (SAR) data can overcome these problems and

various studies demonstrate the potential for mapping LULC and their changes (Pfeifer et al., 2016; Qi et al., 2012; Bovolo et al., 2005), also in the context of deforestation and related processes (Sarker et al., 2013; Reiche et al., 2015a; Englhart et al., 2011; Almeida-Filho et al., 2009). Such mapping approaches become even more attractive due to recent missions with increased repetition rates, higher spatial resolution (e.g. TerraSAR-X and Sentinel-1), as well as better data availability, e.g., by virtue of the Copernicus data policy (Aschbacher et al., 2012). TerraSAR-X and the Sentinel-1 constellation guarantee cloud free coverage within 11 and 6 days respectively, while the repetition rate of the Sentinel-2 constellation (5 days) and Landsat-8 (16 days) might be affected by clouds.

Although the classification accuracy of SAR data can be limited in direct comparison to multi-spectral data, various approaches exist to increase the mapping accuracy. These include the integration of one-pass interferometry (Schlund et al., 2013), contextual spatial information derived from texture parameters or segmentation (Cutler et al., 2012a; Sarker et al., 2013; Schlund et al., 2013; Waske et al., 2008), or the utilization of multi-temporal or multi-sensoral data (Reiche et al., 2013; Stefanski et al., 2014; Waske et al., 2009b). Although limitations of short wavelength SAR data for the classification of dense vegetation are well documented (e.g. Kumar et al., 2013), various studies have highlighted the potentials of this data for LULC mapping (e.g. Schlund et al., 2013; Qi et al., 2015; Uhlmann et al., 2014; Qi et al., 2012; Khatami et al., 2016; Sonobe et al., 2014), e.g. by utilization of multi-temporal data, modern classification algorithms, or spatial context. Multi-temporal data sets are generally more adequate when classes can be characterized by clearly defined temporal signatures, e.g. caused by differences in the phenology of crops, land use management, or seasonal cycles (Blaes et al., 2005; McNairn et al., 2009). While the single classification of a multitemporal data set might be useful for study sites without or long-term changes (Waske et al., 2009b; Stefanski et al., 2014), it might be limited for study sites with temporally high-frequent changes in land cover, e.g. slash-and-burn activities, at arbitrary points in time. Recent studies have shown great potentials to tackle these problems by time series analysis of multispectral data (Zhu et al., 2014), but SAR speckle and quick succession processes still pose difficult challenges using such methods, especially if very long time series are often not available.

In the context of multi-temporal data analysis, a main drawback is often the assumption of non changing land cover during the investigation period. Consequently, temporally dynamic LULC, such as slash-and-burn activities or transitions between clean and shrubby pasture, are neglected. Various studies emphasize the usage of an adequate classification approach to ensure a high mapping accuracy (Liu et al., 2006; Waske et al., 2007; Waske et al., 2009b). Especially the integration of spatial information by means of region-based classification or

spatial features such as texture lead to a gain in accuracy. In addition, Markov Random Fields (MRFs) are a promising approach to integrate spatial context (Moser et al., 2013b; Moser et al., 2013a; Liu et al., 2006). MRFs are employed to model prior knowledge about neighborhood relations within the image, called spatial relations, but can also be extended to describe relations of the same area but at different acquisition dates (temporal relations). Since the early 1990s, approaches based on MRFs have been utilized in remote sensing for various purposes (Bouman et al., 1994; Xie et al., 2002; Tran et al., 2005; Solberg et al., 1996). Liu et al. (2008a) use locally variant transition models to account for spatial heterogeneity and have applied the model on subsets of two Landsat scenes from 1990 and 2001. More recently, Wehmann et al. (2015) have adapted an integrated kernel as proposed by Moser et al. (2013a), and used Iterative Conditional Modes (ICM) as optimization technique with spatially-variant transitions for classifying Landsat data. Hoberg et al. (2015) apply multi-temporal Conditional Random Fields to regularize annual remote sensing imagery from different high resolution scales (IKONOS, RapidEye, Landsat) over the course of five years.

With the emergence of efficient probabilistic classifiers over the last decade, standard MRFs have been extended to discriminative MRFs (Kumar et al., 2003), and turn out to be increasingly useful to optimize land cover classifications (Moser et al., 2010; Tarabalka et al., 2010; Voisin et al., 2013). Liu et al. (2006) highlight the advantages of utilizing non-parametric, probabilistic Support Vector Machines (SVMs, Platt (1999)) over a maximum likelihood classifier. However, although many remote sensing studies highlight the positive capabilities of MRFs, only few studies aim on using MRFs for landscape-scale mapping with multi-temporal data sets (e.g. Cai et al., 2014; Wehmann et al., 2015; Olding et al., 2015), for example, to map forest cover change (Liu et al., 2008b; Liu et al., 2006). If multi-temporal data sets are available, MRFs can also be used to optimize the corresponding maps by considering predefined spatial-temporal inter-dependencies between neighboring pixels, which are stored in transition matrices.

We present a novel framework for classification of a TS-X time series using discriminative MRFs and Import Vector Machine (IVM), a probabilistic, discriminative, non-parametric classifier. Each scene is separately classified using IVM, afterwards MRFs are utilized in an independent step to post-regularize the classification map. We chose IVMs over commonly used probabilistic SVMs, since they have proven to offer a more reliable probabilistic output (Zhu et al., 2005b; Roscher et al., 2012a; Roscher et al., 2012b). For MRF optimization we choose Loopy Belief Propagation (LBP) over ICM as this method has been shown repeatedly to yield higher accuracies (Szeliski et al., 2006; Andres et al., 2010). Few studies have utilized LBP in the field of remote sensing (Li et al., 2012), and as a novelty we integrate

LBP into a multi-temporal setting.

The presented framework aims on the classification of each individual acquisition, and thus enables mapping of high frequency spatial-temporal LULC patterns. In contrast to related studies, we use a multi-temporal MRF model on SAR data to detect short-term transitions within one season and Loopy Belief Propagation (LBP) for inference.

The overall goal of this research is focused on two objectives: (i) to map LULC in a tropical setting with short-term processes, by adapting recent MRF methods, and (ii) to assess the potential for LULC mapping using time-series image data of short wavelength SAR. The specific objective is to map LULC in Pará, Brazil, where transformations of forest to pasture are the major driver of deforestation. Pasture management in the study region tends to fall into one of two categories: long-term processes of intensively managed pasture land (pasto limpo), or short-term processes of episodically managed pasture land with a high degree of successive dynamics (pasto sujo). Pasture management in general is characterized by slash-and-burn processes resulting in sudden changes in LULC.

2.2 Study Area & Data

2.2.1 Study Area

The study area lies in the Northern part of the Novo Progresso municipality (southern Pará state, Brazil), and is intersected by the BR-163 highway in the Southwest 2.1. The BR-163 is accompanied by fishbone structures indicative of deforestation (Ahmed et al., 2013; Coy et al., 2014). A major driver of deforestation in the study area is the transformation of forests into pasture land. The climate in the study region is characterized by a wet and a dry season. While the dry season, between June and September, sees abrupt land cover changes in the form of large scale burning and clear cuts, the wet season is defined by gradual regrowth, yet deforestation rates over the wet season are on the rise.

Table 2.1 Scenes utilized in this study. All scenes were collected over the same area using the same incidence angle.

Date	Polarization
2014-06-08	VV-VH
2014-06-30	HH-HV
2014-07-22	VV-VH
2014-08-24	VV-VH
2014-09-04	HH-HV

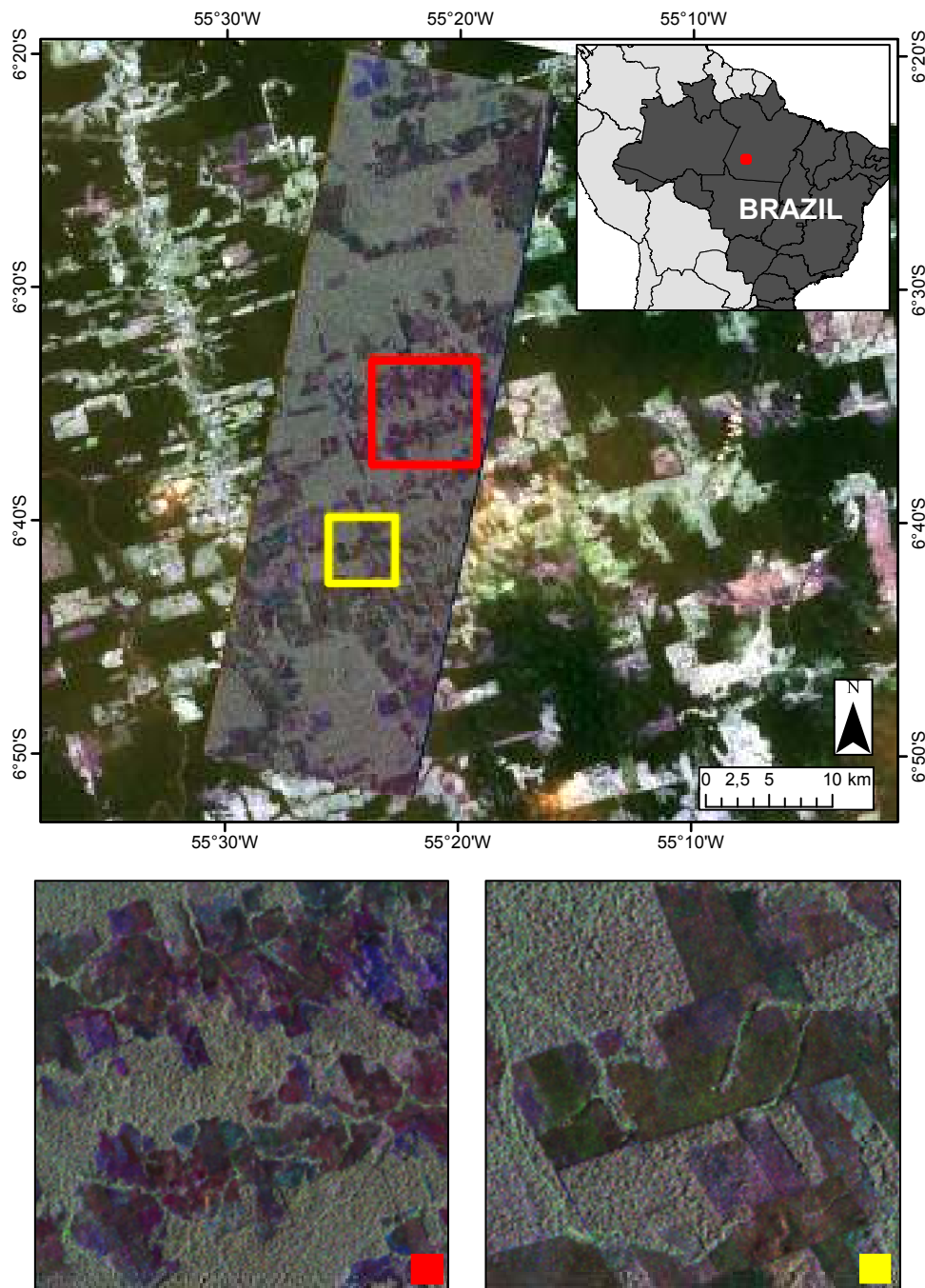


Fig. 2.1 Composite of three TerraSAR-X acquisitions (Red: VV June 8, Green: HH September 4, Blue: VV November 9 of 2014). True color ETM (L8, 12 September 2014) in the background shows the diverse LULC properties.



Fig. 2.2 Photograph illustrating the fluent transitions and interactions of different land cover types in the study region.

2.2.2 Remote Sensing Data

The data base for the study consists of five TS-X strip map scenes with $5m \times 5m$ spatial resolution (Table 2.1). All images are ordered in single-look complex format, comprising different VV-VH and HH-HV polarization at an incidence angle of 37.75° , and cover a swath of roughly $50km \times 15km$ (5663×11856 pixels). Data is calibrated and processed according to common procedures (see Section 2.2.2). Preprocessing in the context of this study includes all necessary steps before random sampling of training and test data is performed. After random sampling, training of IVM, and MRF regularization are taken out, land cover maps are generated and validated, and average measures are calculated.

Preprocessing of the TS-X scenes is conducted using the Sentinel 1-Toolbox and the Geospatial Data Abstraction Library (Team, 2015). All scenes were processed separately in the following order:

Multilooking: 3 range looks, 2 azimuth looks, yielding a ground resolution of $\sim 4.7m \times 4.7m$.

Terrain & Radiometric Correction: Range-Doppler terrain correction (SRTM 3Sec) and resampling to $5m \times 5m$ pixel spacing. The data is projected into UTM Zone 21S. γ^0 radiometric normalization is applied using an SRTM.

GLCM-Texture Texture measurements are widely used to increase the mapping accuracy of SAR data (Sarker et al., 2012; Dekker, 2003; Cutler et al., 2012b). Gray Level Co-occurrence Matrices (GLCM) are calculated with 11×11 moving window size into all symmetric directions with offset one. Probabilistic quantization is conducted into 64 levels. Ten texture parameters are separately derived for any available polarization and any available scene: contrast, dissimilarity, homogeneity, angular second moment (ASM), energy, maximum probability, entropy, GLCM mean, GLCM variance, and GLCM correlation. These will be included as additional features to improve the IVM classification. For more information on GLCM-based texture parameters see Haralick et al. (1973) and Sarker et al. (2012). In respect to findings by Sarker et al. (2013) and Nyongui et al. (2002), and our own experiments, we abstain from combining texture metrics with speckle filtering. Since we use 10 texture measures per layer, we have a total of 22 features per scene for the classification process.

2.2.3 Reference Data

Reference data includes multispectral RapidEye and Landsat data, in situ data, as well as land cover data from various Brazilian agencies (e.g. PRODES, TerraClass). PRODES (Programa de Cálculo do Desflorestamento da Amazônia) is an effort by the Brazilian space agency (INPE) to generate annual maps documenting deforestation of primary forests inside the Legal Amazon with a minimum mapping unit of $6.25ha$ (INPE, 2015). Targeting only the sites that PRODES considers deforested, TerraClass is an effort to determine LULC classes of the affected areas (Almeida et al., 2016). The overall coverage of all available TS-X swaths constitutes the study area (Figure 2.1), and is sufficiently covered by reference information. While forests as well as clean and shrubby pasture are present in the study area, occurrence of water and burnt pasture is overall scarce. To address this issue, polygons are manually distributed over the entire area. Afterwards, each polygon is assigned one class label for each date covered by TS-X to address changes of LULC. If necessary, polygons are split to avoid class ambiguity within different temporal instances. E.g., if a coherent pasture area is only partially burnt, the polygon gets split. The generation of reference data is supported by visual interpretation of RapidEye as well as Landsat 7 ETM+ and Landsat 8 OLI data of the same time period. In addition to Landsat and RapidEye imagery, fire products derived from MODIS are also considered. Moreover, photographs from a field campaign conducted

Table 2.2 Number of sample points available for training distinguished by class, extracted from polygons.







Class	Date				
	06-08	06-30	07-22	08-24	09-04
Burnt Pasture	15	55	139	469	434
Clean Pasture	487	444	375	384	420
Shrubby Pasture	749	783	789	438	428
Water	28	28	28	28	28
Forest	799	701	704	616	516

in August 2014 are available.

Sampling is conducted by two of the authors in close cooperation and was harmonized with classification schemes by INPE (Instituto Nacional de Pesquisas Espaciais). The following LULC classes are considered: clean pasture, shrubby pasture, burnt pasture, water, and forest. Clean pasture, also called *pasto limpo*, describes pasture land that is intensively worked. This includes regular tillage and burning of land to support cattle ranching. Shrubby pasture, also called *pasto sujo*, is not intensively managed and thus affected by bush encroachment. The coarser appearance of shrubby pasture generally allows a visual separation from clean pasture in high resolution images. Burnt pasture includes clean as well as shrubby pasture areas which were recently burned, and are characterized by open soil and vegetation residues. Such areas can be easily identified using false color composites. Forest, beside primary forests, includes areas of secondary vegetation and regeneration as these are usually non-separable by X-band SAR. Forests have a very characteristic appearance in TS-X images and high resolution multispectral imagery. Table 2.2 gives an overview of the number of available training samples for each class and date. It should be underlined that the burning season usually starts around end of July. Hence only few burned pasture areas could be identified before that period. Water bodies are also very scarce and only two lakes over the entire study area are included. Table 2.3 visualizes the classes considered in our classification scheme. The considered LULC classes match comparable studies using TS-X data in Brazilian, or tropical settings, respectively (Garcia et al., 2011; Schlund et al., 2013). As the time period of our study falls into the dry season between June and September, corresponding multispectral remote sensing data could be interpreted sufficiently well. Yet, some challenges remain:

- For the study region two dominating pasture types can be identified: *pasto sujo*, i.e., shrubby pasture, and *pasto limpo*, i.e., clean pasture (Almeida et al., 2008; Adami et al., 2015). While both types are generally used for cattle ranching in this

Table 2.3 Classification scheme.

Class	In-Situ	Multispectral (RE, LS)
Pasto Sujo		
Pasto Limpo		
Pasto Burnt		
Forest		
Water		

region, pasto sujo is characterized by bushes and occasional early stages of succession. However, the transition between these types can be gradual and consequently hard to interpret from remote sensing imagery alone; even at 5m ground resolution as offered by RapidEye.

- Transitions from pasto sujo into early stages of secondary vegetation are hard to distinguish, due to the gradual nature of this process. However, it is not as relevant in our study site since significantly less areas are affected. To allow a solid separation of these classes, we consider multi-annual time series to identify pasture management. In addition, we include information offered by TerraClass which reliably separate different types of secondary vegetation and pasture land.
- Primary and secondary forests, as well as secondary vegetation, are combined into one class, as various studies and own preliminary tests indicate the limitation of X-band for separating these two classes.

2.3 Methods

The proposed framework consists of four steps: (i) preprocessing, (ii) random sampling, (iii) classification of each single scene using IVM, and (iv) optimization of the MRF model. Final validation is performed on averages over 10 independent runs, using a random sampling (50:50) into spatially disjoint train and test polygons. As pixels sampled from training polygons are solely used for IVM parameterization (grid search) and model training, pixels sampled from test polygons enable an independent validation.

Throughout the paper we use the following notation: Let there be a training set $(x_n, y_n) \in \mathcal{T}$ comprising N feature vectors $\{x_1, \dots, x_n, \dots, x_N\}$ and corresponding class labels $y_n \in \{1, \dots, K\}$, distributed over an image lattice l . We later address image samples at any given coordinate as x_i , and probability estimates as $p_i = [p_1, \dots, p_{nk}, \dots, p_{nK}]$ with $p_{nk} = p(y_n = k | x_n)$.

2.3.1 Import Vector Machines

IVM is a discriminative and probabilistic classifier based on kernel logistic regression and has first been introduced by Zhu et al. (2005b). Roscher et al. (2012b) have shown that IVMs provide more reliable probabilities than probabilistic SVMs, since IVMs' probabilities are more balanced, whereas SVMs generally overestimate maximum probabilities. To account for complex decision boundaries between classes, IVM generally benefit from integrating a

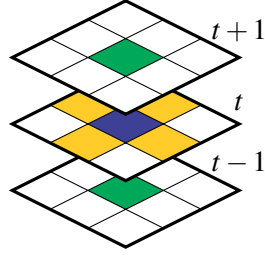


Fig. 2.3 Temporal (green) and spatial (yellow) neighbors of a given pixel (blue).

kernel function. For this study, we utilize the radial basis function (rbf) kernel parameterized by kernel width σ , which is a standard for remote sensing purposes. Parameterization is achieved analogously to standard SVM practices using a grid search, to estimate the cost parameter C and σ . For a more encompassing description of IVM see Zhu et al. (2005b) and Roscher et al. (2012a).

2.3.2 Markov Random Field

In this study, we use post classification MRF with spatio-temporal neighborhood relations between pixels, as illustrated in Figure 2.3. Parameterization is achieved through transition matrices, which are 5×5 matrices indicating spatial and temporal transition probabilities between the five classes. For our description of MRF, we adapt a terminology similar to Moser et al. (2013b) and Melgani et al. (2003). Therefore, with x_i denoting pixel features and y_i its corresponding class label, we reformulate the IVM-based probabilities $p(y_i | x_i)$ as energy terms

$$U_{\mathcal{X}} = - \sum_{i \in I} \ln p(y_i | x_i). \tag{2.1}$$

As the energy $U_{\mathcal{X}}$ are equivalent, minimization of $U_{\mathcal{X}}$ is identical to maximization of P . Now consider a function for the spatial neighborhood U_{sp} , with $i \sim_{sp} j$ applying to any two pixels, which are direct, 4-connected, spatial neighbors, and a function $\delta(y_i, y_j)$ to assign weights to neighboring classes:

$$U_{sp} = \sum_{i \sim_s j} 1 - \delta(y_i, y_j) \tag{2.2}$$

In this case the function δ yields a $K \times K$ matrix which can be used to favor certain neighboring constellations. The function δ is generally defined as Potts model to result in an identity matrix, which encourages the generation of homogeneous areas. The standard

mono-temporal MRF model is given by summation of (2.1) and (2.2)

$$U_{X,sp} = - \sum_{i \in I} \ln p(y_i | x_i) + \beta \sum_{i \sim_s j} 1 - \delta(y_i, y_j), \quad (2.3)$$

with weight parameter β to regulate importance of the spatial component. For the multi-temporal case we consider co-registered images with the temporal neighbors being the spatially congruent cells at the neighboring acquisition times $t - 1$ and $t + 1$. Only if pixel j is the temporal successor of i , $i \sim_{t+1} j$ applies; and only if pixel j is the temporal predecessor of i , $i \sim_{t-1} j$ applies. Temporal energy is hence given by (2.4), analogous to the spatial case.

$$U_{temp} = \sum_{i \sim_{t+1} j} 1 - \tau_1(y_i, y_j) + \sum_{i \sim_{t-1} j} 1 - \tau_2(y_i, y_j) \quad (2.4)$$

Here, τ_1 and τ_2 are $K \times K$ matrices defining the temporal transitions as observed from land cover trajectories. In opposition to the spatial weighting δ , we require multiple, non symmetrical matrices τ to respect trajectories with regard to the future, or the past. The overall energy function is defined by integrating the temporal vicinity into (2.3), which yields

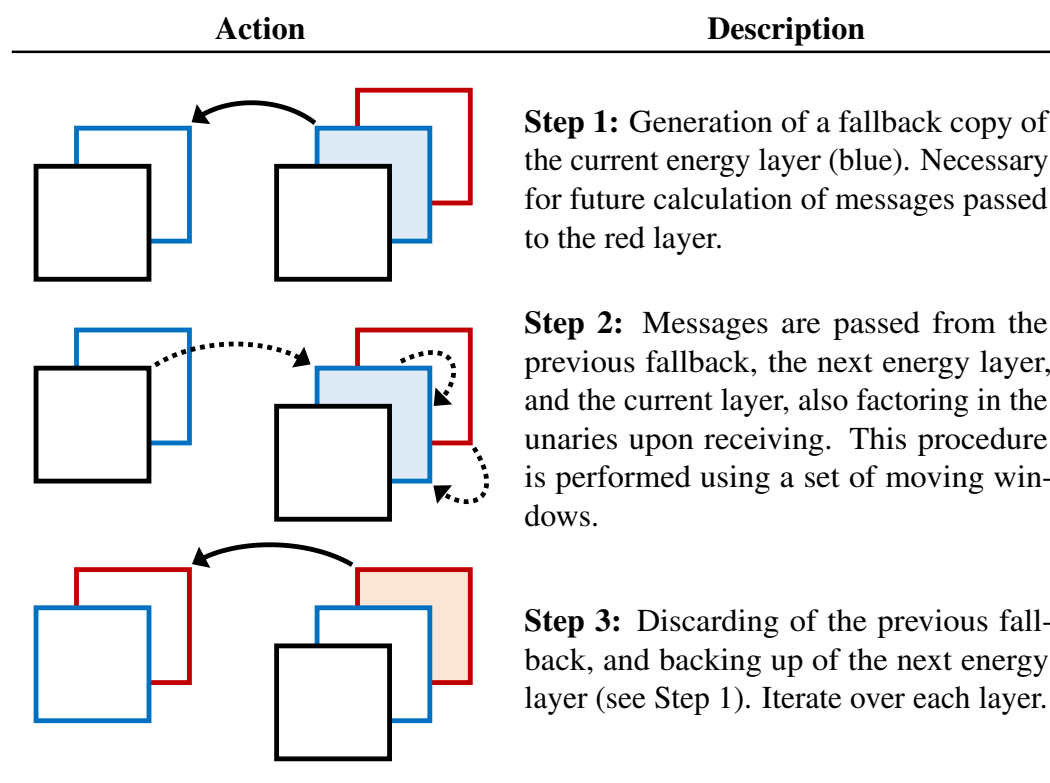
$$U = - \sum_{i \in I} \ln p(y_i | x_i) + \beta_{sp} \sum_{i \sim_s j} 1 - \delta(y_i, y_j) + \beta_{temp} \left(\sum_{i \sim_{t+1} j} 1 - \tau_1(y_i, y_j) + \sum_{i \sim_{t-1} j} 1 - \tau_2(y_i, y_j) \right). \quad (2.5)$$

This function combines (2.3) and (2.4). Weight parameters $\beta_{(\cdot)}$ can be used to adjust the importance of temporal and spatial weights.

2.3.3 Passing scheme & transition matrices

LBP is an inference algorithm utilizing Message Passing (Pearl, 1982), and is shown to approximate maximum values sufficiently well (Murphy et al., 1999). We choose LBP over graph-cut based methods for their more general applicability, as graph-cuts are specifically defined for symmetrical binary factors (Boykov et al., 2001), and can not be applied in non-symmetric environments (Kolmogorov et al., 2004). ICM (Iterated Conditional Modes) is another algorithm which is commonly used to achieve inference, especially in remote sensing and using multi-temporal data sets (Liu et al., 2008b; Liu et al., 2006; Wehmann et al., 2015). While it has low computational cost, it is generally outperformed by LBP in terms of accuracy (Szeliski et al., 2006; Andres et al., 2010). For this reason we formulate an implementation of LBP using moving windows, which can be applied to image stacks

Fig. 2.4 Passing schedule as applied in this study. One pass over all layers corresponds to one iteration of LBP.



of arbitrarily large image stacks sufficiently well. Figure 2.5 illustrates the neighborhood of one pixel in a factor graph, analogous to the MRF neighborhood as described in Section 2.3.2. Using the Potts function to define δ is common practice in remote sensing literature (Moser et al., 2013b), and since the focus of this study lies on the examination of MRF for a multi-temporal linking of classifications, we follow this practice. The Potts function can be represented by an identity matrix, which supports assignment of neighboring pixels to the same class. It is in general not sensible to formulate an asymmetric message passing for the two spatial dimensions, as a pixel will assume the same properties of its left as of its right neighbor. More specifically, the Potts model is a way to reflect Tobler’s assumption on spatial autocorrelation, promoting the idea of close objects to be more alike than distant objects. In contrast to the spatial transitions, utilization of the Potts model for temporal transitions can lead to serious distortions and cause equalization of all subjected probability maps, i.e., it would prohibit any land cover changes from occurring. While we can not assume any spatially directional patterns in the area, and thus rely on the Potts model, a pixel will pass different messages to its temporal successor opposed to its predecessor. Through adjustment of τ it is possible to assign probabilities for all possible types of class transitions. We therefore

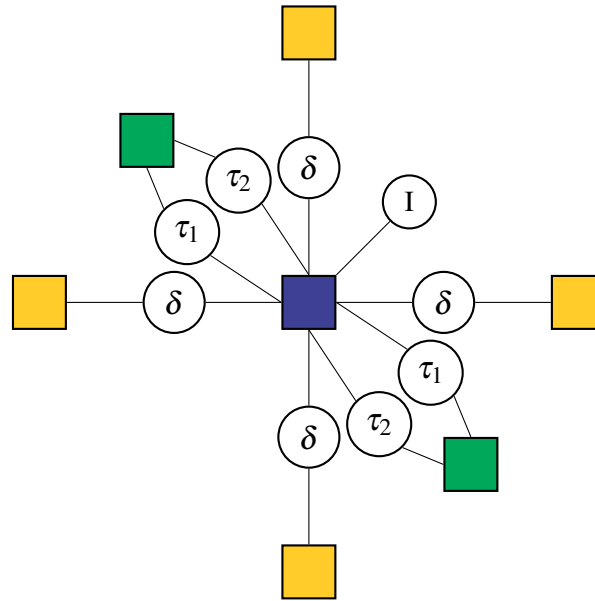


Fig. 2.5 Factor-graph as implemented in this study. Variable nodes illustrated by yellow (spatial neighbor) and green nodes (temporal). Circles mark the corresponding factor nodes and the unary IVM-based energy.

express temporal transitions through two asymmetric transition matrices (τ_1 and τ_2). While matrix τ_1 illustrates the messages pixels pass from the scene at time t to its neighbor at $t - 1$, τ_2 defines the messages the pixels pass from t to $t + 1$. This differentiation is important, e.g. considering that burnt pasture at t will prohibit primary forests at $t + 1$, yet it might endorse pasture at $t - 1$. We integrate the user-defined transition matrices τ_1 and τ_2 as interface to inject a-priori expert knowledge into our regularization model. While not empirically derived, these matrices are based on weak assumptions on land cover trajectories.

The assumptions include that Water and Forest are regarded very consistent classes, yet that pasture areas have some kind of interaction with each other. This especially concerns the transition of pasture land to burnt pasture land, which is explicitly tolerated. Furthermore, forest does not explicitly prohibit predecesing non-forest areas, which is due to forest including secondary vegetation and to offer the model some tolerance with regard to misclassifications. Hence, the formalization of land cover trajectories is relatively straight forward, and not necessarily based on elaborate a-priori knowledge. Previous tests showed a very similar outcome concerning the modification of these parameters, yet using very strict transitions could lead to undesired results and suppress dynamics entirely. In the scope of this study we utilize different transition matrices due to the varying time gap between the five TS-X acquisitions. The revisit rate of TS-X is eleven days, and the available imagery shows one gap of eleven days, two gaps of 22 days, as well as one gap of 33 days in between

neighboring acquisitions. We hence linearly modify the transitions to adjust to the varying temporal resolution, since with increasing time, more change is expected to occur.

The following summarizes the most relevant assumptions we made for specification of the transition matrices.

- Pasture areas can potentially be burnt. After burning, likelihood is high to transition back into clean pasture or shrubby pasture.
- Transitions from shrubby pasture to clean pasture are permitted.
- Clean pasture is considered stable, yet may transition into shrubby pasture or forest. Following observations of TerraClass, for the study region we assume a slow shift from clean pasture into shrubby pasture overall.
- Forest is the most consistent class. It can get removed, yet especially shrubby pasture can develop into forest as the class also includes secondary vegetation.
- Water is used to describe bodies of water which are permanently filled within this dry season.
- For any class there is a small tolerance to evade to counteract inconsistent transitions which may be caused by misclassifications.

2.3.4 Classification & Validation

Three different types of classification are compared: (i) the baseline IVM classification, (ii) the spatial-only MRF with $\beta_t = 0$, from now on referred to as s-MRF, and (iii) the spatial-temporal MRF, referred to as st-MRF. While many studies rely on supervised classification using SVM and Random Forest classifiers, various studies show that IVM perform at least equally well in terms of accuracy (Roscher et al., 2012b; Braun et al., 2012). Therefore the original IVM classification is considered as adequate baseline classification.

Reference polygons exclusively comprise either training or test samples to avoid spatial autocorrelation. For training purposes, 15 samples per polygon are randomly selected, using a minimum sampling distance of 30 meters. A systematic sampling ensures that an adequate number of training samples is selected for all five classes; clean pasture, shrubby pasture, burnt pasture, water, and forest. Validation is conducted considering the current terms of good practice as laid out by Olofsson et al. (2014). Samples are clustered in polygons to improve on the spatial variability of both, training and test samples, with pixels being the assessment unit. This sampling strategy is a necessary trade-off between

ideal conditions of independent random sampling and the difficulties of obtaining large scale, multi-temporal reference data in a challenging environment (Olofsson et al., 2014). Error matrices are derived to serve as a basis for the estimation of overall accuracies (OA), user accuracies (UA), producer accuracies (PA), and their corresponding confidence intervals (CI). In addition, we calculate area measures and their confidence intervals at each acquisition date to estimate the development of burnt pasture land over the entire 2014's dry season. Classification and validation is conducted ten times using different training and test sets and the results are averaged.

2.4 Results

We show that we can benefit from the high repetition rate and high ground resolution of TS-X, and that the proposed framework outperforms common classification approaches in terms of area adjusted mapping accuracy (Olofsson et al., 2014). Table 2.4 illustrates the average area adjusted OA for the five TS-X scenes, using the three different methods. Irrespective of the acquisition date, the accuracy was significantly improved by the MRF, with the s-MRF consistently outperforming the IVM only results, and st-MRF consistently outperforming s-MRF to a lesser degree. The weakest classification of IVM (60%) and s-MRF (69%) could be clearly improved by up to 19 and 10 percentage points compared to the classification results achieved with st-MRF (79%). On average, OA could be improved by 8.6 percentage points using s-MRF, and 12.2 percentage points using st-MRF when compared to the IVM classification. As recommended by Olofsson et al. (2014), we additionally calculated variance measures for results, yet with confidence intervals generally falling well below 1 percentage point, we will not further address these measurements.

Figure 2.6 summarizes the average UA's and PA's of the three approaches (IVM, s-MRF, st-MRF). IVM yields the lowest accuracies, while st-MRF generally shows the highest, and most balanced class-specific accuracies. All approaches are especially reliable concerning

Table 2.4 Area adjusted overall accuracies for different dates. The shown values are means over 10 iterations.

Acquisition Date	Polarization	IVM	s-MRF	st-MRF
2014-06-08	VV-VH	0.65	0.75	0.77
2014-06-30	HH-HV	0.60	0.69	0.79
2014-07-22	VV-VH	0.66	0.76	0.78
2014-08-24	VV-VH	0.69	0.74	0.76
2014-09-04	HH-HV	0.68	0.77	0.78

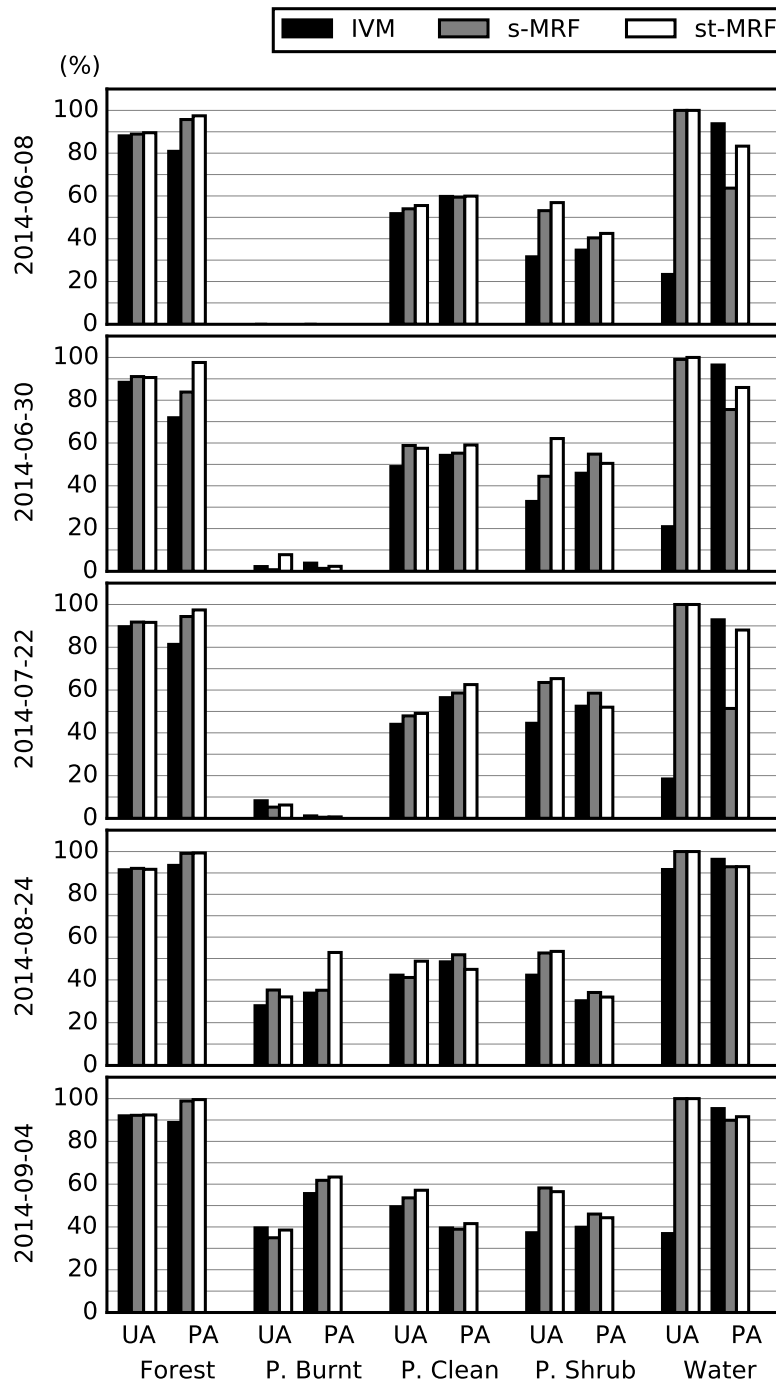
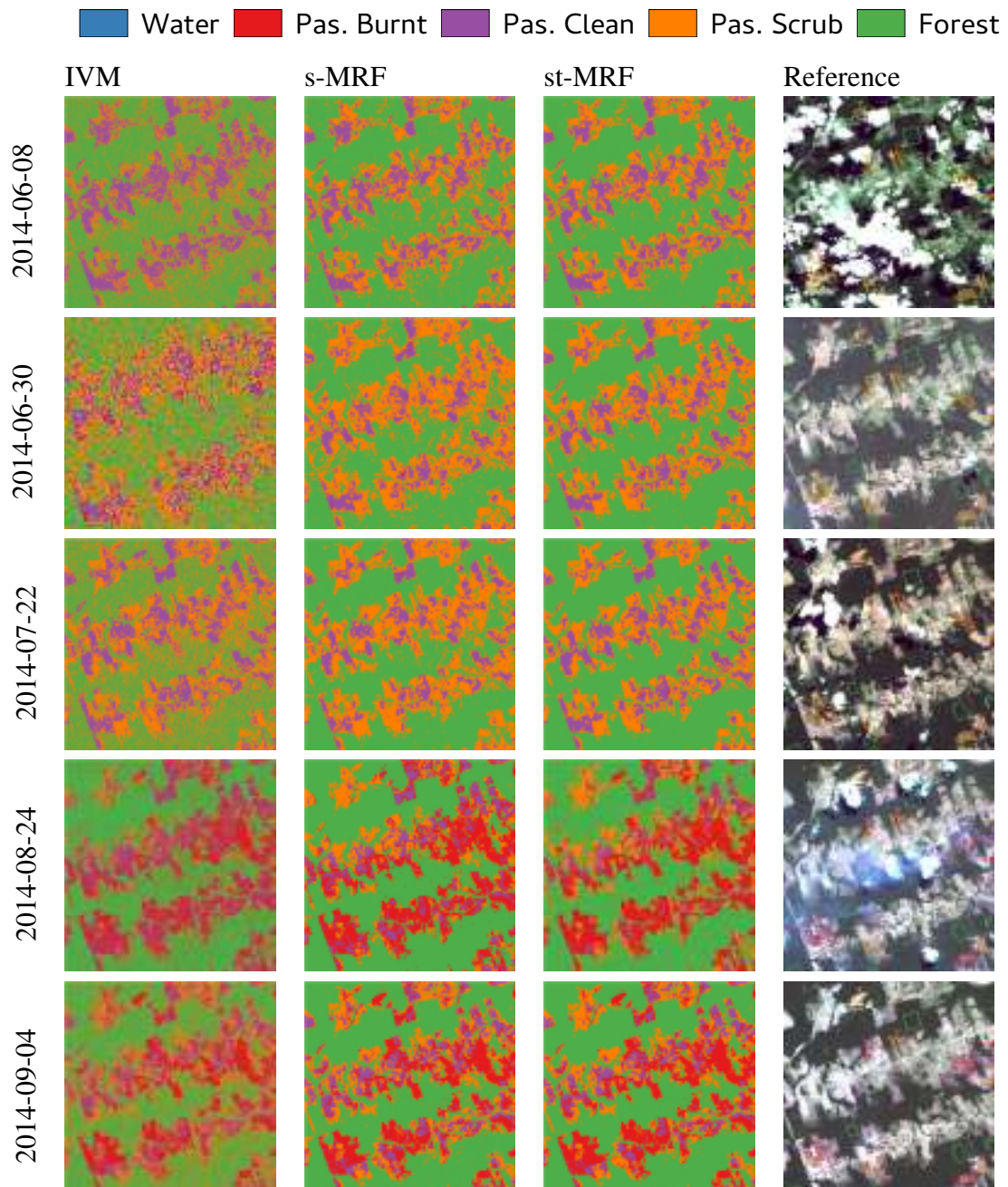


Fig. 2.6 User's and Producer's Accuracy for all the classes at each date.

Table 2.5 Comparison of different classifications inside the subsetting area of Figure 2.1.



the classification of forest areas, with st-MRF achieving especially high PA's for this class ($\geq 90\%$). For any given approach, the three pasture classes are classified with significantly lower accuracies than forest areas. Shrubby pasture and clean pasture are overall underrepresented, with PA's between 30% and 60% depending on the scene and method. Clean pasture generally yields accuracies of approximately 50%, but also classification of this class is particularly problematic concerning the PA of the last scene (around 40%). Weak classification results of the different pasture classes are generally caused by confusion within the different pasture types, and reflects findings of comparable studies which utilize X-band SAR data (Schlund et al., 2013). In general, st-MRF shows higher accuracies, when compared to the classification results achieved by the other approaches, and is capable of mapping burnt pasture starting from 2014-08-24. This is very notable, as a general concern regarding multi-temporal MRF's are its smoothing effects, which could cause the suppression of sporadic events. Due to the low number of burnt pasture areas before the end of July, we are not able to reliably calculate accuracies for burnt pasture areas at every date. Only up to two burnt fields exist for the first two acquisitions, which do not allow for an adequate classification and validation. However, this is also in accordance to the typical land management in the region, insofar slash-and-burn activities usually start later in the season. Nevertheless, the class is kept as st-MRF utilizes any class for the scenes and to have a consistent classification scheme over the entire period. Although some additional burnt pasture areas occur in July (ten areas over the entire study area), the classification accuracy remains very low. Despite consisting of few samples, possibly due to its temporal consistency and very distinct signature, water is mapped especially well. As water encompasses just very few areas over the entire study site, yet yields PAs of 85% and higher for the baseline approach. This weakness appears to get enhanced by the s-MRF approach, which yields a remarkable drop in the PA of water at some dates, while the spatio-temporal MRF appears to ensure its further designation. This behavior underlines capabilities of st-MRF to not only increase mapping accuracy of temporally sporadic classes, such as burnt pasture, but, remarkably, also proves the value of st-MRF regarding the mapping of classes which are static, yet spatially small scaled. Contrastingly, using mono-temporal MRF such classes tend to get suppressed more frequently. Regarding UA, water is mapped very convincingly with accuracies of over 95% using the MRF approaches, yet the IVM classification shows much less reliable accuracies.

The visual assessment of the classification maps underlines the positive effect of the MRF-based approaches (Table 2.5 and 2.8). A large number of speckle induced misclassification can be attributed to any of the maps classified using IVM with texture parameters. This effect is suppressed to some extent by s-MRF, yet individual clusters of misclassification can still

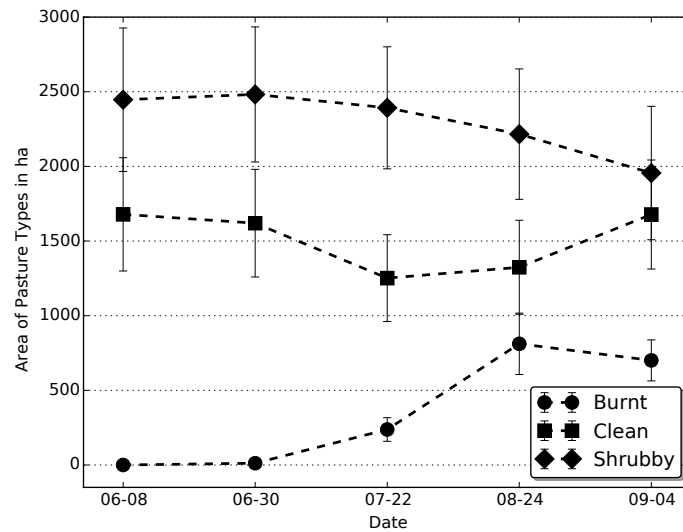


Fig. 2.7 Growth of burnt areas over the 2014 dry season. Error bars are indicative of the 95% confidence interval.

be located. While not entirely homogeneous, st-MRF suppresses the noise considerably, yet maintaining the general spatial patterns of LULC. Fine spatial structures appear to not get suppressed by the st-MRF, despite conservative IVM estimates.

Using land cover maps derived from st-MRF, Figure 2.7 illustrates that clear trends can still be derived using the proposed data and methods. The figure illustrates a high percentage of shrubby pasture land early in the dry season. Over the course of the dry season, this amount is continuously shrinking, while the burning of pasture starts growing exponentially at the end of July. At the end of the dry season, the area of clean pasture land is comparable to that of shrubby pasture.

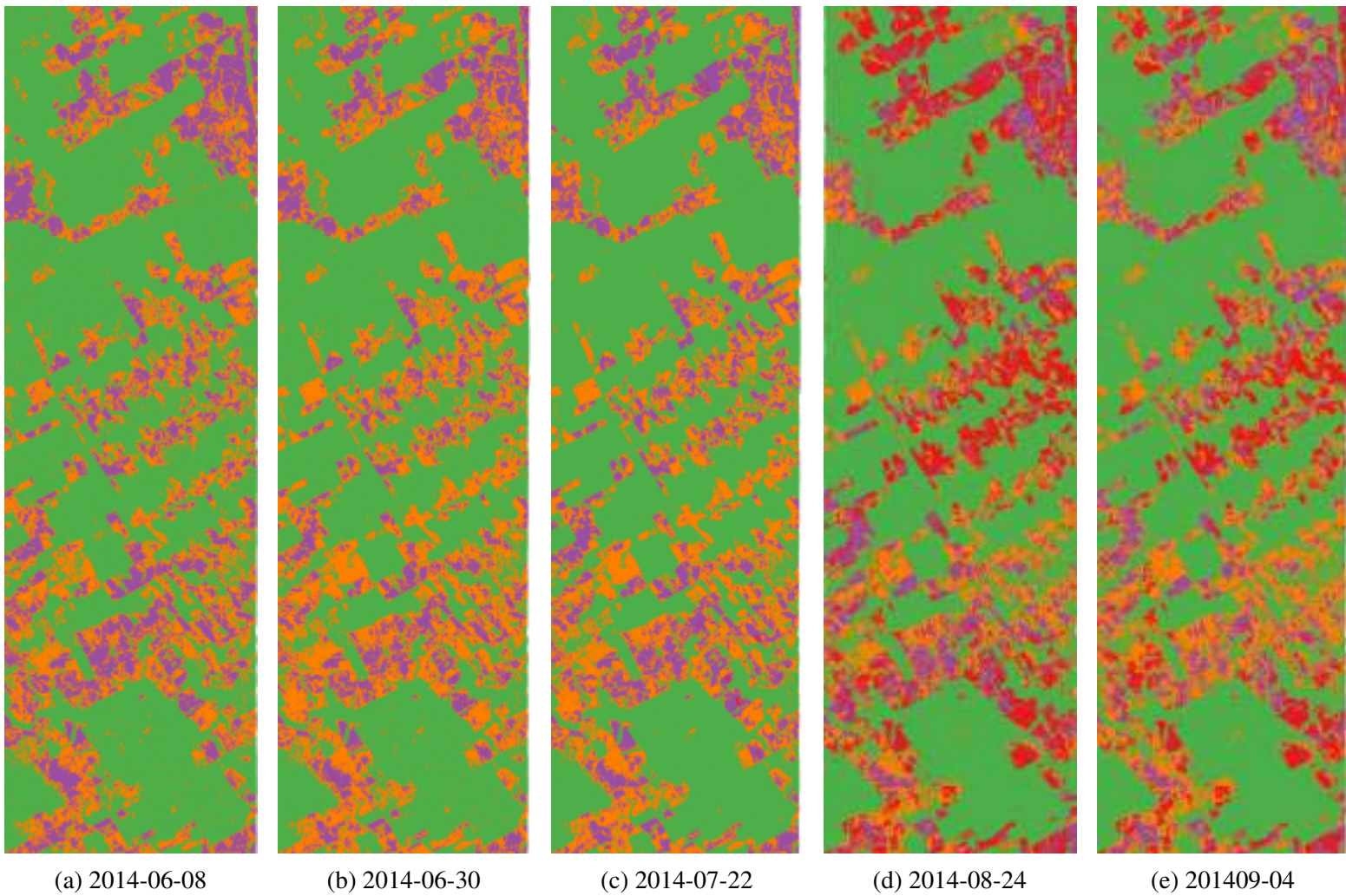


Fig. 2.8 Final classification results using the st-MRF approach.

2.5 Discussion

The main objective of this study, i.e., the adaptation of recent methods for the mapping of dynamic LULC in a tropical setting, is shown to be generally positive in our study. The proposed approach of using spatial-temporal MRF with expert knowledge is generally able to capture short term LULC dynamics, which are challenging to map using standard classification techniques. Although our validation confirms limitations of short-wavelength SAR data (e.g., when differentiating different pasture types, especially mono-temporally), the proposed approach enables the generation of a meaningful time series of homogeneous LULC maps using only SAR data. Consequently, the reliable prompt mapping of LULC change can be achieved independent of cloud cover and atmospheric inference.

The results show that the use of the proposed approach outperforms standard IVM classifications utilizing texture parameters only, as well as common spatial MRF, in terms of classification accuracy. Visual inspection of burnt pasture areas of early dates shows bright and overall heterogeneous backscatter within the class, and similarity to the other pasture classes at TS-X images, while Landsat and RapidEye images unambiguously indicate burnt pasture. Possible reasons for this could be organic debris or wet conditions. Contrary to that, many burnt areas of subsequent scenes, after the occurrence of large scale burning, can be identified more clearly at X-band as areas of low backscatter.

Regarding X-band data the potential transfer of the approach to the wet season, which is characterized by higher saturation of backscatter intensity, is another challenge. While separation of pasture types already appears difficult in the dry season, the integration of temporal context via the MRF might allow for a reliable separation of pasture and forest areas over the wet season. Additional testing showed furthermore that utilization of temporal trajectories alone, despite generally not as effective as utilization of the spatial context (s-MRF), can be used to significantly elevate all accuracies above 70%. In particular the weak classification of 2014-06-30 could benefit from this approach as the variance of classification outcomes is reduced between different scenes.

Our findings are in accordance with the results of other recent studies, which were able to improve the classification accuracy via implementation of multi-temporal MRF (Wehmann et al., 2015; Liu et al., 2008b). While Wehmann et al. (2015) use regionally optimized transition matrices, and a state of the art integrated kernel based on Moser et al. (2013a) to achieve high classification accuracies over long time periods, the proposed method aims on the detection of short term land cover change in SAR imagery, and utilizes LBP for inference as well as IVM for classification. The visual assessment of the classification results confirms the positive effect of the MRF on the classification accuracy. Although the maps provided by the conventional IVM classification show general land use patterns, the results are affected

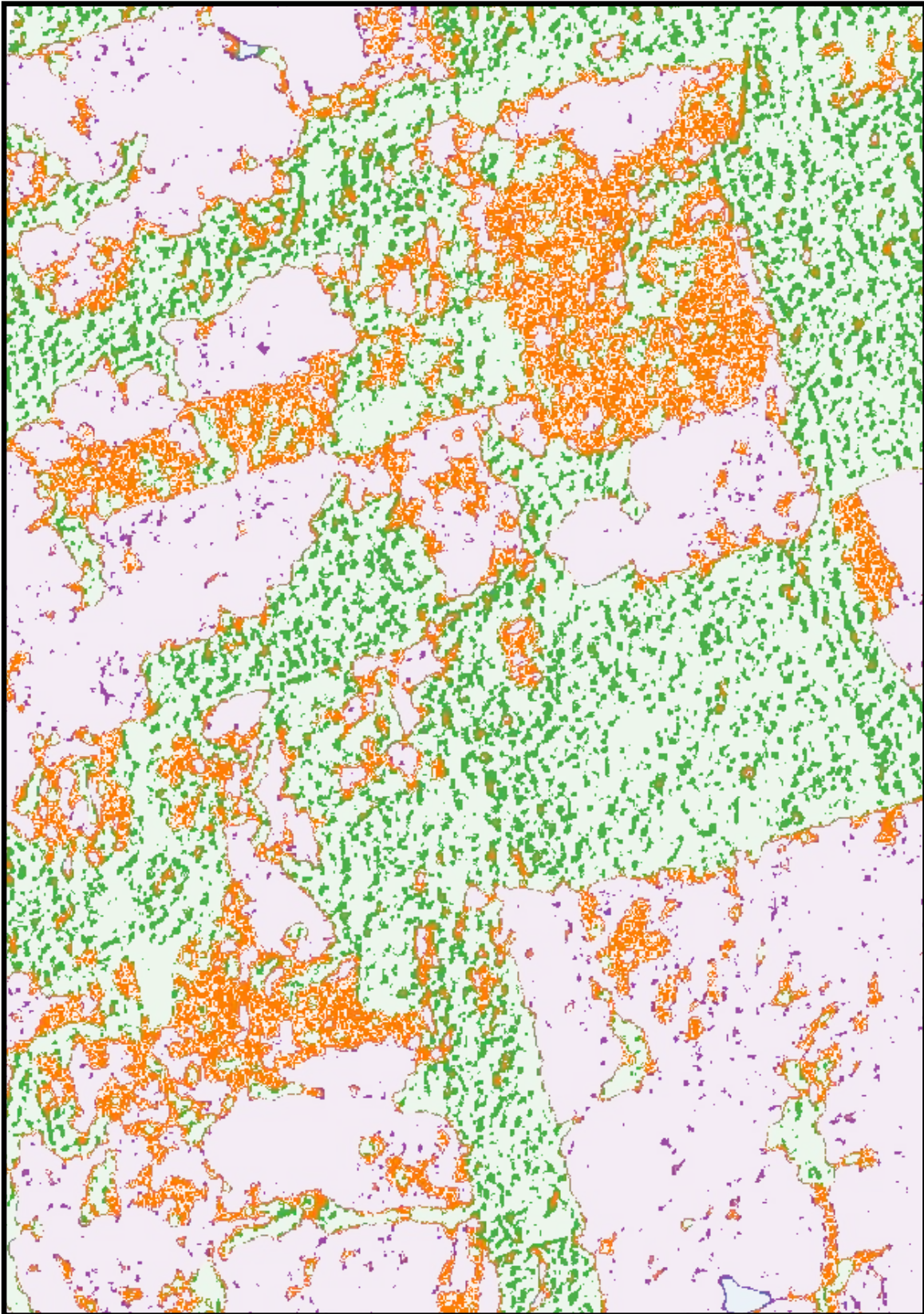


Fig. 2.9 Difference map between 2014-06-30 classifications of st-MRF and IVM. Light colors indicate agreement between the two maps. Dark colors indicate class ambiguities, while the class of the final st-MRF classification is presented.

by typical SAR-inherent noise. Even homogeneous areas appear very noisy, despite texture parameters that were included in the classification procedure. Boundaries between individual land cover and land use classes may appear blurred and are hard to identify. This drawback is significantly reduced by both MRF-based methods. As LBP tries to minimize the transition energy by homogenizing adjacent pixels, areas become overall more concentrated and edges along different LULC classes can be more clearly identified. Benefits can also be attributed to the classification of the interior of areas, as the application of MRF suppresses outliers. Thus, the results confirm the edge preserving capabilities of MRF, even for challenging spatial class transitions (e.g. forest to shrubby pasture).

With regard to class-specific accuracies, the spatio-temporal MRF offers preferable results over just IVM and the spatial-only approach. Figure 2.9 illustrates the differences between a 2014-06-30 classification of the IVM and the st-MRF approaches, underlining the potentials of solving confusion between forest and shrubby pasture. It is colorized to highlight disagreements of the classifications, with pale colors signifying consenting classifications, and opaque colors indicating classes as assigned by st-MRF (for legend see Table 2.5). It is especially obvious that with increasing vegetation density confusion also rises, and that clean pasture is classified congruently in both approaches. While the classification of clean pasture and shrubby pasture remains challenging, TS-X data constitutes an adequate data source for forest / non-forest mapping. The PA and UA for forest are higher compared to the accuracies achieved for the other classes, and are in accordance with the accuracies of comparable studies (Schlund et al., 2013; Garcia et al., 2011). While we did not perform specific analysis on the differences of HH-HV and VV-VH polarized data sets, Table 2.4 shows the OA of the internal HH-HV polarized scenes (06-30) to especially benefit from the multi-temporal integration, and also its neighboring scenes to benefit disproportionately. We can thus assume synergetic effects to be transferable through a multi-temporal MRF, yielding a promising outlook for the multi-sensoral integration of various data sources.

Regarding the low requirements concerning parameterization and the implementation through moving windows, we consider the introduced method to be transferable to other study regions. Adaptation of the transition matrices allows the method to be fitted to more static environments, or also to address multi-annual time series data. Despite the ambitious goals of this study, i.e. to perform land cover mapping in a densely vegetated and dynamic tropical study region using TS-X data, and some documented limitations concerning the separability of different pasture types, we were able to achieve improvements over standard classifications. As the method incorporates adjacency information, potential shortcomings exist when the ground resolution is coarse relative to the mapped land cover. In this case, fragmented structures might get suppressed. Further adjustment would also be required if assumptions on

land cover trajectories are variant in a multi-temporal setup. For example, two scenes from the dry season carry a different transition probability with regard to burning than two scenes from the wet season. While this can be easily solved through different transition models, within this study we just included slight modifications of transition matrices to account for the different intervals between TS-X acquisitions.

2.6 Conclusion

The results show clearly that the integration of spatial-temporal MRFs are advantageous to the baseline classification approach and spatial MRF methods. Especially the classification of forest areas yields very high accuracies. We were able to successfully implement an LBP optimization for the regularization of high resolution, multi-temporal TS-X images of a tropical context. We were furthermore able to give adequate estimates on the spatio-temporal pattern of land use dynamics such as burned pastures. Importantly, the suggested approach is able to handle process of small spatio-temporal scale, and despite its smoothing effects does not suppress fine structures. Separation of different types of pasture (pasto sujo and pasto limpo) remains a challenging task at the short wavelength. Classification of burnt pasture early in the season highlights limitations of the MRF-based model, which arise when the underlying classification accuracy is already limited. While the approach is well suited to regularize small classification errors using contextual information, it is not able to sufficiently address misclassifications in complex, transitional environments with weak classification accuracies. The sometimes relatively low class accuracies are not necessarily a limitation of the proposed method, but rather caused by the short-wave TS-X data as well as class-specific characteristics.

Particularly for study sites which are characterized by land use patterns of high spatial-temporal variability, the proposed approach (i.e., using spatial-temporal MRF with expert knowledge) appears feasible. Using expert knowledge on land cover trajectories, we could positively influence model performance and bypass computationally demanding techniques for the estimation of MRF parameters.

When derived from multiple classifications, change maps are generally strongly affected by weak initial classifications.

The proposed method is formalized to be transferable to large, possibly multi-sensoral, image stacks. For future studies our aim is to integrate the regularization of short-term, intra-annual dynamics with long-term dynamics such as deforestation and agricultural trends, using multi-sensoral imagery.

References

- Adami, M., A. R. Gomes, A. C. Coutinho, J. C.D. M. Esquerdo, and A. Venturieri (2015). “Dinâmica do uso e cobertura da terra no estado do Pará entre os anos de 2008 a 2012”. In: *XVII Simpósio Brasileiro de Sensoriamento Remoto*.
- Ahmed, S. E., C. M. Souza, J. Riberio, and R. M. Ewers (2013). “Temporal patterns of road network development in the Brazilian Amazon”. In: *Reg Environ Change* 13.5, pp. 927–937.
- Almeida, A. S. d. and I. C. G. Vieira (2008). “Dinâmica da cobertura vegetal e uso da terra no município de São Francisco do Pará (Pará, Brasil) com o uso da técnica de sensoriamento remoto”. In: *Boletim do Museu Paraense Emílio Goeldi Ciências Naturais* 3.1, pp. 81–92.
- Almeida, C. A. d., A. C. Coutinho, J. C.D. M. Esquerdo, M. Adami, A. Venturieri, C. G. Diniz, N. Dessay, L. Durieux, and A. R. Gomes (2016). “High spatial resolution land use and land cover mapping of the Brazilian Legal Amazon in 2008 using Landsat-5/TM and MODIS data”. In: *Acta Amaz.* 46.3, pp. 291–302.
- Almeida-Filho, R., Y. E. Shimabukuro, A. Rosenqvist, and G. A. Sanchez (2009). “Using dual-polarized ALOS PALSAR data for detecting new fronts of deforestation in the Brazilian Amazônia”. In: *International Journal of Remote Sensing* 30.14, pp. 3735–3743.
- Andres, B., J. H. Kappes, U. Köthe, C. Schnörr, and F. A. Hamprecht (2010). “An Empirical Comparison of Inference Algorithms for Graphical Models with Higher Order Factors Using OpenGM”. In: *Pattern Recognition*, pp. 353–362.
- Aschbacher, J. and M. P. Milagro-Pérez (2012). “The European Earth monitoring (GMES) programme: Status and perspectives”. In: *Remote Sensing of Environment* 120, pp. 3–8.
- Blaes, X., L. Vanhalle, and P. Defourny (2005). “Efficiency of crop identification based on optical and SAR image time series”. In: *Remote sensing of environment* 96.3, pp. 352–365.
- Bouman, C. A. and M. Shapiro (1994). “A multiscale random field model for Bayesian image segmentation”. In: *Image Processing, IEEE Transactions on* 3.2, pp. 162–177.
- Bovolo, F. and L. Bruzzone (2005). “A detail-preserving scale-driven approach to change detection in multitemporal SAR images”. In: *IEEE Transactions on Geoscience and Remote Sensing* 43.12, pp. 2963–2972.
- Boykov, Y., O. Veksler, and R. Zabih (2001). “Fast approximate energy minimization via graph cuts”. In: *Pattern Analysis and Machine Intelligence, IEEE Transactions on* 23.11, pp. 1222–1239.
- Braun, A. C., U. Weidner, and S. Hinz (2012). “Classification in High-Dimensional Feature Spaces —Assessment Using SVM, IVM and RVM With Focus on Simulated EnMAP

- Data”. In: *IEEE Journal of Selected Topics in Applied Earth Observations and Remote Sensing* 5.2, pp. 436–443.
- Cai, S., D. Liu, D. Sulla-Menashe, and M. A. Friedl (2014). “Enhancing MODIS land cover product with a spatial-temporal modeling algorithm”. In: *Remote Sensing of Environment* 147, pp. 243–255.
- Coy, M. and M. Klingler (2014). “Frentes pioneiras em transformação: o eixo da BR-163 e os desafios socioambientais”. In: *Territórios e Fronteiras* 7.1, pp. 1–26.
- Cutler, M., D. Boyd, G. Foody, and A. Vetrivel (2012a). “Estimating tropical forest biomass with a combination of SAR image texture and Landsat TM data: An assessment of predictions between regions”. In: *ISPRS Journal of Photogrammetry and Remote Sensing* 70, pp. 66–77.
- Cutler, M., D. Boyd, G. Foody, and A. Vetrivel (2012b). “Estimating tropical forest biomass with a combination of SAR image texture and Landsat TM data: An assessment of predictions between regions”. In: *ISPRS Journal of Photogrammetry and Remote Sensing* 70, pp. 66–77.
- Davidson, E. A., A. C. de Araújo, P. Artaxo, J. K. Balch, I. F. Brown, M. M. Bustamante, M. T. Coe, R. S. DeFries, M. Keller, M. Longo, et al. (2012). “The Amazon basin in transition”. In: *Nature* 481.7381, pp. 321–328.
- Dekker, R. J. (2003). “Texture analysis and classification of ERS SAR images for map updating of urban areas in the Netherlands”. In: *Geoscience and Remote Sensing, IEEE Transactions on* 41.9, pp. 1950–1958.
- Englhart, S., V. Keuck, and F. Siegert (2011). “Aboveground biomass retrieval in tropical forests – The potential of combined X- and L-band SAR data use”. In: *Remote Sensing of Environment* 115.5, pp. 1260–1271.
- Foley, J. A. (2005). “Global Consequences of Land Use”. In: *Science* 309.5734, pp. 570–574.
- Garcia, C. E., J. R. dos SANTOS, J. C. Mura, and H. J. H. Kux (2011). “Análise do potencial de imagem TerraSAR-X para mapeamento temático no sudoeste da Amazônia brasileira”. In: *Acta Amazonica* 42.2.
- Hansen, M. C., P. V. Potapov, R. Moore, M. Hancher, S. A. Turubanova, A. Tyukavina, D. Thau, S. V. Stehman, S. J. Goetz, T. R. Loveland, A. Kommareddy, A. Egorov, L. Chini, C. O. Justice, and J. R. G. Townshend (2013). “High-Resolution Global Maps of 21st-Century Forest Cover Change”. In: *Science* 342.6160, pp. 850–853. eprint: <http://science.sciencemag.org/content/342/6160/850.full.pdf>.
- Haralick, R. M., K. Shanmugam, and I. H. Dinstein (1973). “Textural features for image classification”. In: *Systems, Man and Cybernetics, IEEE Transactions on* 6, pp. 610–621.

- Hoberg, T., F. Rottensteiner, R. Queiroz Feitosa, and C. Heipke (2015). “Conditional random fields for multitemporal and multiscale classification of optical satellite imagery”. In: *Geoscience and Remote Sensing, IEEE Transactions on* 53.2, pp. 659–673.
- INPE (2015). *Projeto PRODES - Monitoramento da Floresta Amazonica Brasileira por Satelite*.
- Khatami, R., G. Mountrakis, and S. V. Stehman (2016). “A meta-analysis of remote sensing research on supervised pixel-based land-cover image classification processes: General guidelines for practitioners and future research”. In: *Remote Sensing of Environment* 177, pp. 89–100.
- Kolmogorov, V. and R. Zabini (2004). “What energy functions can be minimized via graph cuts?” In: *Pattern Analysis and Machine Intelligence, IEEE Transactions on* 26.2, pp. 147–159.
- Kumar, S. and Hebert (2003). “Discriminative random fields: a discriminative framework for contextual interaction in classification”. In: *Proceedings Ninth IEEE International Conference on Computer Vision*.
- Kumar, T. and C Patnaik (2013). “Discrimination of mangrove forests and characterization of adjoining land cover classes using temporal C-band Synthetic Aperture Radar data: A case study of Sundarbans”. In: *International Journal of Applied Earth Observation and Geoinformation* 23, pp. 119–131.
- Lapola, D. M., L. A. Martinelli, C. A. Peres, J. P. Ometto, M. E. Ferreira, C. A. Nobre, A. P. D. Aguiar, M. M. Bustamante, M. F. Cardoso, M. H. Costa, et al. (2014). “Pervasive transition of the Brazilian land-use system”. In: *Nature climate change* 4.1, pp. 27–35.
- Li, G., D. Lu, E. Moran, L. Dutra, and M. Batistella (2012). “A comparative analysis of ALOS PALSAR L-band and RADARSAT-2 C-band data for land-cover classification in a tropical moist region”. In: *ISPRS Journal of Photogrammetry and Remote Sensing* 70, 26–38.
- Liu, D., M. Kelly, and P. Gong (2006). “A spatial–temporal approach to monitoring forest disease spread using multi-temporal high spatial resolution imagery”. In: *Remote sensing of environment* 101.2, pp. 167–180.
- Liu, D., K. Song, J. R. Townshend, and P. Gong (2008a). “Using local transition probability models in Markov random fields for forest change detection”. In: *Remote Sensing of Environment* 112.5, pp. 2222–2231.
- (2008b). “Using local transition probability models in Markov random fields for forest change detection”. In: *Remote Sensing of Environment* 112.5, pp. 2222–2231.
- McNairn, H., C. Champagne, J. Shang, D. Holmstrom, and G. Reichert (2009). “Integration of optical and Synthetic Aperture Radar (SAR) imagery for delivering operational annual

- crop inventories”. In: *ISPRS Journal of Photogrammetry and Remote Sensing* 64.5, 434–449.
- Melgani, F. and S. B. Serpico (2003). “A Markov random field approach to spatio-temporal contextual image classification”. In: *Geoscience and Remote Sensing, IEEE Transactions on* 41.11, pp. 2478–2487.
- Moser, G. and S. B. Serpico (2013a). “Combining support vector machines and Markov random fields in an integrated framework for contextual image classification”. In: *Geoscience and Remote Sensing, IEEE Transactions on* 51.5, pp. 2734–2752.
- (2010). “Contextual remote-sensing image classification by support vector machines and Markov random fields”. In: *Geoscience and Remote Sensing Symposium (IGARSS), 2010 IEEE International*. IEEE, pp. 3728–3731.
- Moser, G., S. B. Serpico, and J. A. Benediktsson (2013b). “Land-Cover Mapping by Markov Modeling of Spatial–Contextual Information in Very-High-Resolution Remote Sensing Images”. In:
- Müller, H., P. Rufin, P. Griffiths, A. J. Barros Siqueira, and P. Hostert (2015). “Mining dense Landsat time series for separating cropland and pasture in a heterogeneous Brazilian savanna landscape”. In: *Remote Sensing of Environment* 156, pp. 490–499.
- Murphy, K. P., Y. Weiss, and M. I. Jordan (1999). “Loopy belief propagation for approximate inference: An empirical study”. In: *Proceedings of the Fifteenth conference on Uncertainty in artificial intelligence*. Morgan Kaufmann Publishers Inc., pp. 467–475.
- Nyoungui, A. N., E. Tonye, and A. Akono (2002). “Evaluation of speckle filtering and texture analysis methods for land cover classification from SAR images”. In: *International Journal of Remote Sensing* 23.9, pp. 1895–1925.
- Olding, W. C., J. C. Olivier, and B. P. Salmon (2015). “A Markov Random Field model for decision level fusion of multi-source image segments”. In: *2015 IEEE International Geoscience and Remote Sensing Symposium (IGARSS)*.
- Olofsson, P., G. M. Foody, M. Herold, S. V. Stehman, C. E. Woodcock, and M. A. Wulder (2014). “Good practices for estimating area and assessing accuracy of land change”. In: *Remote Sensing of Environment* 148, pp. 42–57.
- Pearl, J. (1982). “Reverend Bayes on inference engines: A distributed hierarchical approach”. In: *AAAI*, pp. 133–136.
- Pfeifer, M., L. Kor, R. Nilus, E. Turner, J. Cusack, I. Lysenko, M. Khoo, V. Chey, A. Chung, and R. Ewers (2016). “Mapping the structure of Borneo’s tropical forests across a degradation gradient”. In: *Remote Sensing of Environment* 176, pp. 84–97.
- Platt, J. C. (1999). “Probabilistic outputs for support vector machines and comparisons to regularized likelihood methods”. In: *Advances in large margin classifiers*. Citeseer.

- Qi, Z., A. G.-O. Yeh, X. Li, and Z. Lin (2012). “A novel algorithm for land use and land cover classification using RADARSAT-2 polarimetric SAR data”. In: *Remote Sensing of Environment* 118, pp. 21–39.
- Qi, Z., A. G.-O. Yeh, X. Li, S. Xian, and X. Zhang (2015). “Monthly short-term detection of land development using RADARSAT-2 polarimetric SAR imagery”. In: *Remote Sensing of Environment* 164, pp. 179–196.
- Reiche, J., C. M. Souza, D. H. Hoekman, J. Verbesselt, H. Persaud, and M. Herold (2013). “Feature Level Fusion of Multi-Temporal ALOS PALSAR and Landsat Data for Mapping and Monitoring of Tropical Deforestation and Forest Degradation”. In: *IEEE J. Sel. Top. Appl. Earth Observations Remote Sensing* 6.5, pp. 2159–2173.
- Reiche, J., J. Verbesselt, D. Hoekman, and M. Herold (2015a). “Fusing Landsat and SAR time series to detect deforestation in the tropics”. In: *Remote Sensing of Environment* 156, pp. 276–293.
- Roscher, R., W. Förstner, and B. Waske (2012a). “I²VM: Incremental import vector machines”. In: *Image and Vision Computing* 30.4, pp. 263–278.
- Roscher, R., B. Waske, and W. Förstner (2012b). “Incremental import vector machines for classifying hyperspectral data”. In: *Geoscience and Remote Sensing, IEEE Transactions on* 50.9, pp. 3463–3473.
- Rufin, P., H. Müller, D. Pflugmacher, and P. Hostert (2015). “Land use intensity trajectories on Amazonian pastures derived from Landsat time series”. In: *International Journal of Applied Earth Observation and Geoinformation* 41, pp. 1–10.
- Sarker, M. L. R., J. Nichol, H. B. Iz, B. Ahmad, and A. A. Rahman (2013). “Forest Biomass Estimation Using Texture Measurements of High-Resolution Dual-Polarization C-Band SAR Data”. In:
- Sarker, M. L. R., J. Nichol, B. Ahmad, I. Busu, and A. A. Rahman (2012). “Potential of texture measurements of two-date dual polarization PALSAR data for the improvement of forest biomass estimation”. In: *ISPRS Journal of Photogrammetry and Remote Sensing* 69, pp. 146–166.
- Schlund, M., F. von Poncet, D. H. Hoekman, S. Kuntz, and C. Schmullius (2013). “Importance of bistatic SAR features from TanDEM-X for forest mapping and monitoring”. In: *Remote Sensing of Environment*.
- Solberg, A. H. S., T. Taxt, and A. K. Jain (1996). “A Markov random field model for classification of multisource satellite imagery”. In: *Geoscience and Remote Sensing, IEEE Transactions on* 34.1, pp. 100–113.

- Sonobe, R., H. Tani, X. Wang, N. Kobayashi, and H. Shimamura (2014). “Random forest classification of crop type using multi-temporal TerraSAR-X dual-polarimetric data”. In: *Remote Sensing Letters* 5.2, pp. 157–164.
- Stefanski, J., O. Chaskovskyy, and B. Waske (2014). “Mapping and monitoring of land use changes in post-Soviet western Ukraine using remote sensing data”. In: *Applied Geography* 55, pp. 155–164.
- Szeliski, R., R. Zabih, D. Scharstein, O. Veksler, V. Kolmogorov, A. Agarwala, M. Tappen, and C. Rother (2006). “A Comparative Study of Energy Minimization Methods for Markov Random Fields”. In: *Lecture Notes in Computer Science*, pp. 16–29.
- Tarabalka, Y., M. Fauvel, J. Chanussot, and J. A. Benediktsson (2010). “SVM-and MRF-based method for accurate classification of hyperspectral images”. In: *Geoscience and Remote Sensing Letters, IEEE* 7.4, pp. 736–740.
- Team, G. D. (2015). *GDAL - Geospatial Data Abstraction Library, Version 2.0.1*. Open Source Geospatial Foundation.
- Tran, T. N., R. Wehrens, D. H. Hoekman, and L. M. Buydens (2005). “Initialization of Markov random field clustering of large remote sensing images”. In: *Geoscience and Remote Sensing, IEEE Transactions on* 43.8, pp. 1912–1919.
- Uhlmann, S. and S. Kiranyaz (2014). “Classification of dual- and single polarized SAR images by incorporating visual features”. In: *ISPRS Journal of Photogrammetry and Remote Sensing* 90, pp. 10–22.
- Vitousek, P. M. (1997). “Human Domination of Earths Ecosystems”. In: *Science* 277.5325, pp. 494–499.
- Voisin, A., V. A. Krylov, G. Moser, S. B. Serpico, and J. Zerubia (2013). “classification of very high resolution SAR images of urban areas using copulas and texture in a hierarchical Markov random field model”. In: *Geoscience and Remote Sensing Letters, IEEE* 10.1, pp. 96–100.
- Waske, B. and M. Braun (2009b). “Classifier ensembles for land cover mapping using multitemporal SAR imagery”. In: *ISPRS Journal of Photogrammetry and Remote Sensing* 64.5, pp. 450–457.
- Waske, B. and S. van der Linden (2008). “Classifying multilevel imagery from SAR and optical sensors by decision fusion”. In: *Geoscience and Remote Sensing, IEEE Transactions on* 46.5, pp. 1457–1466.
- Waske, B. and J. A. Benediktsson (2007). “Fusion of support vector machines for classification of multisensor data”. In: *Geoscience and Remote Sensing, IEEE Transactions on* 45.12, pp. 3858–3866.

- Wehmann, A. and D. Liu (2015). “A spatial–temporal contextual Markovian kernel method for multi-temporal land cover mapping”. In: *ISPRS Journal of Photogrammetry and Remote Sensing*.
- Wulder, M. A., J. G. Masek, W. B. Cohen, T. R. Loveland, and C. E. Woodcock (2012a). “Opening the archive: How free data has enabled the science and monitoring promise of Landsat”. In: *Remote Sensing of Environment* 122. Landsat Legacy Special Issue, pp. 2–10.
- Xie, H., L. E. Pierce, and F. T. Ulaby (2002). “SAR speckle reduction using wavelet denoising and Markov random field modeling”. In: *Geoscience and Remote Sensing, IEEE Transactions on* 40.10, pp. 2196–2212.
- Zhu, J. and T. Hastie (2005b). “Kernel logistic regression and the import vector machine”. In: *Journal of Computational and Graphical Statistics* 14.1, pp. 185–205.
- Zhu, Z. and C. E. Woodcock (2014). “Continuous change detection and classification of land cover using all available Landsat data”. In: *Remote sensing of Environment* 144, pp. 152–171.

Chapter 3

Evaluation of Multi-Frequency SAR Images for Tropical Land Cover Mapping

Remote Sensing, MDPI AG, 2018, 10, 257

<https://doi.org/10.3390/rs10020257>

Ron Hagensieker and Björn Waske

Abstract

Earth Observation (EO) data plays a major role in supporting surveying compliance of several multilateral environmental treaties, such as UN-REDD+ (United Nations Reducing Emissions from Deforestation and Degradation). In this context land cover maps of remote sensing data are the most commonly used EO products and development of adequate classification strategies is an ongoing research topic. However, the availability of meaningful multispectral data sets can be limited due to cloud cover, particularly in the tropics. In such regions the use of SAR systems (Synthetic Aperture Radar), which are nearly independent from weather conditions, is particularly promising. With an ever-growing number of SAR satellites, as well as the increasing accessibility of SAR data, potentials for multi-frequency remote sensing are becoming numerous. In our study we evaluate the synergistic contribution of multitemporal L-, C-, and X-band data to tropical land cover mapping. We compare classification outcomes of ALOS-2, RADARSAT-2, and TerraSAR-X datasets for a study site in the Brazilian Amazon using a wrapper approach. After preprocessing and calculation of GLCM texture (Grey Level Co-Occurrence), the wrapper utilizes Random Forest classifications to estimate scene importance. Comparing the contribution of different wavelengths, ALOS-2 data perform best in terms of overall classification accuracy, while the classification of TerraSAR-X data yields higher accuracies when compared to the results achieved by RADARSAT-2. Moreover, the wrapper underlines potentials of multi-frequency classification as integration of multi-frequency images is always preferred over multi-temporal, mono-frequent composites. We conclude that despite distinct advantages of certain sensors, for land cover classification multi-sensoral integration is beneficial.

3.1 Introduction

Land Use and Land Cover Change (LUCC) is a main contributor to many acute environmental problems, constituting a loss of biological diversity (Hooper et al., 2012), intensifying the emission of greenhouse gases (Bustamante et al., 2012), and affecting the climate (Foley, 2005; Sombroek, 2001). It is hence a major driver of global environmental change (Lambin et al., 2001). Remote sensing is an important tool, enabling detection and quantification of LUCC on large scales and in regular intervals, emphasizing its prevalent role in LUCC sciences (Beuchle et al., 2015). Mapping and monitoring tropical forests seem particularly relevant, e.g., due to their significant carbon store and rich biodiversity, and remote sensing plays a major role for development of a Measurement, Reporting, and Verification system and the implementation of REDD+ (Reducing Emissions from Deforestation and Degradation).

Change detection is closely linked to land cover mapping. While methods exist to directly detect gradients within remote sensing data (Zhu et al., 2014; Reiche et al., 2015a), many applications are based on the comparison of land cover products at different points in time (Liu et al., 2008a; Müller et al., 2016; Tewkesbury et al., 2015).

The Brazilian Amazon is the largest area of tropical rain forest shared by a single country and for many decades it has been particularly affected by LUCC (Barretto et al., 2013; Nepstad et al., 2014a; Müller et al., 2016). Therefore, many studies use remote sensing data to monitor and quantify different types of land transformation, including deforestation (Nepstad et al., 2014a; Soares-Filho et al., 2014), conservation (Reynolds et al., 2016), or land use intensification (Carreiras et al., 2014).

Although multispectral systems are well established and widely used for LUCC based remote sensing (Hansen et al., 2013; Müller et al., 2016), systems utilizing SAR (Synthetic Aperture Radar) offer additional unique properties. SAR sensors are almost weather-independent, enabling a reliable generation of a time series and thus, a regular monitoring of forest cover. Optical systems are negatively affected by clouds and haze, which occur in particular frequency in tropical regions (Asner, 2001a). Moreover, the number of spaceborne SAR sensors significantly increased during the last several years and further missions will be launched in the future (Ouchi, 2013; Moreira et al., 2013b). With the launch of Sentinel-1 in 2014, the first operational SAR mission is available to offer freely available spaceborne imagery to the public (Aschbacher et al., 2012; McNairn et al., 2009). Considering the impact of freely accessible Landsat imagery (Wulder et al., 2012b), SAR based remote sensing is expected to become increasingly important over the coming years.

The increasing availability of various SAR sensors also fosters the combination of SAR images acquired at different frequencies. While the SIR-C/X-SAR payload onboard the Endeavour space shuttle provided the first spaceborne, multi-frequency (L-, C-, X-band) SAR datasets (Stofan et al., 1995), various satellite missions are in operation nowadays. Missions such as ALOS-2 (AL2), RADARSAT-2 (RS2), TerraSAR-X (TSX), and the recently launched Sentinel-1 enable a harmonized data acquisition, and thus the generation of multi-frequency data sets, consisting of L-, C, and X-band imagery. Concerning the mapping of LUCC and LULC (Land Use and Land Cover), these wavelengths are often used in different study sites to benefit from the particular backscattering characteristics of various land surfaces (e.g., (Schmullius et al., 1997)).

Although X-band data is successfully used for mapping of forests (Schlund et al., 2013), short-wavelength SAR is mainly used for the mapping of low vegetation areas, such as grassland (Schuster et al., 2015), crop types (Sonobe et al., 2014), and urban environments (Ban et al., 2015; Du et al., 2015). On the contrary, L-band sensors are predominantly used for

mapping forests and densely vegetated environments (Rakwatin et al., 2012; Almeida-Filho et al., 2009), while, given its median wavelength and high availability, C-band data is used for a very wide range of applications. This includes the mapping of boreal and tropical forests (Kurvonen et al., 1999; Nelson et al., 2009; Zhang et al., 2012), and urban areas (Taubenböck et al., 2012; Ban et al., 2015). Additionally, C-band data is widely used for mapping agricultural regions, including crop type mapping and changes in agricultural management (Shao et al., 2001; Waske et al., 2009b; McNairn et al., 2009; Stefanski et al., 2014). Still, these examples are not exhaustive. Moreover, the results of many studies prove that the mapping accuracies can be increased when using advanced techniques, e.g., interferometry (Schlund et al., 2013; Jin et al., 2014), spatial features (Cutler et al., 2012b; Du et al., 2015), and state-of-the-art machine learning methods (Voisin et al., 2013; Waske et al., 2008).

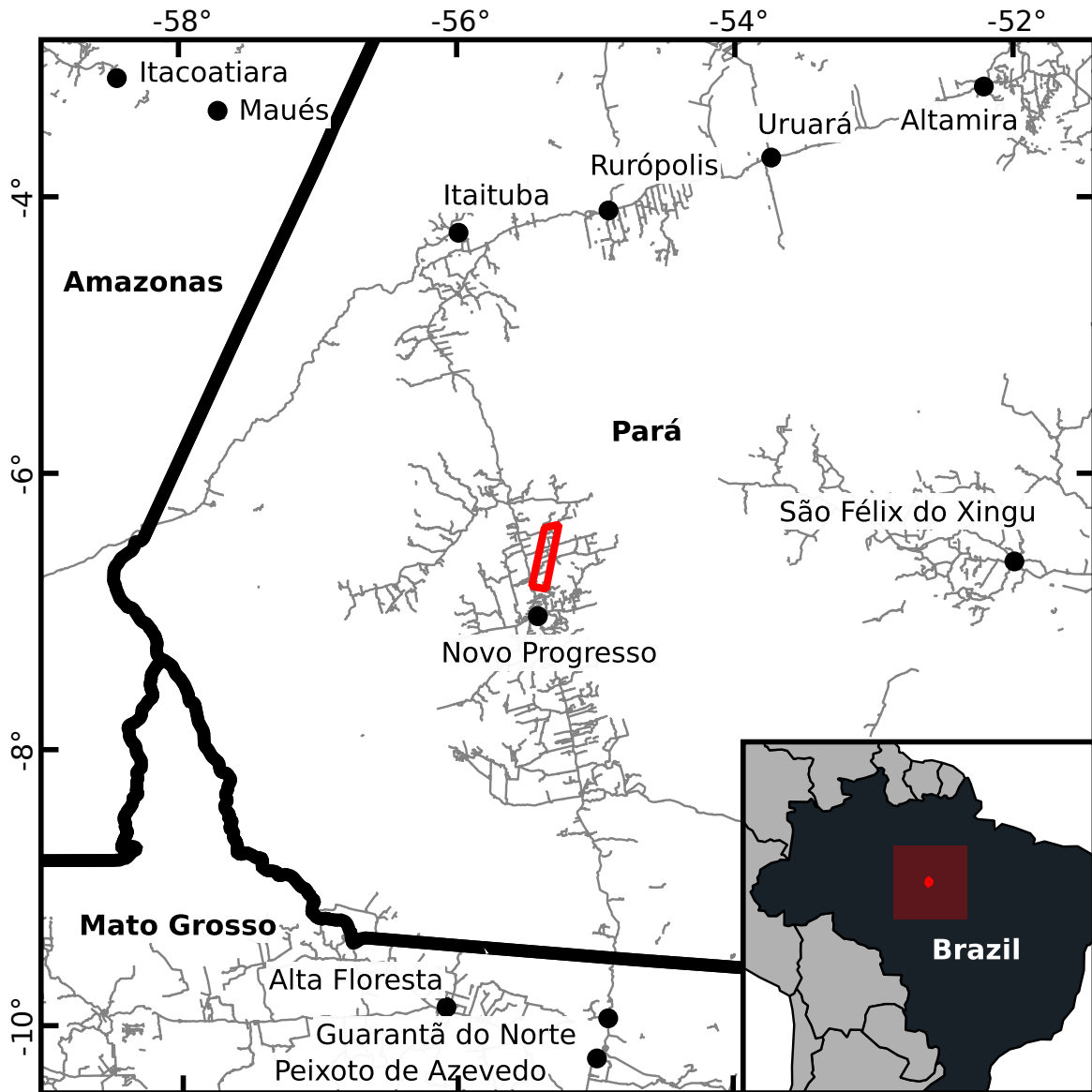
To further benefit from the positive capabilities of multiple frequency remote sensing, various studies aggregate datasets from different sensors. Li et al. (2012) combine multi-temporal ALOS-PALSAR and RS2 products to improve classification accuracies in a tropical context, stressing the positive properties of L-band over C-band.

However, very few studies to date have focused on an encompassing integration of L-, C-, X-band images in the context of land cover mapping. Particularly in the tropics, Wang et al. (2013) observe the backscattering characteristics of different wavelengths with regard to pasture monitoring in a South Australian study site, while Naidoo et al. (2014) and Naidoo et al. (2015) correlate multi-frequency backscatter with above-ground biomass. Similarly, Baghdadi et al. (2009) evaluate the potentials of ALOS-PALSAR (L-Band), ASAR (C-Band), and TSX for sugarcane monitoring. Despite these studies, there is still a lack of research concerning land cover mapping.

The aim of this study is to assess the contribution of multi-temporal, multi-frequency SAR data sets, consisting of AL2, RS2 and TSX images, to LULC mapping in a complex study site in in South Western Pará, in the Brazilian Amazon. The study site is significantly affected by the transformation of forests to pasture, including different types of pasture management and secondary regrowth. We assess the relevance of the different images and potential combinations of data from different sensors through a wrapper approach (Kohavi et al., 1997). This approach enables estimating the importance of different scenes via an iterative generation and evaluation of land cover maps using varying combinations of input scenes. We expect the results to support the understanding of the synergetic potentials of different SAR frequencies in the context of tropical mapping, and offer recommendations for future applications.

3.2 Study Area

The study area lies in South Western Pará state, Brazil, in vicinity to the Novo Progresso municipality (Figure 4.1). The area is a current deforestation frontier and is also affected by post-deforestation dynamics, such as pasture management and secondary regrowth (Fearnside, 2007; Müller et al., 2016). Cattle ranching is the single most dominant form of agricultural land use in the region, despite a slow shift to soy farming, which has recently been affecting farmers in the neighboring, southern state of Mato Grosso (Coy et al., 2014). Hence, with regard to land cover mapping, the aim of this study is to evaluate the potentials of different SAR wavelengths for the separation of the region's most relevant land cover types, i.e., *Primary Forest*, *Secondary Regrowth*, *Clean Pasture*, *Shrubby Pasture*, and *Water*. Within the context of LUCC and management practices, *primary forests* are forests that are unaltered and in their natural state. After degradation and deforestation, two relevant types of land use exist within the study area: *clean pasture* is intensively managed land for cattle ranching often associated with tillage and burning patterns. *Shrubby pasture* is less maintained, with bushes and signs of secondary succession. Lastly, *secondary regrowth* describes areas that are not managed anymore and are densely vegetated up to the stage of secondary forests.



WGS 1984. Administrative data based on Global Administrative Areas and OpenStreetMap.

Fig. 3.1 The study area is defined in an area of severe LULC processes and as the intersection of the available L-, C-, and X-band swaths.

3.3 Data

3.3.1 Remote Sensing Data

For this study, three multi-temporal data sets of current L-, C-, and X-band sensors are considered (Table 3.1). Available imagery includes wet, intermediate, and dry season images, corresponding to acquisitions in January, March, and June, respectively.

PALSAR-2 on AL2 is an L-band system operated by the Japan Aerospace Exploration Agency (JAXA) (Suzuki et al., 2009). AL2 works at a wavelength of 24 cm, which marks the longest currently available wavelength from a spaceborne SAR system for scientific purposes. Long wavelength SAR is generally considered the most promising for the mapping of densely vegetated environments, as the signals can penetrate canopy and backscatter can be correlated to above-ground biomass (Schmullius et al., 1997). Data for this study is available in dual, HH-HV polarization, and acquired in Fine Beam StripMap mode at 10 m target resolution after multi-looking.

Operated at C-band, RS2 is a satellite of the Canadian Space Agency (CSA), which offers a wavelength of 5.5 cm (Morena et al., 2004). Studies have shown RS2 and its predecessor, RADARSAT-1, to be applicable for many purposes, but limitations concerning vegetation mapping are well documented (Sarker et al., 2013). The available data is acquired in Standard Beam mode, at VV-VH polarization, and, after multi-looking, we approximate the recommended operational resolution at 20 m (Morena et al., 2004).

TSX is a German SAR satellite mission for scientific and commercial applications. TSX operates at a wavelength of 3.1 cm (Werninghaus, 2004) and for our study standard StripMap mode data was acquired. While X-band is generally considered less powerful for the mapping of dense vegetation than L-band, due to its high ground resolution and low wavelength TSX could be complementary when used in junction with AL2 data. The recommended nominal resolution of DLR for StripMap TSX imagery is at 5 m, which we approximate through multi-looking.

The subsets in Figure 3.2 give an overview of the different data sets. As expected, all scenes indicate temporal variability within pasture areas, e.g., due to grazing activities and management practices, while forest areas cause high backscatter. While the rectangular borders along individual pasture areas appear blurred in the RS2 image, edges along different natural objects can be visually recognized due to the high spatial resolution of TSX.

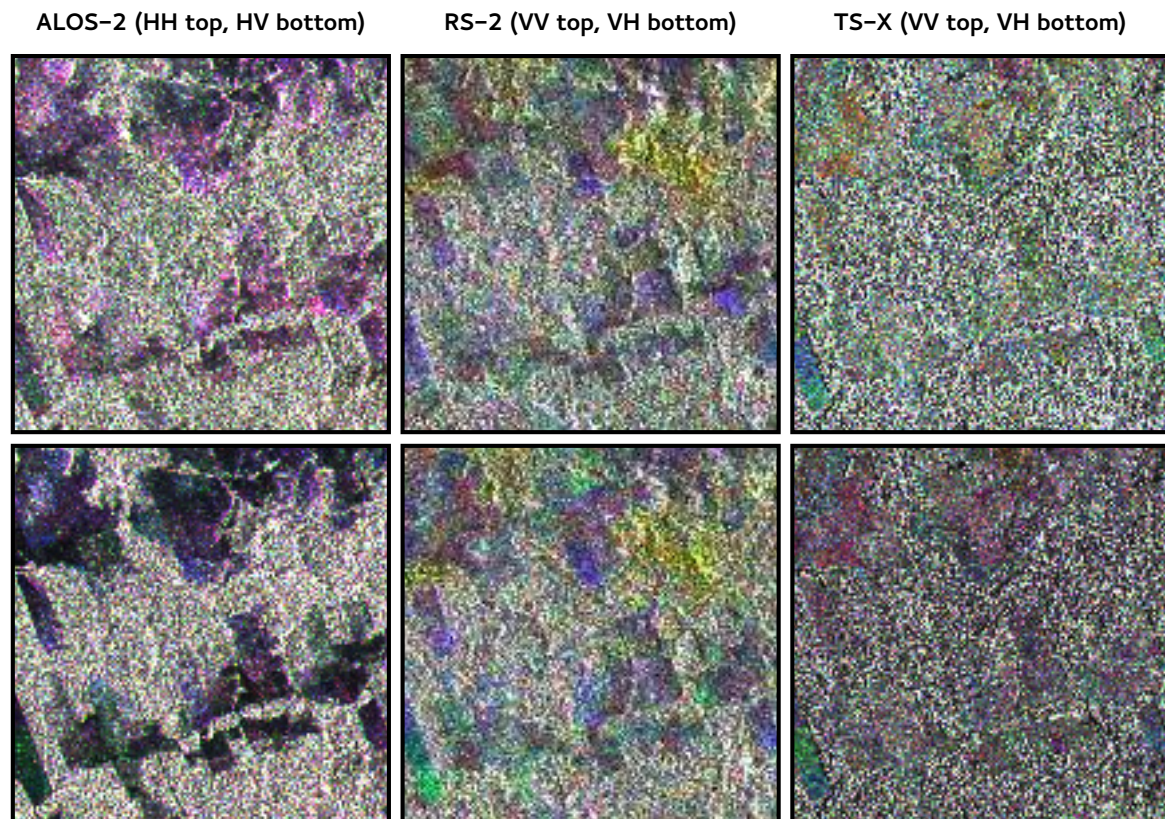


Fig. 3.2 Composites of the available SAR images consisting of January (red), March (green), and June (blue) acquisitions.

Table 3.1 SAR images included in wrapper analysis. TerraSAR-X data acquired as StripMap, RADARSAT-2 in Standard Beam mode, and ALOS-2 as Fine Beam StripMap, at 5 m, 20 m, and 10 m targeted ground resolution, respectively.

Sensor	Date
TerraSAR-X	2015-01-14
RADARSAT-2	2015-01-15
ALOS-2	2015-01-23
TerraSAR-X	2015-02-27
RADARSAT-2	2015-03-04
ALOS-2	2015-03-06
ALOS-2	2015-06-07
RADARSAT-2	2015-06-08
TerraSAR-X	2015-06-17

3.3.2 Reference Data

We use TerraClass (Mapeamento do Uso e Cobertura da Terra na Amazônica Legal Brasileira) as reference data. TerraClass is an effort by INPE, the Brazilian National Institute for Space Research, to manually digitize LULC for the entire Legal Amazon (Almeida et al., 2016). TerraClass addresses areas that are considered deforested according to PRODES (INPE, 2015), and differentiates between 17 LULC classes. PRODES (Programa de Monitoramento do Desflorestamento na Amazônia Legal) is an effort by Brazilian authorities to detect and map deforestation sites based on Landsat and the Moderate Resolution Imaging Spectroradiometer (MODIS) earth observation data, at a minimum mapping unit of 6.5 ha. Due to its exhaustive coverage, and the regional expertise of the interpreters, TerraClass products are considered a meaningful foundation to derive large scale, high quality reference data. As TerraClass is built on 2014 data, comparisons with past TerraClass products (2008, 2010, 2012), show that dynamics can overall be neglected considering the scale of interest. Additionally, our own interpretation using additional RapidEye imagery of 2014 and 2015 furthermore attests its validity. To counteract ambiguities caused by recent deforestation, we use current PRODES data to mask out latest deforestation sites, as deforestation is the most dominant land cover dynamic in the study region (Hansen et al., 2008). While TerraClass encompasses 17 classes, many of these are either not present in the study area (e.g., mining), or they are considered potentially inseparable using the given classification approach and data sets. Therefore, some classes are semantically aggregated into five target LULC classes *Primary Forest*, *Secondary Regrowth*, *Clean Pasture*, *Shrubby Pasture*, and *Water*. Concerning classes of interest within the study area, *primary forest* is analogous to TerraClass' forest class, *secondary regrowth* is composed of TerraClass' secondary vegetation and regeneration with pasture classes, *clean pasture* is a combination of TerraClass' pasture with exposed soil and clean pasture, while *shrubby pasture* and *water* are used synonymously. Masked out are the four TerraClass classes encompassing recent deforestation, other areas, utilization, and non observed areas. In summary, reference areas encompass 277.3 km² for *forest*, 208.1 km² for *clean pasture*, 24.2 km² for *shrubby pasture*, 40.9 km² for *secondary vegetation*, and 0.4 km² for *water*, while 18.5 km² are masked out. These areas are rasterized into an image of 5 by 5 m pixel resolution to sample pixels for training and testing. Due to TerraClass being collected based on optical data, which is predominantly available in the dry season between June and September, areas of *clean pasture* in the reference data can be assumed to be overrepresented due to intra-annual dynamics (Hagensieker et al., 2017a).

3.4 Methods

3.4.1 Preprocessing

All data sets are processed following current standard practices. In a first step, Single Look Complex (SLC) data of all sensors is radiometrically corrected to yield γ^0 terrain-flattened, normalized data (Small, 2011). Multi-looking is applied to approximate target resolutions of AL2, RS2, and TSX, at 10 m, 20 m and 5 m, respectively. Afterwards, Range-Doppler Terrain-Correction with an 3 s SRTM is performed. Images are projected into Lambert Azimuthal Equal Area using the SAD69 spheroid, which corresponds to the available TerraClass data. Additionally, images are sampled to exactly meet their intended target resolutions. Following findings by Sarker et al. (2013), 10 GLCM texture parameters are derived per polarization and scene. Subsequent filtering (GammaMap) is applied on the γ^0 layers only (Haralick et al., 1973; Baraldi et al., 1995). To ensure homogeneity of the resolutions, these steps are performed using windows of approximately $100\text{ m} \times 100\text{ m}$ for any sensor, and the number of grey levels is adjusted accordingly. The derived texture parameters are *Contrast*, *Dissimilarity*, *Homogeneity*, *Angular Second Moment*, *Energy*, *Maximum Probability*, *Entropy*, *GLCM Mean*, *GLCM Variance*, and *GLCM Correlation*. While we acknowledge the existence of correlation and redundancy between different GLCM attributes, our own testing in the past showed these effects to be negligible as long as a capable classifier and a sufficient amount of training data are provided. For this study, we utilize the filtered intensity layers in combination with texture parameters, which were derived from the unfiltered products.

3.4.2 Classification

A random sampling stratified by class is conducted using the reference data set (see Section 3.3.2). Three thousand samples per class (i.e., *Primary Forest*, *Secondary Regrowth*, *Clean Pasture*, *Shrubby Pasture* and *Water*) are selected for classifier training, while the remaining reference data is used for validation. Training samples are drawn point based with a minimal distance of 50 m to avoid redundancy and reduce the effect of spatial correlation. For testing, locations of all RS2 pixels are considered, and contained TSX as well as AL2 pixels are selected. Polygons are drawn well within the interpreted class borders from the optical and TerraClass reference image. While this might weaken the expressiveness of the classification and its validation for regions at class borders, it ensures that border discrepancies stemming from varying image resolutions are reduced.

Classifications are performed using Random Forest (RF), which is successfully used for various remote sensing applications, including the classification of SAR data (Waske

et al., 2008; Du et al., 2015). A detailed description of RF is given by Breiman (2001b), and detailed overviews in the context of remote sensing by Belgiu et al. (2016), and Waske et al. (2009b).

We apply a wrapper approach (Kohavi et al., 1997; Chan et al., 2008; Waske et al., 2009a; Maghsoudi et al., 2013) with a forward feature search strategy (FFS) to assess the contribution of the different SAR images on the classification accuracy. By sequentially selecting the next most relevant data set, in our study, each SAR acquisition with the corresponding texture layers from both polarizations, the impact of the different data sets on classification accuracy is assessed. A wrapper is based on a classification algorithms (here: RF) and a specified accuracy measure. Let us assume that we have a set of N candidate SAR images $A = \{\alpha_1, \dots, \alpha_N\}$, and a set of selected images $\Omega = \{\}$. A total of N iterations are conducted. At each iteration, unions of Ω and any element of A get classified and evaluated, resulting in $|A|$ classifications per iteration, with $|A|$ the number of elements in A . The candidate image associated with the highest classification accuracy then gets removed from A and integrated into Ω . Afterwards, the next iteration commences. The order of selection refers to the relevance of each data set in terms of classification accuracy.

As an accuracy measure, we choose the area adjusted overall accuracy as discussed by Olofsson et al. (2014). For this measure, area adjusted accuracies are derived from a population error matrix. This approach is particularly useful if class occurrences are uneven. In addition, it can be used to yield confidence intervals for the generated accuracy measures. Entries of the population error matrix are estimated by Equation (4.1):

$$p_{ij} = W_i \frac{n_{ij}}{n_i}. \quad (3.1)$$

Contrary to a conventional confusion matrix, p_{ij} are proportion area elements, stemming from the corresponding sample counts n_{ij} of the confusion matrix, and the total area proportion W_i of class i . Accordingly, the overall accuracy is the sum of the main diagonal of this population error matrix.

3.5 Results

Table 4.1 shows the overall accuracies achieved on the individual acquisitions (i.e., iteration 1) and the various combinations, using an RF-based wrapper approach (i.e., iteration 2–9). Confidence intervals of all measures are generated to verify significance.

Table 3.2 Area adjusted overall accuracy (%) for each dataset and iteration of the wrapper.

Scene	Iteration								
	1	2	3	4	5	6	7	8	9
AL2-Jan	62.23								
AL2-Mar	59.60	64.05	66.26	68.07	68.54	68.81	69.02		
AL2-Jun	60.62	64.50	66.75	68.26	68.64	68.87	68.97	69.21	
RS2-Jan	48.93	65.56	67.79						
RS2-Mar	39.15	64.62	66.84	68.40					
RS2-Jun	46.76	65.28	67.23	68.26	68.64	68.87			
TSX-Jan	56.25	65.33	66.58	68.24	68.67	68.83	69.00	69.15	69.27
TSX-Mar	57.53	65.24	66.71	68.27	68.67				
TSX-Jun	55.51	65.78							

Comparing all mono-temporal, single-sensor results, i.e., the results achieved in the first wrapper iteration, it can be assessed that the AL2 data yields the highest accuracies, even when the weakest AL2 classification (AL2-Mar, 59.60%) performs better than the best non-AL2 dataset (TSX-Mar, 57.53%). As these accuracies are based on Olofsson et al. (2014), calculation of standard errors of these accuracies is also feasible. Having used exhaustive TerraClass data as test data, the associated standard errors are all well below 0.001%. This is also emphasized by a visual interpretation of the best classification results, achieved by a single data source (see Figure 3.3 for reference). It can further be observed that TSX overall outperforms RS2, which is notable given the wavelength and the area of application, and might be a consequence of the favorable spatial resolution of TSX.

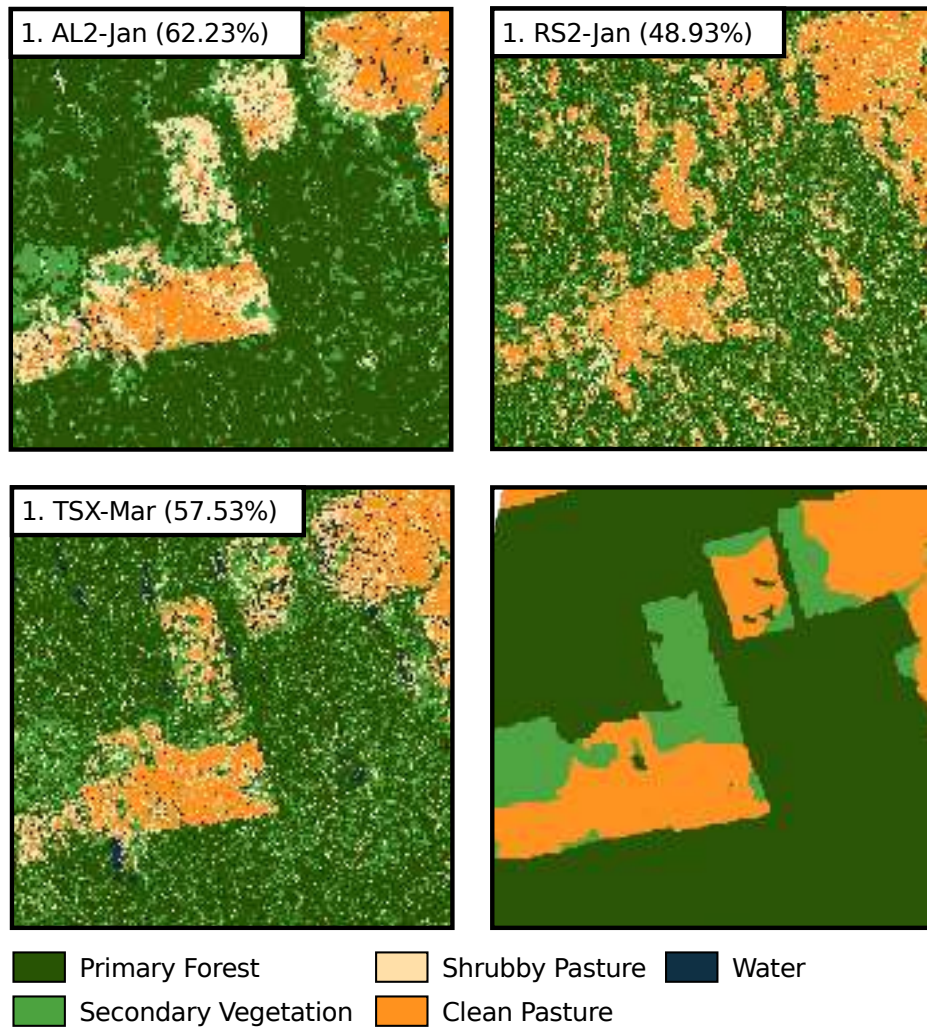


Fig. 3.3 Comparison of the single scene mapping capabilities. Scenes are shown that yield the highest overall accuracy per sensor. The bottom right shows the TerraClass reference image.

The visual interpretation of the results underlines the strong contribution of AL2 data to tropical land cover mapping. Areas are generally correctly classified, and few misclassifications can be observed. Contrary to TSX and AL2, RS2 shows very high confusion not only between *Clean Pasture* and *Shrubby Pasture*, as well as *Primary Forests* and *Secondary Vegetation*, but additionally between managed and non-managed regions (e.g., *Primary Forest* and *Shrubby Pasture*). Accuracies of RS2 are significantly lower when compared to the results achieved by TSX data, and especially RS2-Mar is a negative outlier.

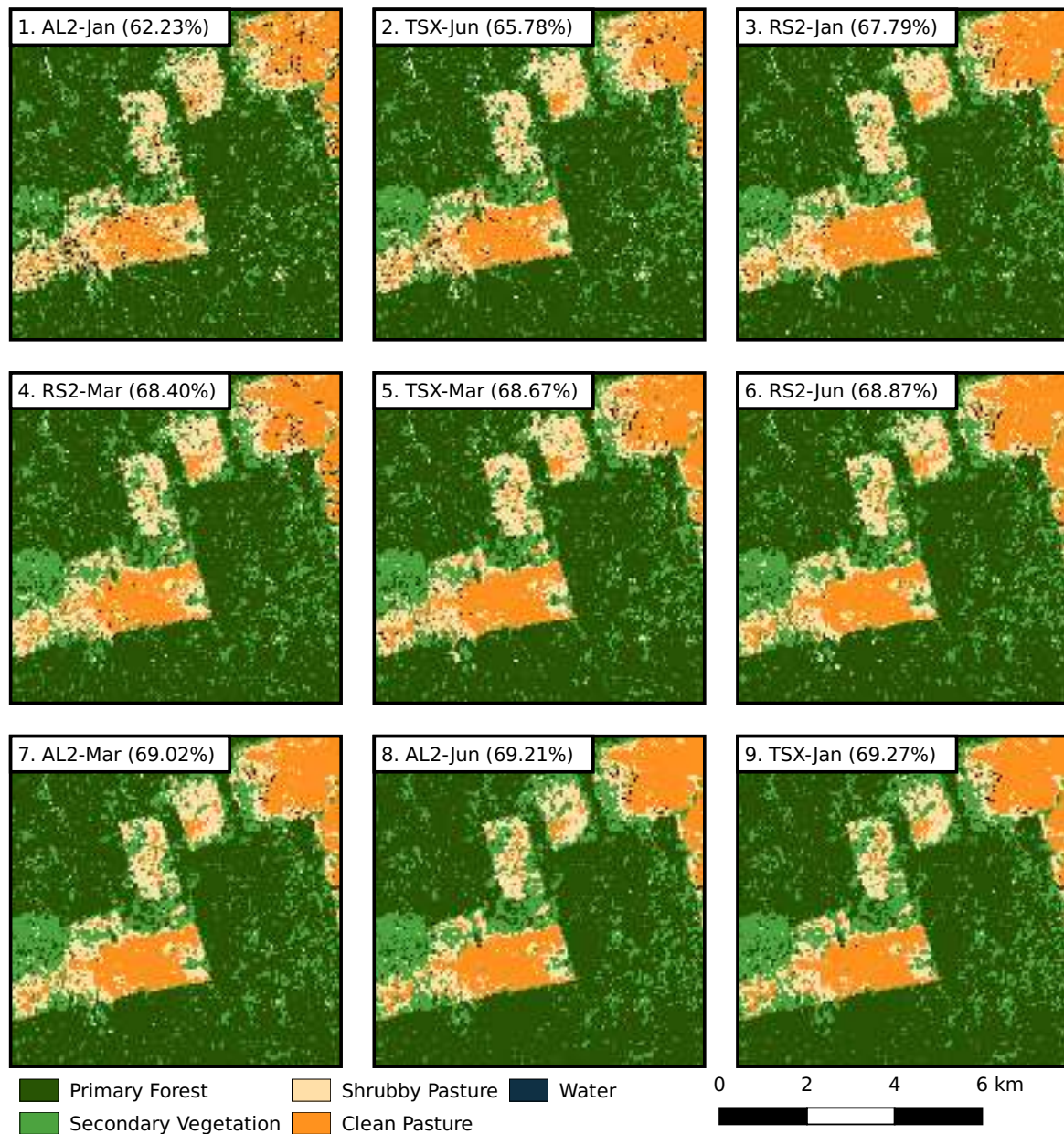


Fig. 3.4 Subsets of the classification result, achieved after each iteration of the wrapper. The classification is based on all specified data sets, e.g.,: the RS2-Jan is selected as the third data set and added to the AL2-Jan and TSX-Jun, which have been selected beforehand. The classification of these three datasets results in an accuracy of 67.79%.

As expected, the classification accuracy increases steadily with increasing number of acquisitions, ranging from 62.23% up to 69.27%. Comparing the results of iteration 2, it can be assessed that the combination of the AL2-Jan with additional AL2 images performs worst in terms of accuracy. Despite the documented lower accuracies at iteration 1, RS2 offers results that are comparable to AL2 and TSX in terms of accuracy. Nevertheless, the

combination of one AL2 and one TSX scene is most adequate, resulting in the highest gain of 3.55 percentage points using the TSX-Jun image. The dataset is complemented by RS2 images in the third iteration. However, from iteration three onwards, and including scenes from all three sensors, the positive impact of additional scenes on the accuracy is significantly reduced. The visual assessment of the classification results (Figure 3.4) underlines these findings. The numeration in Figure 3.4 indicates the corresponding iteration of the wrapper approach and the added scene. For example, after selecting AL2-Jan at the first iteration, the TSX acquisition from June is selected at iteration two. Classification of these two scenes results in an area adjusted OA of 65.78%. Although all maps show the general structures of the classified area, some maps are noisy even in homogeneous areas. Borders along the edges appear blurred and hard to identify. This drawback is significantly reduced by combining different data sets.

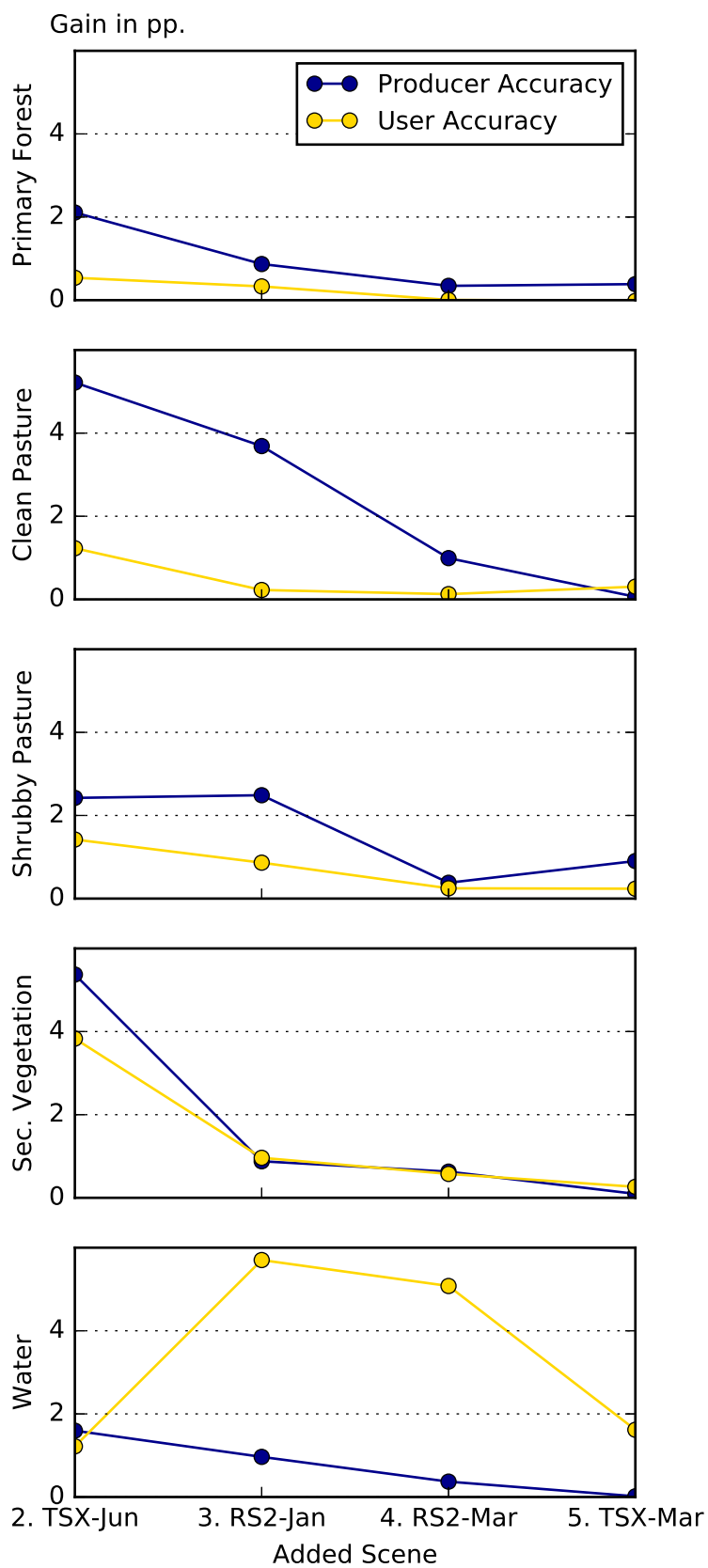


Fig. 3.5 Gains in User and Producer Accuracy for wrapper iterations 2–5.

The contribution of the SAR data to the tropical LULC mapping is also underlined by an analysis of the Producer and User Accuracies (PA, UA). Figure 4.2 shows the gains in area adjusted UA's and PA's achieved by the RF-wrapper approach. Correlating with the receding increase of overall accuracy, UA's and PA's mark high gains for the first additional scenes, before the gains are approaching zero. The figure shows that the PA of *clean pasture* benefits overall very well from the inclusion of further scenes in addition to the original AL2-Jan scene. Figure 3.6 compares the final multi-temporal, multi-frequency land cover product with the reference data derived by TerraClass. The corresponding confusion matrix is shown in Table 3.3.



Fig. 3.6 Final classification product using multi-temporal, multi-frequency imagery compared to TerraClass reference data set. Note that inconsistent classes from the TerraClass dataset are masked out white.

As noted previously, the highest confusion exists between *Primary Forest* and *Secondary Vegetation*, as well as between *Clean Pasture* and *Shrubby Pasture*. Notably, many *Clean Pasture* regions are misclassified as *Shrubby Pasture*, while *Shrubby Pasture* is generally not labeled *Clean Pasture*. Additionally, many *Primary Forests* are classified as *Secondary*

Vegetation and vice versa. While confusion exists between *Secondary Vegetation* and *Shrubby Pasture*, it is not as prevalent.

Table 3.3 Population error matrix derived from classification of the full dataset and TerraClass reference data. Numbers reflect area adjusted percentages as introduced by Equation (4.1).

Classification	Reference					Sum	User's Accuracy
	1	2	3	4	5		
1 Primary Forest	39.27	1.94	0.27	2.04	0.00	43.51	90.26
2 Clean Pasture	1.13	24.05	1.00	0.79	0.00	27.01	89.04
3 Shrubby Pasture	2.23	8.42	2.55	1.25	0.00	14.46	17.64
4 Secondary Vegetation	7.32	3.44	0.57	3.33	0.00	14.66	22.72
5 Water	0.04	0.21	0.01	0.02	0.08	0.36	22.22
Sum	49.99	38.07	4.44	7.43	0.08	100	
Producer's Accuracy	78.56	63.17	57.43	44.81	100		

3.6 Discussion

As expected, the combination of multitemporal SAR data from different sensors sets proves useful for tropical land cover mapping. Obtained overall accuracies are higher than those achieved by single source data sets. The results clearly underline the relevance of the AL2 scenes, which yield the highest accuracies when compared to the TSX and RS2 data. This reflects the general consensus in literature, which acknowledges systems of longer wavelengths to be favorable concerning vegetation mapping (Naidoo et al., 2015; Schmillius et al., 1997; Sarker et al., 2013). AL2 is in particular the most adequate sensor for mono-frequent, mono-temporal classifications (Table 4.1) and, thus, seems sufficient when data availability is limited. A visual interpretation of the classification results confirms these findings (Figure 3.3). While *Primary Forest* and *Secondary Vegetation* tend to be less confused when using AL2 data, *Secondary Vegetation* is overestimated by TSX data. However, the positive effects of the high spatial resolution of TSX are clearly visible in the classification results. Edges along individual land cover types, e.g., the nearly rectangular pasture area, can be more clearly identified, while these boundaries appear blurred in the results achieved by RS2 and AL2 data. Moreover, the differentiation between managed and unmanaged areas is challenging for RS2 data, indicated by many patches of Primary Forest that are misclassified as Pasture. While any individual AL2 acquisition outperforms any RS2 as well as any TSX scene, the wrapper selects a TSX at the second iteration. Even the combination of one AL2

scene with a RS2 scene outperforms the classification results achieved by two AL2 scenes. The positive impact of combining multi-frequency data is further underlined by the third iteration of the wrapper. After integration of the first TSX scene at the second iteration, RS2 images lead to the strongest gains in accuracy, despite their weak initial performances. Hence, acquisitions of each sensor are utilized after just three iterations, underlining the potential of including multi-frequency SAR images for land cover mapping. This is in accordance with previous findings, e.g., by Naidoo et al. (2015), who also document slight advantages of multi-frequency integration, yet remark on limited gains over L-band data alone for the purpose of biomass mapping.

After scenes of each sensor are integrated, gains in accuracy are receding rapidly. Additionally, it appears that the advantages of AL2 and TSX do not appear to transfer over to the subsequent iterations. Two times RS2 is chosen over AL2 and TSX (iterations 5 and 6), yet all scenes are performing very similarly as they yield a low variance in accuracy. The range of accuracies for the fifth iteration is already very narrow at 0.13 pp., and the gain of the fifth over fourth iteration is only at 0.27 pp. The population error matrix (Table 3.3) reflects the stratified sampling, with *Shrubby Pasture* and *Water* being overrepresented. The confusion between pasture areas deserves special attention in particular. While TerraClass products imply *Clean Pasture* and *Shrubby Pasture* to be stable over the years, we observe these classes to be very ambiguous. Inspection of the land cover maps shows the confusion of *Pasture* classes to often affect continuous areas that are misattributed (see Figure 3.3). Counterintuitively, we observe that *Shrubby Pasture* areas do not necessarily align with regions of increased backscatter. Reasons might be a high inner-class and intra-annual variance, seasonality overall, and possibly limitations concerning the interpretation of the two classes in the TerraClass dataset. Intra-annual variance is of particular interest, as the underlying SAR acquisitions are spread over the entire dry period, which in general also coincide with a decrease of *shrubby*, in favor of *clean pasture* (Hagensieker et al., 2017a). Since these effects are present in the training as well as testing data, classification outcomes are affected to a certain degree. In particular, results of classifications that might be capable of separating the pasture types might be lessened, as the inherent variance could introduce non-recoverable confusion. This is also indicated by the lower confusion between *Secondary Vegetation* and *Shrubby Pasture*, which can be separated more reliably despite being very similar in visual appearance. In contrast, the confusion between *Secondary Vegetation* and *Primary Forest* appears to be more random and is distributed spatially, while individual small regions of *Secondary Vegetation* can generally be made out. Consequently, these classes might not be classified well even with available L-band imagery, which might be a direct consequence of the saturation of L-band in environments of high biomass (Yu et al., 2016;

Mermoz et al., 2015). Comparing the reference classification as shown by Figure 3.3 with the classification outcomes of the first iteration, TSX shows the potential to improve on the *Pasture* classes. However, these potentials are not reflected after integration of TSX scenes into the fused product (Figure 3.4).

Given its low resolution and all of the data being upsampled to TSX' spatial resolution, RS2 should be affected more positively by spatial autocorrelation than the other sensors, yet these effects appear to be miniscule. Additional tests also show a very limited effect of the chosen upsampling strategy with regard to the confidences of accuracies, which remains on a comparably high level even when just an eighth of the testing data is utilized.

Some factors are not considered in this study. Data is obtained in the standard operation modes of the examined sensors. While other acquisition modes might lead to more similar data sets regarding spatial resolution, spatial extent, or polarization, the authors had no influence in e.g., the acquisition of AL2 data, which is HH-HV polarized. A potential consequence could be a higher gain in accuracy at the second iteration for non-AL2 scenes, as not only the benefits of including an additional wavelength are factored in, but also the benefits of including an additional polarization. As 45 models have to be trained using 15,000 samples with up to 198 features, and the classification of entire images has to be conducted to estimate area adjusted accuracies, the study is effortlessly handled by a common desktop PC (i7-3770 @ 3.40 Ghz). In case of accessible multi-frequency SAR data, it is possible to utilize current open source packages, i.e., ESA's Snap, GDAL, Python, Q-GIS, to conduct powerful land cover analyses using a combination of standard workflows. Limitations can be caused by a mixture of ascending and descending passes, as well as inconsistent looking directions. Having considered this and not aiming for interferometric accuracy, coregistration of images could be achieved without manual adjustments even at varying looking angles. Reference data was mainly collected using alternative sources, which we highly recommend in any case for conducting land cover analyses on SAR data.

3.7 Conclusions

In the presented study, the contribution of multi-frequency SAR data to topical land cover mapping was analyzed. However, a complementary integration of additional X- and C-band images yield higher accuracies when compared to the classification of multi-temporal AL2 scenes alone. Moreover, the results show that TSX outperforms RS2 for individual classifications in terms of accuracy. Given a set of multi-frequency imagery, the integration of additional scenes leads to an increase in accuracy, yet this effect is weakened with a growing number of scenes. In addition, advantages of adding multiple AL2 over TSX or

RS2 scenes do not exist if an AL2 scene is integrated already. For this reason, when adding scenes to a dataset that is already multi-frequency, advantages of adding certain frequencies are also negligible. Finally, we show that a wrapper can be implemented effortlessly and is very applicable for the identification of most relevant acquisitions. Generally, the results show that the use of multisensor SAR data is worthwhile and the classification accuracy is significantly increased by such data sets. Moreover, classifiers such as Random Forest prove useful in various studies for handling large and multisource data sets. This is particularly important with respect to recent and planned missions with increased revisit times and better spatial resolutions such as Sentinel-1 (C-band), the NASA-ISRO Synthetic Aperture Radar (NISAR, L/S-band), or High Resolution Wide Swath (HRWS, X-band).

References

- Almeida, C. A. d., A. C. Coutinho, J. C.D. M. Esquerdo, M. Adami, A. Venturieri, C. G. Diniz, N. Dessay, L. Durieux, and A. R. Gomes (2016). “High spatial resolution land use and land cover mapping of the Brazilian Legal Amazon in 2008 using Landsat-5/TM and MODIS data”. In: *Acta Amaz.* 46.3, pp. 291–302.
- Almeida-Filho, R., Y. E. Shimabukuro, A. Rosenqvist, and G. A. Sanchez (2009). “Using dual-polarized ALOS PALSAR data for detecting new fronts of deforestation in the Brazilian Amazônia”. In: *International Journal of Remote Sensing* 30.14, pp. 3735–3743.
- Aschbacher, J. and M. P. Milagro-Pérez (2012). “The European Earth monitoring (GMES) programme: Status and perspectives”. In: *Remote Sensing of Environment* 120, pp. 3–8.
- Asner, G. P. (2001a). “Cloud cover in Landsat observations of the Brazilian Amazon”. In: *International Journal of Remote Sensing* 22.18, 3855–3862.
- Baghdadi, N., N. Boyer, P. Todoroff, M. El Hajj, and A. Bégué (2009). “Potential of SAR sensors TerraSAR-X, ASAR/ENVISAT and PALSAR/ALOS for monitoring sugarcane crops on Reunion Island”. In: *Remote Sensing of Environment* 113.8, 1724–1738.
- Ban, Y., A. Jacob, and P. Gamba (2015). “Spaceborne SAR data for global urban mapping at 30m resolution using a robust urban extractor”. In: *ISPRS Journal of Photogrammetry and Remote Sensing* 103, 28–37.
- Baraldi, A. and F. Parmiggiani (1995). “A refined gamma MAP SAR speckle filter with improved geometrical adaptivity”. In: *IEEE Transactions on Geoscience and Remote Sensing* 33.5, 1245–1257.
- Barretto, A. G.O. P., G. Berndes, G. Sparovek, and S. Wirsenius (2013). “Agricultural intensification in Brazil and its effects on land-use patterns: an analysis of the 1975-2006 period”. In: *Global Change Biology* 19.6, 1804–1815.
- Belgiu, M. and L. Drăguț (2016). “Random forest in remote sensing: A review of applications and future directions”. In: *ISPRS Journal of Photogrammetry and Remote Sensing* 114, 24–31.
- Beuchle, R., R. C. Grecchi, Y. E. Shimabukuro, R. Seliger, H. D. Eva, E. Sano, and F. Achard (2015). “Land cover changes in the Brazilian Cerrado and Caatinga biomes from 1990 to 2010 based on a systematic remote sensing sampling approach”. In: *Applied Geography* 58, 116–127.
- Breiman, L. (2001b). “Random forests”. In: *Machine learning* 45.1, pp. 5–32.
- Bustamante, M. M., C. A. Nobre, R. Smeraldi, A. P. Aguiar, L. G. Barioni, L. G. Ferreira, K. Longo, P. May, A. S. Pinto, and J. P. Ometto (2012). “Estimating greenhouse gas emissions from cattle raising in Brazil”. In: *Climatic change* 115.3-4, pp. 559–577.

- Carreiras, J. M. B., J. Jones, R. M. Lucas, and C. Gabriel (2014). “Land Use and Land Cover Change Dynamics across the Brazilian Amazon: Insights from Extensive Time-Series Analysis of Remote Sensing Data”. In: *PLoS ONE* 9.8. Ed. by B. Hérault, e104144.
- Chan, J. C.-W. and D. Paelinckx (2008). “Evaluation of Random Forest and Adaboost tree-based ensemble classification and spectral band selection for ecotope mapping using airborne hyperspectral imagery”. In: *Remote Sensing of Environment* 112.6, 2999–3011.
- Coy, M. and M. Klingler (2014). “Frentes pioneiras em transformação: o eixo da BR-163 e os desafios socioambientais”. In: *Territórios e Fronteiras* 7.1, pp. 1–26.
- Cutler, M., D. Boyd, G. Foody, and A. Vetrivel (2012b). “Estimating tropical forest biomass with a combination of SAR image texture and Landsat TM data: An assessment of predictions between regions”. In: *ISPRS Journal of Photogrammetry and Remote Sensing* 70, pp. 66–77.
- Du, P., A. Samat, B. Waske, S. Liu, and Z. Li (2015). “Random Forest and Rotation Forest for fully polarized SAR image classification using polarimetric and spatial features”. In: *ISPRS Journal of Photogrammetry and Remote Sensing* 105, 38–53.
- Fearnside, P. M. (2007). “Brazil’s Cuiabá- Santarém (BR-163) Highway: The Environmental Cost of Paving a Soybean Corridor Through the Amazon”. In: *Environmental Management* 39.5, 601–614.
- Foley, J. A. (2005). “Global Consequences of Land Use”. In: *Science* 309.5734, pp. 570–574.
- Hagensieker, R., R. Roscher, J. Rosentreter, B. Jakimow, and B. Waske (2017a). “Tropical land use land cover mapping in Pará (Brazil) using discriminative Markov random fields and multi-temporal TerraSAR-X data”. In: *International Journal of Applied Earth Observation and Geoinformation* 63, pp. 244–256.
- Hansen, M, Y Shimabukuro, P Potapov, and K Pittmann (2008). “Comparing annual MODIS and PRODES forest cover change data for advancing monitoring of Brazilian forest cover”. In: *Remote Sensing of Environment* 112.10, 3784–3793.
- Hansen, M. C., P. V. Potapov, R. Moore, M. Hancher, S. A. Turubanova, A. Tyukavina, D. Thau, S. V. Stehman, S. J. Goetz, T. R. Loveland, A. Kommareddy, A. Egorov, L. Chini, C. O. Justice, and J. R. G. Townshend (2013). “High-Resolution Global Maps of 21st-Century Forest Cover Change”. In: *Science* 342.6160, pp. 850–853. eprint: <http://science.sciencemag.org/content/342/6160/850.full.pdf>.
- Haralick, R. M., K. Shanmugam, and I. H. Dinstein (1973). “Textural features for image classification”. In: *Systems, Man and Cybernetics, IEEE Transactions on* 6, pp. 610–621.
- Hooper, D. U., E. C. Adair, B. J. Cardinale, J. E. Byrnes, B. A. Hungate, K. L. Matulich, A. Gonzalez, J. E. Duffy, L. Gamfeldt, and M. I. OConnor (2012). “A global synthesis

- reveals biodiversity loss as a major driver of ecosystem change”. In: *Nature* 486.7401, pp. 105–108.
- INPE (2015). *Projeto PRODES - Monitoramento da Floresta Amazonica Brasileira por Satelite*.
- Jin, H., G. Mountrakis, and S. V. Stehman (2014). “Assessing integration of intensity, polarimetric scattering, interferometric coherence and spatial texture metrics in PALSAR-derived land cover classification”. In: *ISPRS Journal of Photogrammetry and Remote Sensing* 98, 70–84.
- Kohavi, R. and G. H. John (1997). “Wrappers for feature subset selection”. In: *Artificial Intelligence* 97.1-2, 273–324.
- Kurvonen, L., J. Pulliainen, and M. Hallikainen (1999). “Retrieval of biomass in boreal forests from multitemporal ERS-1 and JERS-1 SAR images”. In: *IEEE Transactions on Geoscience and Remote Sensing* 37.1, 198–205.
- Lambin, E. F., B. Turner, H. J. Geist, S. B. Agbola, A. Angelsen, J. W. Bruce, O. T. Coomes, R. Dirzo, G. Fischer, C. Folke, and et al. (2001). “The causes of land-use and land-cover change: moving beyond the myths”. In: *Global Environmental Change* 11.4, 261–269.
- Li, G., D. Lu, E. Moran, L. Dutra, and M. Batistella (2012). “A comparative analysis of ALOS PALSAR L-band and RADARSAT-2 C-band data for land-cover classification in a tropical moist region”. In: *ISPRS Journal of Photogrammetry and Remote Sensing* 70, 26–38.
- Liu, D., K. Song, J. R. Townshend, and P. Gong (2008a). “Using local transition probability models in Markov random fields for forest change detection”. In: *Remote Sensing of Environment* 112.5, pp. 2222–2231.
- Maghsoudi, Y., M. J. Collins, and D. G. Leckie (2013). “Radarsat-2 Polarimetric SAR Data for Boreal Forest Classification Using SVM and a Wrapper Feature Selector”. In: *IEEE Journal of Selected Topics in Applied Earth Observations and Remote Sensing* 6.3, 1531–1538.
- McNairn, H., C. Champagne, J. Shang, D. Holmstrom, and G. Reichert (2009). “Integration of optical and Synthetic Aperture Radar (SAR) imagery for delivering operational annual crop inventories”. In: *ISPRS Journal of Photogrammetry and Remote Sensing* 64.5, 434–449.
- Mermoz, S., M. Réjou-Méchain, L. Villard, T. Le Toan, V. Rossi, and S. Gourlet-Fleury (2015). “Decrease of L-band SAR backscatter with biomass of dense forests”. In: *Remote Sensing of Environment* 159, 307–317.
- Moreira, A., P. Pratstiraola, M. Younis, G. Krieger, I. Hajnsek, and K. P. Papathanassiou (2013b). “A Tutorial on Synthetic Aperture Radar”. In:

- Morena, L., K. James, and J Beck (2004). “An introduction to the RADARSAT-2 mission”. In: *Canadian Journal of Remote Sensing* 30.3, pp. 221–234.
- Müller, H., P. Griffiths, and P. Hostert (2016). “Long-term deforestation dynamics in the Brazilian Amazon—Uncovering historic frontier development along the Cuiabá–Santarém highway”. In: *International Journal of Applied Earth Observation and Geoinformation* 44, 61–69.
- Naidoo, L., R. Mathieu, R. Main, W. Kleynhans, K. Wessels, G. Asner, and B. Leblon (2015). “Savannah woody structure modelling and mapping using multi-frequency (X-, C- and L-band) Synthetic Aperture Radar data”. In: *ISPRS Journal of Photogrammetry and Remote Sensing* 105, 234–250.
- Naidoo, L., R. Mathieu, R. Main, W. Kleynhans, K. Wessels, G. P. Asner, and B. Leblon (2014). “The assessment of data mining algorithms for modelling Savannah Woody cover using multi-frequency (X-, C- and L-band) synthetic aperture radar (SAR) datasets”. In: *2014 IEEE Geoscience and Remote Sensing Symposium*.
- Nelson, M. D., K. T. Ward, and M. E. Bauer (2009). “Forest-cover-type separation using RADARSAT-1 synthetic aperture radar imagery”. In: *Notes*.
- Nepstad, D., D. McGrath, C. Stickler, A. Alencar, A. Azevedo, B. Swette, T. Bezerra, M. DiGiano, J. Shimada, R. S. da Motta, et al. (2014a). “Slowing Amazon deforestation through public policy and interventions in beef and soy supply chains”. In: *Science* 344.6188, pp. 1118–1123.
- Olofsson, P., G. M. Foody, M. Herold, S. V. Stehman, C. E. Woodcock, and M. A. Wulder (2014). “Good practices for estimating area and assessing accuracy of land change”. In: *Remote Sensing of Environment* 148, pp. 42–57.
- Ouchi, K. (2013). “Recent Trend and Advance of Synthetic Aperture Radar with Selected Topics”. In: *Remote Sensing* 5.2, pp. 716–807.
- Rakwatin, P., N. Longépé, O. Isoguchi, M. Shimada, Y. Uryu, and W. Takeuchi (2012). “Using multiscale texture information from ALOS PALSAR to map tropical forest”. In: *International Journal of Remote Sensing* 33.24, pp. 7727–7746.
- Reiche, J., J. Verbesselt, D. Hoekman, and M. Herold (2015a). “Fusing Landsat and SAR time series to detect deforestation in the tropics”. In: *Remote Sensing of Environment* 156, pp. 276–293.
- Reynolds, J., K. Wesson, A. Desbiez, J. Ochoa-Quintero, and P. Leimgruber (2016). “Using Remote Sensing and Random Forest to Assess the Conservation Status of Critical Cerrado Habitats in Mato Grosso do Sul, Brazil”. In: *Land* 5.2, p. 12.

- Sarker, M. L. R., J. Nichol, H. B. Iz, B. Ahmad, and A. A. Rahman (2013). "Forest Biomass Estimation Using Texture Measurements of High-Resolution Dual-Polarization C-Band SAR Data". In:
- Schlund, M., F. von Poncet, D. H. Hoekman, S. Kuntz, and C. Schmullius (2013). "Importance of bistatic SAR features from TanDEM-X for forest mapping and monitoring". In: *Remote Sensing of Environment*.
- Schmullius, C. C. and D. L. Evans (1997). "Review article Synthetic aperture radar (SAR) frequency and polarization requirements for applications in ecology, geology, hydrology, and oceanography: A tabular status quo after SIR-C/X-SAR". In: *International Journal of Remote Sensing* 18.13, 2713–2722.
- Schuster, C., T. Schmidt, C. Conrad, B. Kleinschmit, and M. Förster (2015). "Grassland habitat mapping by intra-annual time series analysis—Comparison of RapidEye and TerraSAR-X satellite data". In: *International Journal of Applied Earth Observation and Geoinformation* 34, pp. 25–34.
- Shao, Y., X. Fan, H. Liu, J. Xiao, S. Ross, B. Brisco, R. Brown, and G. Staples (2001). "Rice monitoring and production estimation using multitemporal RADARSAT". In: *Remote Sensing of Environment* 76.3, 310–325.
- Small, D. (2011). "Flattening Gamma: Radiometric Terrain Correction for SAR Imagery". In: *IEEE Transactions on Geoscience and Remote Sensing* 49.8, 3081–3093.
- Soares-Filho, B., R. Rajão, M. Macedo, A. Carneiro, W. Costa, M. Coe, H. Rodrigues, and A. Alencar (2014). "Cracking Brazil's Forest Code". In: *Science* 344.6182, pp. 363–364.
- Sombroek, W. (2001). "Spatial and Temporal Patterns of Amazon Rainfall". In: *AMBIO: A Journal of the Human Environment* 30.7, 388–396.
- Sonobe, R., H. Tani, X. Wang, N. Kobayashi, and H. Shimamura (2014). "Random forest classification of crop type using multi-temporal TerraSAR-X dual-polarimetric data". In: *Remote Sensing Letters* 5.2, pp. 157–164.
- Stefanski, J., O. Chaskovskyy, and B. Waske (2014). "Mapping and monitoring of land use changes in post-Soviet western Ukraine using remote sensing data". In: *Applied Geography* 55, pp. 155–164.
- Stofan, E., D. Evans, C. Schmullius, B. Holt, J. Plaut, J. van Zyl, S. Wall, and J. Way (1995). "Overview of results of Spaceborne Imaging Radar-C, X-Band Synthetic Aperture Radar (SIR-C/X-SAR)". In: *IEEE Transactions on Geoscience and Remote Sensing* 33.4, 817–828.
- Suzuki, S., Y. Osawa, Y. Hatooka, Y. Kankaku, and T. Watanabe (2009). "Overview of Japan's Advanced Land Observing Satellite-2 mission". In: *Sensors, Systems, and Next-Generation Satellites XIII*. Ed. by R. Meynart, S. P. Neeck, and H. Shimoda.

- Taubenböck, H, A Felbier, T Esch, A Roth, and S Dech (2012). “Pixel-based classification algorithm for mapping urban footprints from radar data: a case study for RADARSAT-2”. In: *Canadian Journal of Remote Sensing* 38.03, pp. 211–222.
- Tewkesbury, A. P., A. J. Comber, N. J. Tate, A. Lamb, and P. F. Fisher (2015). “A critical synthesis of remotely sensed optical image change detection techniques”. In: *Remote Sensing of Environment* 160, pp. 1–14.
- Voisin, A., V. A. Krylov, G. Moser, S. B. Serpico, and J. Zerubia (2013). “classification of very high resolution SAR images of urban areas using copulas and texture in a hierarchical Markov random field model”. In: *Geoscience and Remote Sensing Letters, IEEE* 10.1, pp. 96–100.
- Wang, X., L. Ge, and X. Li (2013). “Pasture Monitoring Using SAR with COSMO-SkyMed, ENVISAT ASAR, and ALOS PALSAR in Otway, Australia”. In: *Remote Sensing* 5.7, 3611–3636.
- Waske, B., S. van der Linden, J. Benediktsson, A. Rabe, and P. Hostert (2009a). “Impact of different morphological profiles on the classification accuracy of urban hyperspectral data”. In: *2009 First Workshop on Hyperspectral Image and Signal Processing: Evolution in Remote Sensing*.
- Waske, B. and M. Braun (2009b). “Classifier ensembles for land cover mapping using multitemporal SAR imagery”. In: *ISPRS Journal of Photogrammetry and Remote Sensing* 64.5, pp. 450–457.
- Waske, B. and S. van der Linden (2008). “Classifying multilevel imagery from SAR and optical sensors by decision fusion”. In: *Geoscience and Remote Sensing, IEEE Transactions on* 46.5, pp. 1457–1466.
- Werninghaus, R. (2004). “TerraSAR-X mission”. In: *SAR Image Analysis, Modeling, and Techniques VI*. Ed. by F. Posa.
- Wulder, M. A., J. G. Masek, W. B. Cohen, T. R. Loveland, and C. E. Woodcock (2012b). “Opening the archive: How free data has enabled the science and monitoring promise of Landsat”. In: *Remote Sensing of Environment* 122, 2–10.
- Yu, Y. and S. Saatchi (2016). “Sensitivity of L-Band SAR Backscatter to Aboveground Biomass of Global Forests”. In: *Remote Sensing* 8.6, p. 522.
- Zhang, F., M. Xu, C. Xie, Z. Xia, K. Li, and X. Wang (2012). “Forest and deforestation identification based on multitemporal polarimetric RADARSAT-2 images in Southwestern China”. In: *Journal of Applied Remote Sensing* 6.1, pp. 063527–1.
- Zhu, Z. and C. E. Woodcock (2014). “Continuous change detection and classification of land cover using all available Landsat data”. In: *Remote sensing of Environment* 144, pp. 152–171.

Chapter 4

Land Cover Classification based on interferometric TanDEM-X Imagery in the Brazilian Amazon

submitted for publication in *Geoscience and Remote Sensing Letters*, IEEE
Ron Hagensieker, Ivo Zeller, and Björn Waske

Abstract

With TanDEM-X for the first time single-pass interferometric information is gathered as part of a continuous mission. We investigate potentials of TanDEM-X imagery for the land cover mapping of densely vegetated forest areas, in particular the benefits of integrating interferometric coherence and elevation information. Besides interferometric information, textural features are derived. The specific objective is the classification of forest and different types of pasture in a study site located in the Brazilian Amazon. In order to evaluate the potential of TanDEM-X, we perform four classifications, using a Random Forest classifier and different feature sets. Integrating all features yields an overall accuracy of 89 %, opposed to 55 % when relying on dual-pol SAR intensity alone. Moreover, results underline that both aspects, the integration of InSAR information as well as texture metrics, prove useful in terms of classification accuracy. Overall, TanDEM-X data seems promising for tropical land cover mapping.

4.1 Introduction

Land use, land use change, and forestry are defined by the United Nations Framework Convention on Climate Change as human activities that directly impact carbon sinks. In the past, remote sensing has played an important role in monitoring the anthropogenic impact on forest ecosystems (Butler, 2014). Besides multi-spectral systems, SAR has proven to be particularly relevant for mapping land cover as well as the detection of land cover change (Joshi et al., 2016). While long wavelength SAR, such as PALSAR's L-band, has been shown to be positively correlated to aboveground biomass (Rakwatin et al., 2012), shorter wavelength SAR is often used to discriminate forested areas and shrubby succession or pasture land (Li et al., 2012; Hagensieker et al., 2017b). The TanDEM-X (TD-X) mission by DLR utilizes a short wavelength X-band system in a constellation consisting of two twin satellites, enabling the derivation of single pass interferometric products (Moreira et al., 2004). First studies have discussed the capabilities of TD-X data for mapping forest areas (Schlund et al., 2013) and estimating forest biomass (Treuhft et al., 2015; Soja et al., 2017). Recently, Martone et al. (2018) have provided a global forest/non-forest map, which was also derived from interferometric TanDEM-X data.

The main objective is to evaluate the contribution of TD-X data for tropical land cover mapping. As previous studies have highlighted capabilities of including spatial features, e.g. via image segmentation or texture features (Stefanski et al., 2013; Schlund et al., 2013), we include textural information as well as interferometric features. The specific objective of our

study is the classification of TD-X data of a study site within the Brazilian Amazon. We aim at the separation of *forest* and different types of *pasture*. In order to evaluate the potential of TD-X data for tropical land cover mapping, we assess the impact of the different features on the classification accuracy in detail.

4.2 Data & Study area

The study area is located close to the current deforestation frontier of the Brazilian Amazon region in the state of Pará, about 50 km north of the municipality of Novo Progresso. It spans from $6^{\circ}29'47''$ S to $6^{\circ}54'22''$ S and from $55^{\circ}13'8''$ W to $55^{\circ}26'54''$ W, is 42.845 km in azimuth extent, 17.420 km in range extent and covers an area of 750.745 km² (Figure 4.1).

The study area is comprised of *primary forest*, *pasture* (separated into *clean* and *shrubby*), and secondary vegetation from different stages. While many studies particularly focus on forest cover mapping, we also aim on the separation of the two pasture types. Both pasture types are generally used for cattle ranching in this region, but differ on land management. *Shrubby pasture* is characterized by bushes and occasional early stages of succession, while *clean pasture* is intensely managed pasture land, often composed by patches affected by grazing, tilling, or slash and burn practices. Tree crowns of *primary forests* can reach up to 40 m in height. Over the dry season, leaf fall can be observed through decrease of backscatter intensity. While this might affect classification outcome, these observations are hard to quantify and warrant further investigation. Secondary vegetation and water bodies have been omitted due to only occasional occurrence and difficulties of providing a legitimate interpretation in case of secondary vegetation.

Acquired as part of the TanDEM-X science phase, five interferometric, VH-VV dual-polarized TD-X scenes could be acquired at experimental across-track baselines of up to 3 km. Initial testing has revealed four of the acquired scenes to be unusable due to decorrelation caused by the baseline, which is in accordance with Krieger et al. (2007), and the general recommendation of across-track baseline for forest height estimation between 100 m and 300 m. The last image pair was taken on 2015 – 10 – 8 at a baseline of 208.68 m, and with a coherence of 0.81 the images appear suited for the envisioned task. For the sampling of reference data, additional RapidEye and scenes from the Landsat 8 OLI (Operational Land Imager) are utilized, as well as TerraClass and Prodes data (Almeida et al., 2016; Instituto Nacional de Pesquisas Espaciais (INPE), 2015). Acquisition dates of the corresponding RapidEye and Landsat 8 OLI scenes are 2015 – 9 – 18 and 2015 – 10 – 17, respectively. Both optical scenes are cloud free, and despite the one month gap show negligible land cover change. As the TD-X acquisition lies in between, its land cover is assumed not to deviate

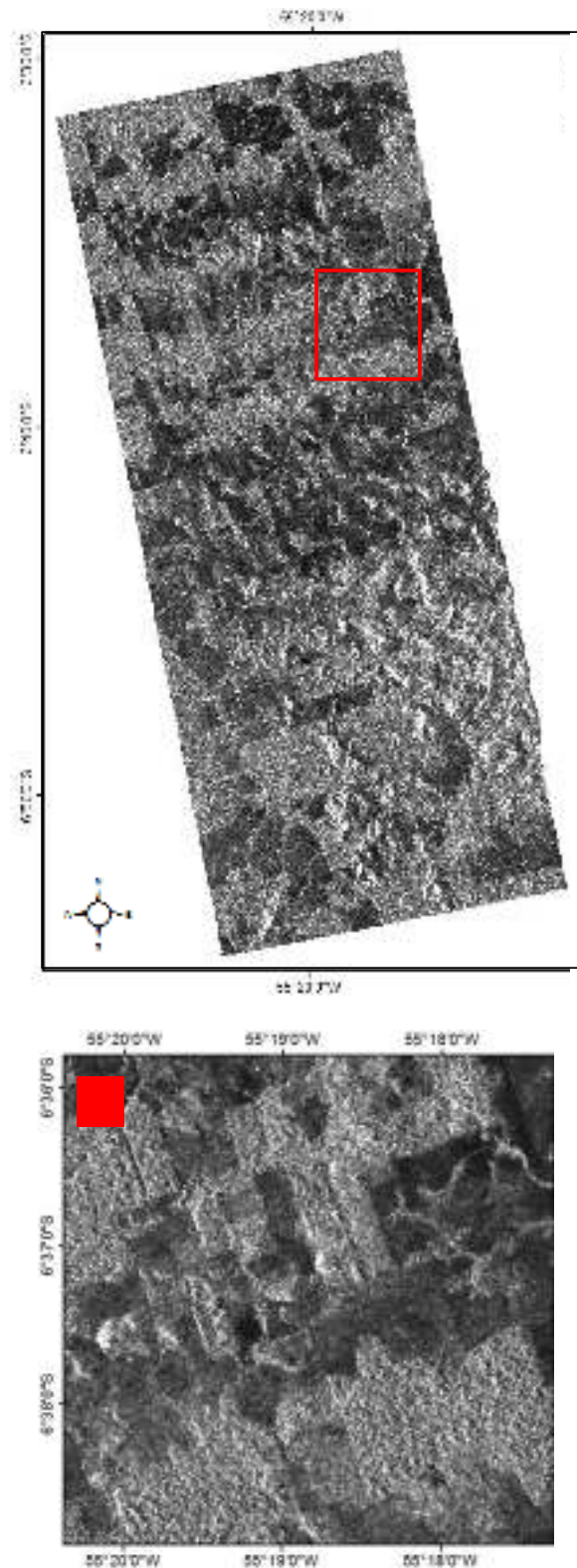


Fig. 4.1 The utilized StripMap scene. Position of the subset in the lower part is indicated by the red window.

from these two scenes. Thus, the optical data seems adequate for the collection of reference data for our TD-X scene, which was acquired within this time period.

4.3 Methods

Preprocessing was performed in SNAP, following the standard practices for both polarizations VH and VV: i) Generation of interferograms & coherence estimation, ii) Goldstein filtering, iii) Topographic Phase Removal, iv) Multi-Looking, v) Phase Unwrapping (snaphu), vi) Phase to height conversion, and vii) Range-Doppler Terrain correction. Analogously, non-interferometric intensity products are a) multi-looked, b) speckle filtered, and c) geocoded using Range-Doppler Terrain correction. Afterwards, Grey Level Cooccurrence Matrix (GLCM) based texture parameters are derived from all resulting products; i.e. Contrast, dissimilarity, homogeneity, angular second moment (ASM), energy, MAX, entropy, GLCM mean, GLCM variance and GLCM correlation. GLCM texture is a way to integrate information on spatial vicinity into the classification, which is derived through discretization of the pixel's values into bins and subsequently counting neighboring patterns at predefined directions. A detailed description is given in Haralick et al. (1973).

For classification, we utilize the R implementation of Random Forests (RF) (Breiman, 2001b). RF's are well suited for classifying SAR data and outperform other algorithms in terms of accuracy. Another advantage of RF is its simple handling and computational efficiency (Waske et al., 2009b). We randomly select 200 samples per class for model training and the same number of independent test samples. A total of 1200 samples are hence raised well distributed over the extent of the entire StripMap scene. All accuracy estimates in this manuscript are based on area-adjusted accuracy measures as introduced by Olofsson et al. (2014). For area-adjusted accuracy metrics, entries of the population error matrix are estimated by (4.1).

$$p_{ij} = W_i \frac{n_{ij}}{n_i} \tag{4.1}$$

In contrast to conventional confusion matrices, p_{ij} are proportion area elements stemming from the corresponding sample counts n_{ij} of the confusion matrix, and the total area proportion mapped as class i , W_i . The Overall Accuracy (OA) is hence given by the sum of the main diagonal. Also note the dot operator \cdot in the denominator, which signifies the sum over the corresponding matrix vector, in this case the i th row of n . Analogously to conventional population error matrices, it is further possible to estimate class-based user's accuracies signifying the proportion of areas mapped as some class i with reference class i via (4.2).

$$U_i = p_{ii} / p_i \tag{4.2}$$

Its complementary metric, the producer's accuracy, which signifies the proportion of class j 's area to be mapped as class j is yielded by (4.3).

$$P_j = p_{jj}/p_{\cdot j} \quad (4.3)$$

Having determined these basic metrics, it is further possible to derive additional statistics such as variances as well as area proportions. For a more in-depth overview see Olofsson et al. (2014).

4.4 Results

To assess the potential of TD-X data for tropical land cover mapping in terms of accuracy we perform a detailed accuracy assessment for the following four different classifications:

1. *SAR*: Classification of only the original SAR images
2. *InSAR*: Classification of original SAR images + Coherence images + DEM
3. *SAR+T*: Classification of original SAR images + corresponding GLCM
4. *InSAR+T*: Classification of original SAR images + Coherence images + DEM's + corresponding GLCM for any band

The classification of original *SAR* images only results in a 55 % OA. Misclassification for this feature set is particularly present for the class *shrubby pasture*, which shows high confusion with both, *forest* and *clean pasture*. The map appears noisy even in homogeneous areas, and a quarter of all forest pixels is classified as *shrubby pasture* (Figure 4.3). Integration of interferometric information (i.e., coherence as well as DEM) increases the classification accuracy significantly to 78 %. The result shows a strong decrease in misclassified *forest* areas, and misclassifications within *clean pasture* areas can often be attributed to the effects of individual trees.

Despite the absence of spatial texture information, classification accuracy of *InSAR* also surpasses *SAR+T*, which yields an OA of 72 %. While effects of speckle are reduced even further for this approach, strong confusion remains for *shrubby pasture*. Combining all data, *InSAR+T* yields a very high OA of 89 %. The effects of speckle are overwhelmingly suppressed, and forest is classified particularly well at 95 % (Figure 4.3). These findings are also underlined by a comparison of the derived User's (UA) and Producer's Accuracies (PA) (Figure 4.2). The class accuracies are increased by using interferometric and textural features.

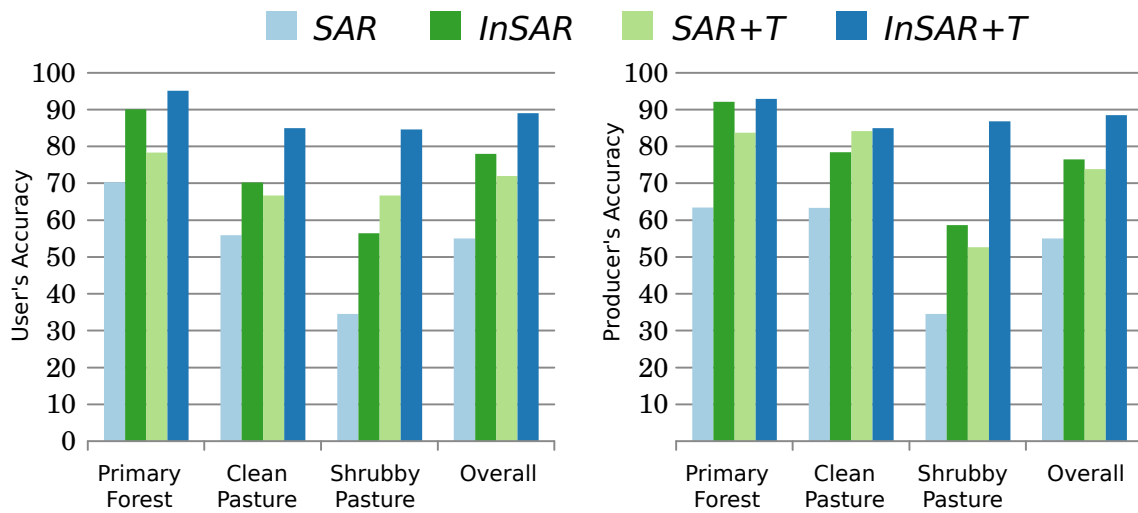


Fig. 4.2 Comparison of UA's and PA's.

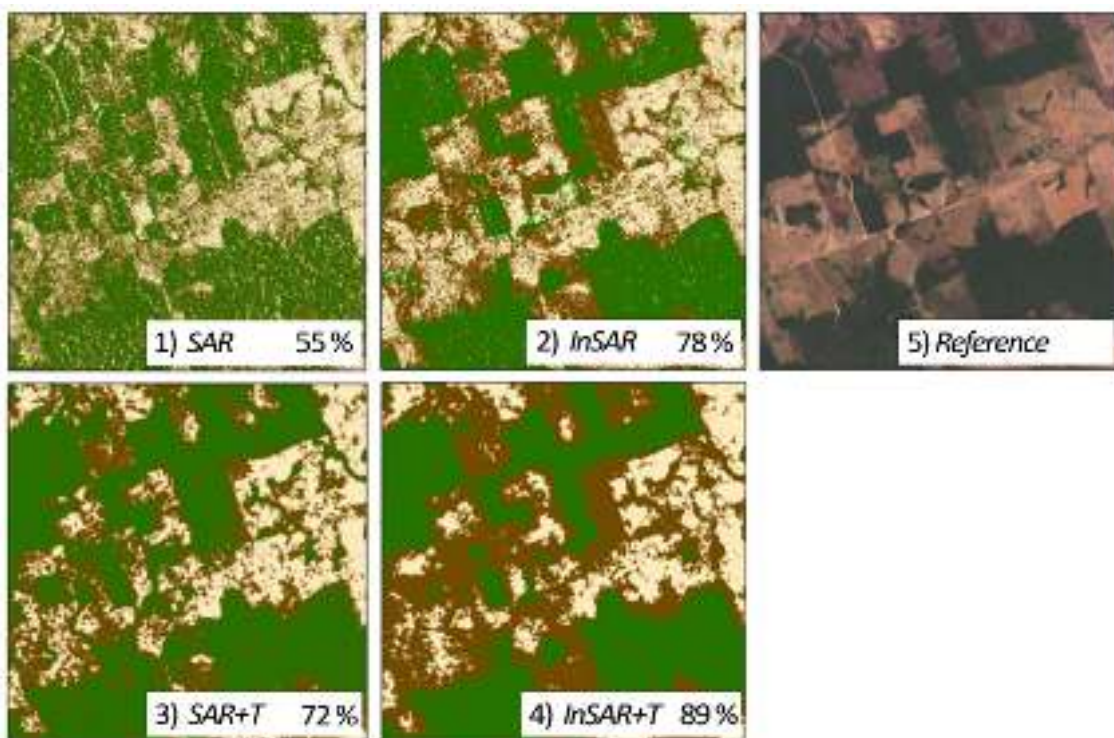


Fig. 4.3 Visual comparison of generated land cover products.

The final land cover map, derived using all available features, is given by Figure 4.4. The map illustrates particularly well the separability of *clean pasture* and *forest* areas, and also indicates increasingly dense vegetation at *forest* edges. The corresponding confusion matrix is given by Table 4.1. Very evidently, there is no confusion between *forests* and *clean pasture*, and it also indicates the more common occurrence of *shrubby pasture's* over *clean pasture* in the study region.

Table 4.1 Area proportion matrix for the InSAR+T approach.

Class	Forest	Clean Pasture	Shrubby Pasture	PA
Forest	0.39	0.00	0.03	0.93
Clean Pasture	0.00	0.17	0.03	0.85
Shrubby Pasture	0.02	0.03	0.33	0.87
UA	0.95	0.85	0.85	0.89

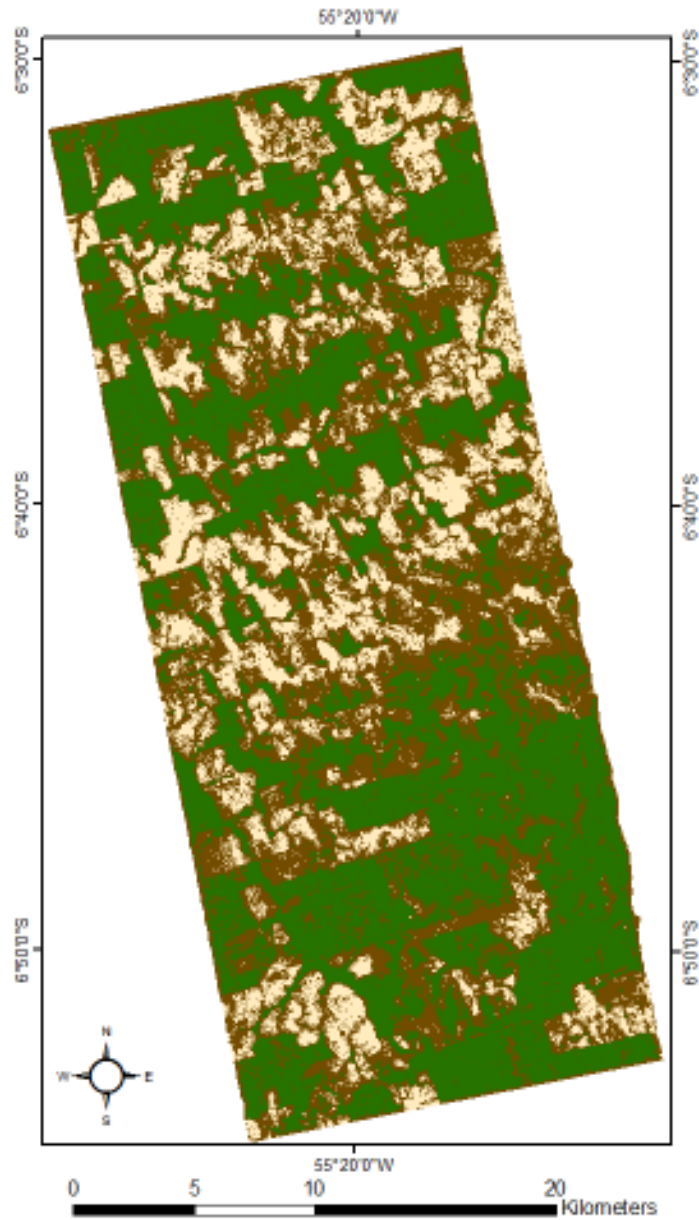


Fig. 4.4 Final land cover map using the *InSAR+T* data set.

4.5 Discussion

It is well known that SAR data with short wavelengths (X-band) has limitations for the classification of densely vegetated areas. Concerning the integration of interferometric coherence, this study underlines its usefulness to differentiate *forest* from *non-forest*. The classification accuracy increases by 10 p.p., from 55 % to 65.7 % when coherence is added to the SAR images. Yet using interferometric coherence alone is not sufficient to accurately separate *shrubby pasture* from the other classes, which is also confirmed by Schlund et al. (2013). Additional inclusion of a DEM yields a significant increase of 16 p.p.. Consistent with Santos et al. (2010a), this study shows the high significance of texture analysis for separability. Since texture analysis can possibly omit small scale variations within the map, such as individual trees or bushes, its integration should be considered carefully. In comparison with studies utilizing different sensors, yet are located in the same study region using similar classes, accuracies of this approach are on par with an approach based on Landsat time series (Jakimow et al., 2018).

In case a very high resolution is mandatory, *InSAR* offers the highest accuracy without the filtering effect of texture. When comparing the area of *clean pasture* and *shrubby pasture* for *InSAR*, they are almost equal at 21 214 ha \pm 8 % for *clean pasture*, to 19 734 ha \pm 11 % for *shrubby pasture*, with \pm indicating a 95 % confidence interval. In contrast, *InSAR+T* yields a 1 : 2 ratio for *clean* and *shrubby pasture*, with 14 979 ha \pm 9 % for *clean* and 29 210 ha \pm 15 % for *shrubby pasture*. This strong decrease in *clean pasture* when comparing texture vs. no texture shows that a pixel based approach acknowledges smaller patches of *clean pasture* while a texture based approach incorporates these patches more readily into *shrubby pasture*. In general, the use of texture information increases *forest* areas and *shrubby pasture*, and decreases the area of *clean pasture*. It can further be assumed that the high UA's of 95.1 % for *forest*, 85 % for *clean pasture*, and 84.6 % for *shrubby pasture* produce a fairly accurate representation of class proportions in the study area.

However, the results using SAR images, interferometric coherence, the phase generated DEM, and their texture information yield great success with an overall classification accuracy of 89 %.

4.6 Conclusion

TD-X delivers bi-static, weather independent images with high resolution. It is the first mission to simultaneously utilize two orbiting sensors to obtain across-track bistatic scenes enabling interferometric analysis. Although a simple distinction between *forest* and *non-*

forest can be achieved for all setups, separation between different *pasture* types is much more challenging. However, both feature sets, i.e., interferometric as well as textural features, lead to an increase in the mapping accuracy. The final overall classification accuracy of the three classes *primary forest*, *clean pasture* and *shrubby pasture* is increased from 55 % from SAR images alone to 89 %, by integrating interferometric and texture features. Comparing the two feature sets, it can be assessed that the interferometric features outperform the textural information in terms of accuracies.

References

- Almeida, C. A. d., A. C. Coutinho, J. C.D. M. Esquerdo, M. Adami, A. Venturieri, C. G. Diniz, N. Dessay, L. Durieux, and A. R. Gomes (2016). “High spatial resolution land use and land cover mapping of the Brazilian Legal Amazon in 2008 using Landsat-5/TM and MODIS data”. In: *Acta Amaz.* 46.3, pp. 291–302.
- Breiman, L. (2001b). “Random forests”. In: *Machine learning* 45.1, pp. 5–32.
- Butler, D. (2014). “Earth observation enters next phase”. In: *Nature* 508.7495, pp. 160–161.
- Hagensieker, R., R. Roscher, J. Rosentreter, B. Jakimow, and B. Waske (2017b). “Tropical land use land cover mapping in Pará (Brazil) using discriminative Markov random fields and multi-temporal TerraSAR-X data”. In: *International Journal of Applied Earth Observation and Geoinformation* 63, pp. 244–256.
- Haralick, R. M., K. Shanmugam, and I. H. Dinstein (1973). “Textural features for image classification”. In: *Systems, Man and Cybernetics, IEEE Transactions on* 6, pp. 610–621.
- Instituto Nacional de Pesquisas Espaciais (INPE) (2015). *Projeto PRODES - Monitoramento da Floresta Amazonica Brasileira por Satelite*.
- Jakimow, B., P. Griffiths, S. van der Linden, and P. Hostert (2018). “Mapping pasture management in the Brazilian Amazon from dense Landsat time series”. In: *Remote Sensing of Environment* 205, pp. 453–468.
- Joshi, N., M. Baumann, A. Ehammer, R. Fensholt, K. Grogan, P. Hostert, M. Jepsen, T. Kuemmerle, P. Meyfroidt, E. Mitchard, and et al.s (2016). “A Review of the Application of Optical and Radar Remote Sensing Data Fusion to Land Use Mapping and Monitoring”. In: *Remote Sensing* 8.1, p. 70.
- Krieger, G., A. Moreira, H. Fiedler, I. Hajnsek, M. Werner, M. Younis, and M. Zink (2007). “TanDEM-X: A satellite formation for high-resolution SAR interferometry”. In: *IEEE Transactions on Geoscience and Remote Sensing* 45.11, pp. 3317–3341.
- Li, G., D. Lu, E. Moran, L. Dutra, and M. Batistella (2012). “A comparative analysis of ALOS PALSAR L-band and RADARSAT-2 C-band data for land-cover classification in a tropical moist region”. In: *ISPRS Journal of Photogrammetry and Remote Sensing* 70, 26–38.
- Martone, M., P. Rizzoli, C. Wecklich, C. González, J.-L. Bueso-Bello, P. Valdo, D. Schulze, M. Zink, G. Krieger, and A. Moreira (2018). “The global forest/non-forest map from TanDEM-X interferometric SAR data”. In: *Remote Sensing of Environment* 205, pp. 352–373.
- Moreira, A., G. Krieger, I. Hajnsek, D. Hounam, M. Werner, S. Riegger, and E. Settelmeier (2004). “TanDEM-X: a terraSAR-X add-on satellite for single-pass SAR interferometry”.

- In: *IEEE International IEEE International IEEE International Geoscience and Remote Sensing Symposium, 2004. IGARSS '04. Proceedings. 2004.*
- Olofsson, P., G. M. Foody, M. Herold, S. V. Stehman, C. E. Woodcock, and M. A. Wulder (2014). “Good practices for estimating area and assessing accuracy of land change”. In: *Remote Sensing of Environment* 148, pp. 42–57.
- Rakwatin, P., N. Longépé, O. Isoguchi, M. Shimada, Y. Uryu, and W. Takeuchi (2012). “Using multiscale texture information from ALOS PALSAR to map tropical forest”. In: *International Journal of Remote Sensing* 33.24, pp. 7727–7746.
- Santos, J., J. Mura, H. Kux, C. Garcia, S Kuntz, I. Brown, and N. Pantoja (2010a). “Classification of TerraSAR-X imagery for the characterization of Amazon tropical forests”. In: *30th EARSeL Symposium: Remote Sensing for Science, Education and Culture*. Vol. 31, pp. 329–334.
- Schlund, M., F. von Poncet, D. H. Hoekman, S. Kuntz, and C. Schmullius (2013). “Importance of bistatic SAR features from TanDEM-X for forest mapping and monitoring”. In: *Remote Sensing of Environment*.
- Soja, M. J., J. I. Askne, and L. M. Ulander (2017). “Estimation of Boreal Forest Properties From TanDEM-X Data Using Inversion of the Interferometric Water Cloud Model”. In: *IEEE Geoscience and Remote Sensing Letters*.
- Stefanski, J., B. Mack, and B. Waske (2013). “Optimization of object-based image analysis with random forests for land cover mapping”. In: *IEEE Journal of Selected Topics in Applied Earth Observations and Remote Sensing* 6.6, pp. 2492–2504.
- Treuhaft, R., F. Gonçalves, J. R. dos Santos, M. Keller, M. Palace, S. N. Madsen, F. Sullivan, and P. M. Graça (2015). “Tropical-Forest Biomass Estimation at X-Band From the Spaceborne TanDEM-X Interferometer”. In: *Geoscience and Remote Sensing Letters, IEEE* 12.2, pp. 239–243.
- Waske, B. and M. Braun (2009b). “Classifier ensembles for land cover mapping using multitemporal SAR imagery”. In: *ISPRS Journal of Photogrammetry and Remote Sensing* 64.5, pp. 450–457.

Chapter 5

Mapping Deforestation from Height Differences of multi-temporal Tandem-X Images

Ron Hagensieker, Patrick Lubig, and Björn Waske

Abstract

TanDEM-X is the first spaceborne mission to allow single-pass bi-static interferometry as part of a continuous effort. In this study we investigate its multi-temporal capabilities for the detection of deforestation sites. Specifically, two height models and two intensity images are derived for two continuous years, before differences are calculated between the height and intensity images, respectively. With the help of optical RapidEye and Landsat images, reference information on land cover change is collected, and Random Forest classifications are performed on the difference images to derive deforestation maps. Using this method, accuracies of 89 % for the detection of forest are achieved, with an overall mapping accuracy of 89 %. The proposed method is applicable using currently available open source packages, requiring only few adaptations, e.g. to address effects such as interferometric ramp building.

5.1 Introduction

Changes in land use and land cover (LUCC) directly influence the earth's carbon stock, with the high deforestation rates of the 20th century contributing to anthropogenically released CO₂ in a major way (Canadell et al., 2008). Besides its effects on the global carbon cycle, forests directly influence regional climate and hydrology (Makarieva et al., 2006), and they are further hotspots of biodiversity (Lawton et al., 1998).

Deforestation is defined as active removal of forests toward areas with crown cover below 10 % (UN-REDD Programme Collaborative Online Workspace 2015). Information on land cover is conventionally derived from optical remote sensing imagery, yet technological progress allows for an increasing quality of SAR-based mapping (Kumar et al., 2017; Kuntz, 2010). Moreover, SAR data seem particularly interesting in the context of forest mapping, because deforestation often takes place in regions that are affected by dominant cloud cover, such as the Brazilian Amazon. Due to the characteristics of backscatter, SAR is especially capable for estimating biomass and the mapping of wetlands (Saatchi et al., 2011; Evans et al., 2013). In addition, many studies have highlighted the potential of SAR within the context of tropical classification (Grover et al., 1999). The authors used C- and L-band interferometry to perform land cover classification and change detection. More recently, the utilization of time series data and multi-sensoral integration with optical data plays an important role (Reiche et al., 2015b; Reiche et al., 2018).

TanDEM-X (TD-X) is a constellation maintained by DLR, and consists of two twin satellites which acquire interferometric SAR images at high revisit rates and high spatial resolution. Due to its attractive properties, in recent years various studies utilized interfer-

ometric TerraSAR-X and TD-X data in the context of forest mapping (Karila et al., 2015; Liesenberg et al., 2013; Schlund et al., 2013). Schlund et al. (2013) show that utilization of bi-static SAR images can improve the classification accuracy of several vegetated classes and forest types by up to 10 % compared to monostatic SAR. Karila et al. (2015) utilize interferometric TD-X to derive forest inventory data such as trunk diameter, tree height, basal area, and Magnard et al. (2016) classify trees using multi-baseline SAR using experimental aerial Ka-band sensors. Santos et al. (2010b) use dual polarized SAR images to test different classification methods.

Overall, with the increasing availability of interferometric SAR data over the last years, many studies are beginning to uncover its various capabilities. The main objective of this study is to investigate the potential multitemporal TD-X data to map different types of land use change in the Brazilian Amazon. The specific objective of our study is the classification of multiple CoSSC TD-X scenes, acquired over a study area in the North of federal state of Mato Grosso, Brazil.

5.2 Data & Study area

The federal state Mato Grosso (MT) is located in central Brazil and encompasses a total area of 900 000 km². It's dominated by two biomes, the cerrado and, particularly in the north-west, the Brazilian Amazon. MT experienced peak deforestation in 2005 with 12 000 km² per year (Morton et al., 2011). This peak was followed by a strong, Amazon wide decrease in the following years to 3000 km² per year (Morton et al., 2011), which was discussed heavily in literature (Nepstad et al., 2014b; Souza Jr et al., 2013). Reasons behind deforestation in MT are traditionally cattle ranching, and more recently, cultivation of areas for soy farming.

The study area encompasses an area of about 1000 km² and is located at the southern edge of the Brazilian Amazon, close to the border of neighboring state Pará, and in vicinity to the transcontinental BR-163 highway (Figure 5.1). Within the study area there are primary forests, especially in the central, north-western and eastern parts. It is overall dominated by agricultural areas of different succession stages. There are no closed municipal areas, but farming along the road network.

The study area is covered by the swath of multiple CoSSC TD-X scenes from the 2012 and 2013 experimental acquisition phase. Within this phase, the baseline of multiple acquisitions surpassed the critical threshold, and in particular acquisitions from 2012-12-19 and 2013-10-23 are considered for the analysis. Data is acquired in StripMap mode at HH single polarization.

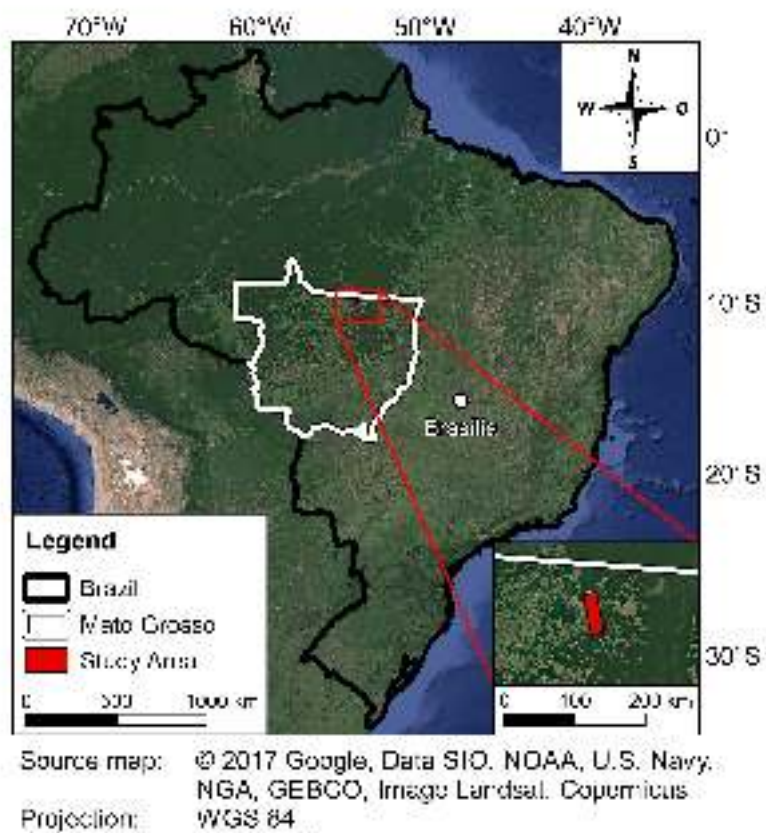


Fig. 5.1 Location and extent of the study region in central Brazil.

5.3 Methods

InSAR is based on relating phase information of multiple comparable SAR acquisitions. There are two principles to enable InSAR, which are along-track and across-track interferometry (Moreira et al., 2013a). For both methods the acquisition of multiple images from slightly different angles is critical. Along-track interferometry achieves this, in the general case, by a single sensor taking acquisitions from a revisiting orbit, albeit slightly shifted in position. Across-track interferometry, on the other hand, requires two sensors in an offset constellation, to gather imagery in parallel. TD-X particularly enables the latter. If acquisitions are coherent, the phase of an interferogram illustrates phase differences between the two interferometric images, which allows for the extraction of meaningful patterns. Coherence is a measure for the correlation of two SAR scenes. It is particularly affected by signal to noise ratios and even miniscule differences in surface structure between two scenes. Further problems can arise in areas of low coherence and through repetitive phase information (Zebker et al., 1992). These problems are in direct relation to the ground resolution and the baseline of the two sensors. It is addressed by phase unwrapping which includes external information on the topography and offers an estimation of signal continuity (Davidson et al., 1999).

Using Snap 5.0, interferograms are generated from the CoSSC images of the years 2012 and 2013, and layers of intensity, phase, and coherence are calculated for both dates. Afterwards, DHM's of relative height are derived. To correct noise in the interferogram and to eliminate height ambiguities within the unwrapping procedure, a Goldstein Phase filter is applied (Goldstein et al., 1998). Phase unwrapping is conducted through Snaphu using the TOPO mode, and Minimum Cost Flow (MCF) as initial method (Hooper, 2010). After preprocessing images for both years, two difference maps are generated for height and intensity, respectively. These layers will be the key features within this study, as the classification is ultimately based on detecting deforestation sites from the derived height and intensity differences. All datasets are geocoded into UTM using Range-Doppler Terrain Correction.

5.4 Reference Data

The particular focus of this study lies on the detection of deforestation. Beside deforestation, different types of similar LUCC can be identified (grazing, slash and burn farming, tillage). Delineating these processes is an important interpretation task, yet the scope of the subsequent classification lies on the detection of deforestation. It is addressed through the labeling of all detectable changes into seven distinct classes, using a strictly defined scheme based on

available SAR and optical images. In total, 202 change areas could be identified, spanning an area of 2254 ha, which we assume covers all change within the investigation period. Out of the 202 detected changes, deforestation of primary forests contributes 51 polygons, while deforestation of secondary forests contributes 25 polygons. The total area of deforestation is below one quarter of all LUCC. The final data set is split in two parts, resulting in two spatially disjointed data sets, for training and validation.

5.5 Methods

The classification is conducted through Random Forests (RF) using a total of 1,000 test and 1,000 training pixels, which are extracted from the digitized change areas. RF are an ensemble method based on classification trees, which are capable to address multi-dimensional data with complex class distributions (Breiman, 2001b). In the field of remote sensing, they are widely used for the classification of multi-temporal SAR data (e.g. Waske et al. (2009b), Stefanski et al. (2014), and Du et al. (2015)).

For an opposing class, an additional 1,000 pixels are sampled for training and testing, respectively. To particularly highlight the importance of separating different types of change, a stratified sampling strategy is chosen to include 500 samples from non-deforestation areas, and 500 samples from the remaining areas of the image.

5.6 Results

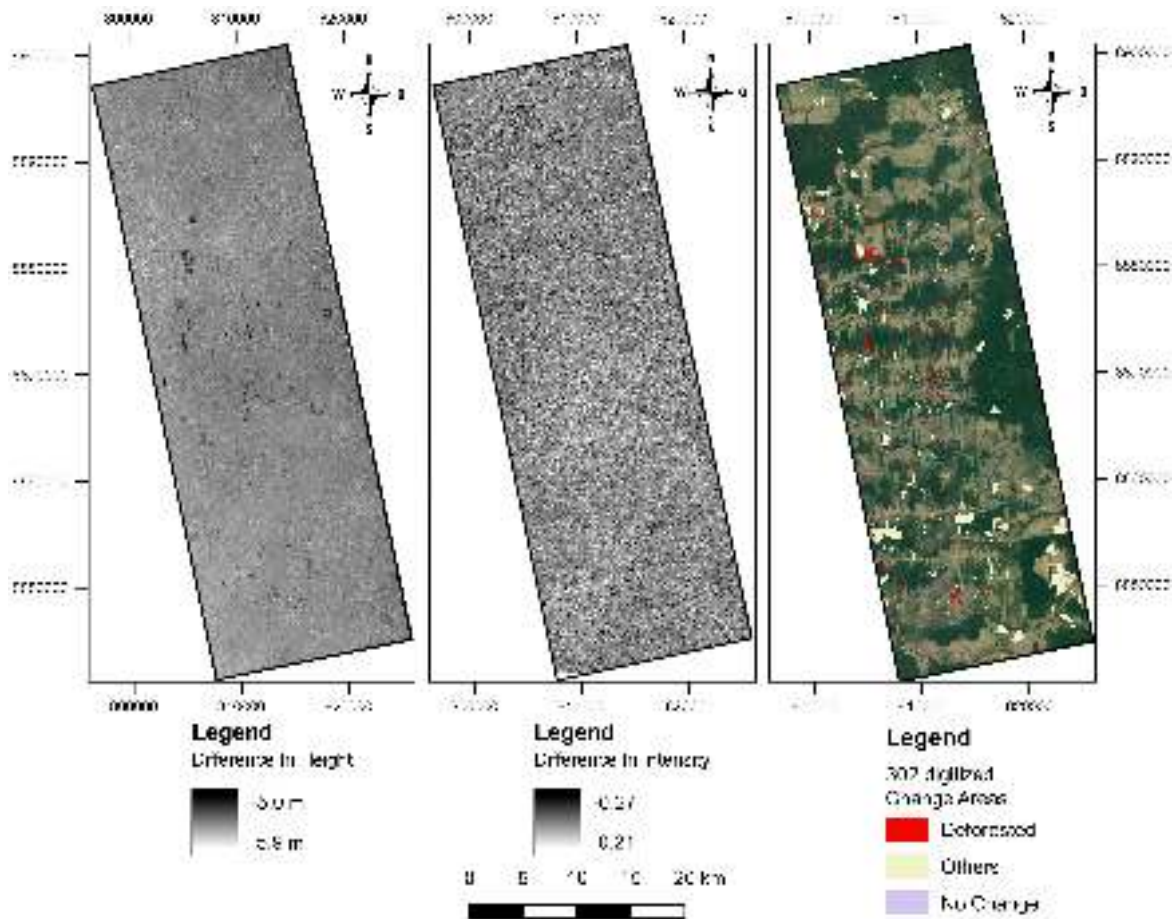


Fig. 5.2 Summary of relevant input layers: differences in height, differences in intensity, and digitized areas of change, respectively.

A visual comparison already underlines the advantages of deriving height differences in comparison to intensity differences. Dark areas in Figure 5.2 indicate reduction of heights and intensities, and especially height differences appear as characteristic rectangular shapes indicative of deforestation. In contrast, differences in intensity are more subtle and sites of LUCC are harder to make out using intensity difference images. Note that there is a large number of change areas, which are not considered deforestation. Other changes include pasture management, secondary regrowth, and degradation. These are the layers utilized for the classification procedure to discriminate deforestation from other change and non-change sites. Utilizing these layers, Figure 5.3 illustrates the final results of the RF classification. An overall classification accuracy of 88 % is achieved when all difference layers are included.

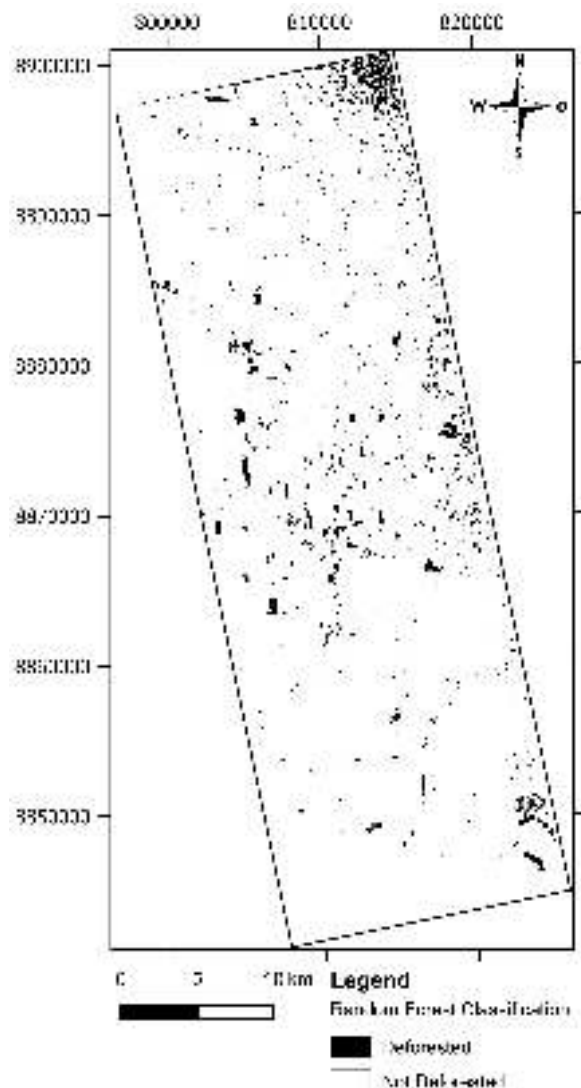


Fig. 5.3 Deforestation map of the study region.

The confusion matrix shows well balanced User Accuracies (UA) and Producer Accuracies (PA) between the classes (Table 5.1). Consider that sampling has not been conducted entirely random but was stratified, and hence, a relatively high number of change sites is included for the validation. Deforestation sites appear to be slightly underrepresented, which is indicated by their relatively low PA of 85.6%, while non-deforestation sites are detected more precisely (90.2%).

Table 5.1 Confusion matrix for the classification. Test data was sampled over the entire extent of the available data.

	Reference		
	Deforested	Other	PA (%)
Deforested	856	144	85.6
Other	98	902	90.2
UA (%)	89.7	86.2	
Overall Accuracy	87.9 %		

5.7 Discussion

Utilization of difference images from two bistatic TD-X acquisitions appears well suited to sufficiently detect sites of deforestation.

Weaknesses of the approach can be observed in the northern area of the study region, where an overestimation of deforestation sites took place (Figure 5.3). This systematic error is caused by a ramp, which is an artifact from the phase to height preprocessing (Simons et al., 2007). Similar observations are made by Neelmeijer et al. (2017), who corrected this gradient via a 2D quadratic phase model followed by an extra tilt-removal during the alignment to an external DEM (Digital Elevation Model). For ramp removal we chose a simple method based on an IDW interpolation (Inverted Distance Weighting). For this, we sampled multiple bare points, which we know should not yield significant height differences, such as road intersections or bare ground. While we were able to generally suppress the ramp, some effects remain noticeable, especially in the north eastern part of the study area.

Additionally, the analysis is affected by *interferometric height* (Hoekman et al., 2001). Interferometric height describes a displacement error caused by tree top penetration, which has been shown to be also present at X-band. Since it is highly correlated to true tree heights, its effects concerning the subsequent classification are minor. Still, it decreases the interpretative value of the illustrated height differences as heights appear reduced.

Except for these, the outcome appears very homogeneous considering the speckling characteristics of SAR, and the overall problems of utilizing short wavelength SAR for mapping of densely vegetated areas.

5.8 Conclusion

In this study we propose an applicable workflow for the derivation of deforestation maps from multi-temporal across-track interferometric imagery with baselines below 300 m. The processing can be achieved using freely available software, such as Snap, snaphu, and Python.

Height differences are particularly useful as they offer powerful features for the classification. Limitations are posed by the ramp effect as well as the ambiguities caused by interferometric height. While the first one can be addressed using various methods, the effects of interferometric height remain an interpretative challenge requiring further research in the future.

References

- Breiman, L. (2001b). “Random forests”. In: *Machine learning* 45.1, pp. 5–32.
- Canadell, J. G. and M. R. Raupach (2008). “Managing Forests for Climate Change Mitigation”. In: *Science* 320.5882, pp. 1456–1457.
- Davidson, G. W. and R. Bamler (1999). “Multiresolution phase unwrapping for SAR interferometry”. In: *IEEE Transactions on Geoscience and Remote Sensing* 37.1, pp. 163–174.
- Du, P., A. Samat, B. Waske, S. Liu, and Z. Li (2015). “Random Forest and Rotation Forest for fully polarized SAR image classification using polarimetric and spatial features”. In: *ISPRS Journal of Photogrammetry and Remote Sensing* 105, 38–53.
- Evans, T. L. and M. Costa (2013). “Landcover classification of the Lower Nhecolândia subregion of the Brazilian Pantanal Wetlands using ALOS/PALSAR, RADARSAT-2 and ENVISAT/ASAR imagery”. In: *Remote Sensing of Environment* 128, 118–137.
- Goldstein, R. M. and C. L. Werner (1998). “Radar interferogram filtering for geophysical applications”. In: *Geophysical research letters* 25.21, pp. 4035–4038.
- Grover, K., S. Quegan, and C. da Costa Freitas (1999). “Quantitative estimation of tropical forest cover by SAR”. In: *IEEE Transactions on Geoscience and Remote Sensing* 37.1, pp. 479–490.
- Hoekman, D. H. and C. Verekamp (2001). “Observation of tropical rain forest trees by airborne high-resolution interferometric radar”. In: *IEEE Transactions on Geoscience and remote sensing* 39.3, pp. 584–594.
- Hooper, A. (2010). “A statistical-cost approach to unwrapping the phase of InSAR time series”. In: *Proceeding of international workshop on ERS SAR interferometry, Frascati, Italy*. Vol. 30.
- Karila, K., M. Vastaranta, M. Karjalainen, and S. Kaasalainen (2015). “Tandem-X interferometry in the prediction of forest inventory attributes in managed boreal forests”. In: *Remote Sensing of Environment* 159, pp. 259–268.
- Kumar, S., U. G. Khatri, S. Chandola, S. Agrawal, and S. P. Kushwaha (2017). “Polarimetric SAR Interferometry based modeling for tree height and aboveground biomass retrieval in a tropical deciduous forest”. In: *Advances in Space Research* 60.3, pp. 571–586.
- Kuntz, S. (2010). “Potential of spaceborne SAR for monitoring the tropical environments”. In: *Tropical Ecology* 51.1, pp. 3–10.
- Lawton, J. H., D. E. Bignell, B. Bolton, G. F. Bloemers, P. Eggleton, P. M. Hammond, M. Hodda, R. D. Holt, T. B. Larsen, N. A. Mawdsley, N. E. Stork, D. S. Srivastava, and A. D. Watt (1998). “Biodiversity inventories, indicator taxa and effects of habitat modification in tropical forest”. In: *Nature* 391.6662, pp. 72–76.

- Liesenberg, V. and R. Gloaguen (2013). "Evaluating SAR polarization modes at L-band for forest classification purposes in Eastern Amazon, Brazil". In: *International Journal of Applied Earth Observation and Geoinformation* 21, pp. 122–135.
- Magnard, C., F. Morsdorf, D. Small, U. Stilla, M. E. Schaepman, and E. Meier (2016). "Single tree identification using airborne multibaseline SAR interferometry data". In: *Remote Sensing of Environment* 186, pp. 567–580.
- Makarieva, A. M. and V. G. Gorshkov (2006). "Biotic pump of atmospheric moisture as driver of the hydrological cycle on land". In: *Hydrology and Earth System Sciences Discussions* 3.4, pp. 2621–2673.
- Moreira, A., P. Pratstiraola, M. Younis, G. Krieger, I. Hajnsek, and K. P. Papathanassiou (2013a). "A Tutorial on Synthetic Aperture Radar". In:
- Morton, D. C., M. H. Sales, C. M. Souza, and B. Griscom (2011). "Historic emissions from deforestation and forest degradation in Mato Grosso, Brazil: 1) source data uncertainties". In: *Carbon Balance and Management* 6.1, p. 18.
- Neelmeijer, J., M. Motagh, and B. Bookhagen (2017). "High-resolution digital elevation models from single-pass TanDEM-X interferometry over mountainous regions: A case study of Inylchek Glacier, Central Asia". In: *ISPRS Journal of Photogrammetry and Remote Sensing* 130, pp. 108–121.
- Nepstad, D., D. McGrath, C. Stickler, A. Alencar, A. Azevedo, B. Swette, T. Bezerra, M. DiGiano, J. Shimada, R. S. da Motta, et al. (2014b). "Slowing Amazon deforestation through public policy and interventions in beef and soy supply chains". In: *Science* 344.6188, pp. 1118–1123.
- Reiche, J., J. Verbesselt, D. Hoekman, and M. Herold (2015b). "Fusing Landsat and SAR time series to detect deforestation in the tropics". In: *Remote Sensing of Environment* 156, pp. 276–293.
- Reiche, J., E. Hamunyela, J. Verbesselt, D. Hoekman, and M. Herold (2018). "Improving near-real time deforestation monitoring in tropical dry forests by combining dense Sentinel-1 time series with Landsat and ALOS-2 PALSAR-2". In: *Remote Sensing of Environment* 204, pp. 147–161.
- Saatchi, S., M. Marlier, R. L. Chazdon, D. B. Clark, and A. E. Russell (2011). "Impact of spatial variability of tropical forest structure on radar estimation of aboveground biomass". In: *Remote Sensing of Environment* 115.11, pp. 2836–2849.
- Santos, J., J. Mura, H. Kux, C. Garcia, S. Kuntz, I. Brown, and N. Pantoja (2010b). "Classification of TerraSAR-X imagery for the characterization of Amazon tropical forests". In: *30th EARSeL Symposium: Remote Sensing for Science, Education and Culture*. Vol. 31, pp. 329–334.

- Schlund, M., F. von Poncet, D. H. Hoekman, S. Kuntz, and C. Schmullius (2013). “Importance of bistatic SAR features from TanDEM-X for forest mapping and monitoring”. In: *Remote Sensing of Environment*.
- Simons, M. and P. Rosen (2007). “Interferometric Synthetic Aperture Radar Geodesy”. In: *Treatise on Geophysics*. Elsevier, pp. 391–446.
- Souza Jr, C. M., J. V. Siqueira, M. H. Sales, A. V. Fonseca, J. G. Ribeiro, I. Numata, M. A. Cochrane, C. P. Barber, D. A. Roberts, and J. Barlow (2013). “Ten-Year Landsat Classification of Deforestation and Forest Degradation in the Brazilian Amazon”. In: *Remote Sensing* 5.11, pp. 5493–5513.
- Stefanski, J., O. Chaskovskyy, and B. Waske (2014). “Mapping and monitoring of land use changes in post-Soviet western Ukraine using remote sensing data”. In: *Applied Geography* 55, pp. 155–164.
- Waske, B. and M. Braun (2009b). “Classifier ensembles for land cover mapping using multitemporal SAR imagery”. In: *ISPRS Journal of Photogrammetry and Remote Sensing* 64.5, pp. 450–457.
- Zebker, H. A. and J. Villasenor (1992). “Decorrelation in interferometric radar echoes”. In: *IEEE Transactions on geoscience and remote sensing* 30.5, pp. 950–959.

Chapter 6

Synthesis

6.1 Main findings

In the following section, the aims as defined in Chapter 1 are gauged with the findings of the conducted research from Chapters 2 to 5.

6.1.1 Chapter 2 - Discriminative MRF

Due to being less affected by clouds and the potentials of acquiring gapless time series data, multi-temporal analysis of SAR images is promising. On the other hand, speckle is widely considered a serious impediment for land cover analysis based on SAR, and also multi-temporal mapping within tropical ecosystems faces challenges due to rapid changes of the land surface. It is thus essential to develop methods that can handle these challenges.

In Chapter 2, a method is presented to utilize spatial and temporal pixel neighborhoods to improve the outcome of probabilistic land cover classifications. Overall accuracies are elevated by an average of 12 % through utilization of spatial neighborhoods and information on land cover trajectories. Variance between classification accuracies of multiple scenes are reduced, leading to more reliable outcome, and especially benefiting scenes with initially weak classifications. Interestingly, the worst classification result before application of the spatial-temporal MRF after application yields the highest accuracy. As a multi-temporal setup over one dry season is considered, the study shows growth of clean pasture as well as the decline of shrubby pasture areas between the dry season's months June and August. The method is particularly able to take into consideration estimates on land cover dynamics, which are formulated in advance and used for model parameterization. The method is robust and potentially transferable to multi-sensoral cases, as it is based just on probabilistic classifications of land cover, and is hence agnostic to the underlying input of these classifications.

6.1.2 Chapter 3 - Multi-frequency SAR

The number of active earth observation SAR-satellites is rapidly growing, and data policies of these systems increasingly permit free use of remote sensing imagery. There are hence obvious potentials to fuse multi-frequency and multi-temporal images to enhance land cover mapping.

As part of Chapter 3, advantages of a combined utilization of different wavelength SAR for the purpose of tropical mapping are discussed. While at L-band it is already possible to distinctly map primary forests, through integration of multi-frequency data a distinction of additional vegetated classes such as pasture areas and secondary regrowth can be achieved. Single classification of the most accurate scenes of ALOS-2, RS-2, and TS-X yield accuracies

of 62 %, 47 %, and 58 %, respectively. A combined utilization of ALOS-2 and TS-X data yields a 66 % accuracy, while the additional inclusion of RS-2 raises accuracies to 68 %. Classification using the entire data set, consisting of 9 scenes in total, leads to an accuracy of 69 %.

Surprisingly, in particular TS-X appears more capable for the task than RS-2, which operates at a longer wavelength albeit at lower spatial resolution. The combination of three scenes to yield the highest accuracy is a combination consisting of all, an X-, C-, and L-band acquisition, which underlines the potentials of multi-frequency applications. While the combination of different frequencies is advisable, gains in accuracy saturate quickly as a growing number of scenes is added.

6.1.3 Chapters 4 and 5 - Interferometric SAR

TanDEM-X is the first commercially available constellation which acquires single-pass interferometric SAR data. Interferometry enables to derive additional structural surface information as well as the estimation of ground heights, yet it requires a sensitive preprocessing, which includes an interferometric coregistration, as well as phase unwrapping in order to avoid phase shifts.

In Chapters 4 and 5 the potentials of interferometrically derived features to assist land cover mapping in central Brazilian study sites are investigated. While Chapter 4 focuses on the evaluation of interferometric coherence as an additional attribute for land cover classification, Chapter 5 aims at the utilization of multiple interferometrically derived height models to perform detection of deforestation. Chapter 4 shows an overall accuracy of 78 % over 55 %, when interferometric coherence is included. Similarly, in the case of a texture-based classification, interferometric coherence can raise the accuracy from 72 % to 89 %. In Chapter 5, with the help of height information derived from interferometric images, an overall accuracy of 88 % is achieved for the detection of deforestation sites.

6.2 Conclusion and prospects

A typical SAR classification workflow can be subdivided into several distinct stages. After acquisition, images require preprocessing before classification and post-classificative methods can be applied. All stages are topics of investigation in current remote sensing literature, and, focusing on the demands of tropical land cover mapping, this work as well grazes all parts of this processing chain. The suitability of L-band data, yet also the potentials of high resolution imagery as offered by TS-X, as well as the benefits of multi-frequency remote sensing are

highlighted by Chapter 3. Chapter 4 and Chapter 5 underline capabilities of interferometric images, in particular for the separation of vegetation classes, which conventional SAR generally struggles with. Finally, Chapter 2 utilizes probabilistic classifications and an innovative, applicable method to link land cover information and expert knowledge to optimize classification outcome.

Considering the growing importance of deep learning as well as the rapidly growing number of spaceborne SAR sensors (LeCun et al., 2015; Joshi et al., 2016), the findings of this study should be discussed with regard to these developments. The potentials of deep neural networks for classification have been discussed in various recent articles (LeCun et al., 2015; Schmidhuber, 2015), and some early applications have been conducted within the remote sensing domain (Kampffmeyer et al., 2016; Romero et al., 2016; Volpi et al., 2016). Most prominently, Convolutional Neural Nets (CNN's) offer a very efficient way to learn, supervisedly or unsupervisedly, spatial features from image data (Lee et al., 2009). Based on these features, which are extracted by filters that scan for recurring, characteristic patterns, the final layers conduct a classification to yield a probabilistic output.

Parallels hence exist to the approach undertaken in Chapter 2, and potential ways to combine these efforts. Utilizing a CNN for classification, the integration of GLCM texture parameters can be considered redundant as the network is able to learn superior spatial features within its various hidden layers. Instead of a pure post-classificative definition, like it is implemented in Chapter 2, MRF's could instead be integrated as additional layers within the model, in a way that model training can already respect the effect of regularization and adapt parameters accordingly. As the applied method of message passing just introduces multiplication by constant weight parameters, integration of such an operation would not break the fundamental principle of being derivable through to perform backpropagation, which underlies most current deep learning architectures. Moreover, the developed approach in Chapter 2 to utilize pixel vicinity in multi-temporal neighborhoods can analogously be extended to CNN's. In the same way CNN's are considering two spatial dimensions to aggregate information on neighborhoods from different scales, implementation of temporal convolution and pooling appears like an obvious extension, which is a particularly interesting application for gapless (i.e. cloud free), i.e. SAR, remote sensing time series. With regard to SAR, such methods are furthermore of particular interest, as they not only might assist with the suppression of speckle effects, but might potentially be able to learn spatial patterns directly from the speckle. Implementation of such a system would be straight-forward and could be achieved using modern deep learning libraries.

The remaining Chapters 3 to 5 are particularly relevant with regard to future sensor systems and the increasing amount of freely accessible data. Modern classifiers allow a

straight-forward integration of various types of features, which can stem from multi-frequency data, interferometry, or multi-temporal acquisitions. A growing number of operational SAR systems therefore will directly contribute to products of higher accuracy. Still, observations of Chapter 3 show L-band and images of high resolution to be preferable for vegetation mapping, while observations of Chapter 4 and 5 underline the potentials attached to interferometric analysis. Besides the large volume of SAR data, which will be gathered within the next years, TanDEM-L is a constellation planned by DLR, that answers most of these demands, and could truly expand the possibilities of SAR-based remote sensing in the tropics (Moreira et al., 2015).

At a broader scope, new methods and sensors will not only contribute to increases in accuracy, but will allow to tap on new fields of research and practical applications. For example, within the last years, the management practice of integrated systems has gained importance in central Brazil (Gil et al., 2015). Yet, due to the fine scale of these systems and its intrinsic interactions of land cover types, continued quantification via SAR-based remote sensing, at the current point, might not appear feasible. In addition, global phenomena like forest dieback or more subtle tasks like mapping invasive species (Allen, 2009), which require the detection of slight gradual shifts, could sufficiently be covered by better data and more powerful methods. More than ever before, these topics can only be addressed adequately if true syntheses between disciplines can be established, and the specialized expertise of multiple highly specialized domains is integrated to gather new knowledge.

References

- Allen, C. D. et al. (2009). “Climate-induced forest dieback: an escalating global phenomenon”. In: *Unasylva* 231.232, p. 60.
- Gil, J., M. Siebold, and T. Berger (2015). “Adoption and development of integrated crop–livestock–forestry systems in Mato Grosso, Brazil”. In: *Agriculture, Ecosystems & Environment* 199, pp. 394–406.
- Joshi, N., M. Baumann, A. Ehammer, R. Fensholt, K. Grogan, P. Hostert, M. Jepsen, T. Kuemmerle, P. Meyfroidt, E. Mitchard, and et al.s (2016). “A Review of the Application of Optical and Radar Remote Sensing Data Fusion to Land Use Mapping and Monitoring”. In: *Remote Sensing* 8.1, p. 70.
- Kampffmeyer, M., A.-B. Salberg, and R. Jenssen (2016). “Semantic segmentation of small objects and modeling of uncertainty in urban remote sensing images using deep convolutional neural networks”. In: *Proceedings of the IEEE Conference on Computer Vision and Pattern Recognition Workshops*, pp. 1–9.
- LeCun, Y., Y. Bengio, and G. Hinton (2015). “Deep learning”. In: *Nature* 521.7553, pp. 436–444.
- Lee, H., R. Grosse, R. Ranganath, and A. Y. Ng (2009). “Convolutional deep belief networks for scalable unsupervised learning of hierarchical representations”. In: *Proceedings of the 26th Annual International Conference on Machine Learning - ICML 2009*.
- Moreira, A., G. Krieger, I. Hajnsek, K. Papathanassiou, M. Younis, P. Lopez-Dekker, S. Huber, M. Villano, M. Pardini, M. Eineder, F. D. Zan, and A. Parizzi (2015). “Tandem-L: A Highly Innovative Bistatic SAR Mission for Global Observation of Dynamic Processes on the Earth's Surface”. In: *IEEE Geoscience and Remote Sensing Magazine* 3.2, pp. 8–23.
- Romero, A., C. Gatta, and G. Camps-Valls (2016). “Unsupervised Deep Feature Extraction for Remote Sensing Image Classification”. In: *IEEE Transactions on Geoscience and Remote Sensing* 54.3, pp. 1349–1362.
- Schmidhuber, J. (2015). “Deep learning in neural networks: An overview”. In: *Neural Networks* 61, pp. 85–117.
- Volpi, M. and D. Tuia (2016). “Dense Semantic Labeling of Subdecimeter Resolution Images With Convolutional Neural Networks”. In: *IEEE Transactions on Geoscience and Remote Sensing*.